THE APPLICATION OF THE MODIFIED FORM OF BÅTH'S LAW TO THE FAULT ZONES IN TURKEY

by

Tuğba Öztürk Gökgöl

B.S., Physics, IŞIK University, 2004

Submitted to the Institute for Graduate Studies in
Science and Engineering in partial fulfillment of
the requirements for the degree of
Master of Science

Graduate Program in Physics

Boğaziçi University

2008

ACKNOWLEDGEMENTS

I would like to express my thanks to Prof. Dr. Levent Kurnaz for his comments, help and supervision on the topic, and for understanding my faults.

I would like to thank Prof. Dr. Niyazi Türkelli and Assist. Prof. Dr. İbrahim Semiz for evaluating my thesis.

I would like to thank Dr. Doğan Kalafat for his great help and time, and my friend Şükrü Murat Cebeci for his help.

Lastly, I would like to thank my husband for his help and my family for their psychological support.

ABSTRACT

THE APPLICATION OF THE MODIFIED FORM OF BÅTH'S LAW TO THE FAULT ZONES IN TURKEY

Båth's law is an empirical law which says that any mainshock is followed by an aftershock approximately 1.2 less than its mainshock in magnitude, regardless of mainshock magnitude. In modified form of Båth's law, we infer the largest aftershock of a mainshock from an extrapolation of the Gutenberg-Richter statistics. In this thesis, application of the modified version of the Båth's law to the fault zones in Turkey, and nearby countries, and to the San Andreas Fault Zone in California was studied. We considered 41 earthquakes occuring in and near Turkey between 1900 and 2005 with magnitude equal to or greater than $m_{ms} \geq 5.7$. The earthquake catalogs that are provided by Boğaziçi University Kandilli Observatory and Earthquake Research Institute were used in this application. Nine large earthquakes that occured in California between 1987 and 2003 with magnitudes equal to or greater than $m_{ms} \geq 5.5$ were also considered. For California region, earthquake catalogs that are provided by the Southern California Earthquake Center, Southern California Seismic Network catalog, and the Northern California Earthquake Data Center, Northern California Seismic Network catalog were used. We also categorized the mainshocks according to their fault zones. It was concluded that the modified form of Båth's law is not applicable to the fault zones in Turkey.

ÖZET

GELİŞTİRİLMİŞ BÅTH YASASININ TÜRKİYEDEKİ FAY HATLARINA UYGULANIŞI

Båth yasası; ana depremlerin büyüklükleri ile bu depremler sonrasında kaydedilen en büyük artçı sarsıntıların büyüklükleri arasındaki farkı sabit ve yaklaşık 1.2 civarında kabul eden ampirik bir yasadır. Geliştirilmiş Båth yasasında, ana depremin en büyük artçı sarsıntısını Gutenberg-Richter frekans-büyüklük istatistiğine dışdeğer biçim uygulanması ile elde ederiz. Bu çalışmada, geliştirilmiş yasanın uygulanabilirliğini test etmek amacıyla Türkiye ve Türkiye'nin yakın sınır komşuları içindeki fay hatları, ve California'daki San Andreas fay hattı incelenmiştir. 1900-2005 yılları arasında Türkiye ve Türkiye'nin yakın sınır komşuları içerisinde, büyüklüğü 5.7 ve 5.7'den büyük 41 deprem göz önüne alındı. Bu çalışmada, Boğaziçi Üniversitesi Kandilli Rasathanesi ve Deprem Araştırma Enstitüsü'nün deprem katalogları kullanılmıştır. California'da ise 1987-2003 yılları arasındaki 5.5 ve daha büyük 9 deprem göz önüne alınmıştır. California Bölgesi için ise, Güney California Deprem Veri Merkezi, Güney California Sismik Ağ Kataloğu, Kuzey California Deprem Veri Merkezi ve Güney California Sismik Ağ Kataloğu'ndan elde edilen veriler kullanılmıştır. Bu çalışmada ayrıca ana depremler, üzerinde gerçekleştikleri fay hatlarına göre gruplanmıştır. Båth Yasasının Türkiyedeki fay zonlarına uygulanamayacağı sonucuna varılmıştır.

TABLE OF CONTENTS

LIST OF FIGURES

LIST OF TABLES

LIST OF SYMBOLS

a	the total seismicity rate of the region
b	the exponent constant
L	The linear extent of the aftershock zone
L_x	Linear extent in the East-West direction
L_y	Linear extent in the North-South direction
M or m	Magnitude of the earthquake
m_{as}^{max}	The magnitude of the largest detected aftershock
m_{ms}	The magnitude of the mainshock
m^*	The magnitude of the largest inferred aftershock
$N(\geq m)$	The cumulative number of earthquakes with magnitudes greater than or equal to m occurring in a specified area and time window
R	The radius of the Earth: taken as 6378 km
Δm	The difference between the mainshock and the largest detected aftershock
Δm^*	The difference between the mainshock and the largest inferred aftershock
$\overline{\Delta m^*}$	The mean of the differences between mainshocks and the inferred aftershocks
$EAFZ$	East Anatolian Fault Zone
$NAFZ$	North Anatolian Fault Zone
$SEAFZ$	South-East Anatolian Fault Zone
$SAFZ$	San Andreas Fault Zone
$U.S.$	United States

1. INTRODUCTION

Earthquakes are extreme and complex phenomena. Earthquakes are among the most powerful events on earth, and their results can be terrifying. A severe earthquake may release energy $10,000$ times as great as that of the first atomic bomb. Rock movements during an earthquake can make rivers change their course. Large earthquakes can create a series of huge, destructive waves called tsunamis that flood coasts for many miles. Earthquakes can trigger landslides that cause serious destruction and loss of life.

Turkey covers one of the most seismically active regions on the earth. The complex plate interaction among Arabia, Eurasia and Africa has created different fault systems in Anatolia and the surrounding region (Figure 1.1). The North Anatolian Fault Zone (NAFZ) and the East Anatolian Fault Zone (EAFZ) are the main strike-slip fault zones in Turkey. Aegean Graben System and Cyprus Arc Zone are the other main fault zones. There were lots of destructive earthquakes in the past and it will occur in the future as well.

It is impossible to know exactly earthquake occurrence time, place and its magnitude. Because of this ambiguity, people are afraid of earthquakes and want to know when this devastating event occurs. Many scientific studies are interested in this subject. Statistical approach is one of these research areas. Aftershocks that are occurring after mainshock are also important, because severe mainshocks have severe aftershocks too. It is very important for people to know aftershock's magnitude as well. There are many statistical studies about aftershocks.

This thesis is about aftershock statistics too. In seismology, the statistical properties of aftershock sequence are associated with three empirical scaling relations. One of these scaling relations is Gutenberg-Richter magnitude-frequency relationship [1]. The

Gutenberg-Richter scaling law is an empirical law, which states that the logarithm of the cumulative frequency $N(\geq m)$ of earthquakes with magnitude larger than m is proportional to the magnitude. The other empirical law is the Omori's law for the temporal decay of aftershocks [2]. Omori stated that aftershock frequency decreases by roughly the reciprocal of time after the mainshock. Båth's law for the magnitude of the largest aftershock is another empirical relation [3]. According to the Båth's law, the magnitude difference between mainshock and the following largest aftershock must be approximately 1.2, regardless of the mainshock magnitude. Båth's law is also important because it gives a prediction of the expected size of the potentially most destructive aftershock that follows a mainshock. A modified version of Båth's law has been proposed by Shcherbakov and Turcotte and is based on an extrapolation of Gutenberg-Richter statistics for aftershocks [4]. In this version of Båth's law, the magnitude of the largest aftershock is inferred from an extrapolation of the Gutenberg-Richter frequency-magnitude statistics of the aftershock sequence of a given mainshock.

In this thesis, we applied the modified version of the Båth's law to the fault zones in and near Turkey, and San Andreas Fault Zone in California. We used the earthquake catalogs that are provided by Boğaziçi University Kandilli Observatory and Earthquake Research Institute [5]. For California region, we used catalogs that are provided by the Southern California Earthquake Center, Southern California Seismic Network catalog [6], and the Northern California Earthquake Data Center, Northern California Seismic Network catalog [7]. We consider 41 earthquakes occuring in and near Turkey between 1900 and 2005 with magnitude equal to or greater than $m_{ms} \geq 5.7$. These 41 earthquakes' aftershock sequences do not overlap since they were separated in time and coordinates. There were approximately 200 earthquakes occuring in and near Turkey between 1900 and 2005 with mainshock magnitude equal to or greater than $m_{ms} \geq 5.7$. The 41 earthquakes were chosen according to two criteria among approximately 200 earthquakes. One of these criteria is that the earthquake must have sufficient number of aftershocks. In our criterion, this number is 5, because otherwise the statistical calculations are not possible. Other

criterion is that the r-square value of the graph of the cumulative number of earthquakes with magnitudes greater than m versus magnitude m must be equal to or greater than 0.95. These 41 earthquakes were chosen by considering these criteria. We used U. S. Geological Survey Earthquake Database to check our data with the other catalogs. We did the same analysis for some earthquakes in Turkey by using U. S. catalog [8]. There are some earthquakes that occur in the Greece in our analysis. We also used catalog provided by Institute of Geodynamics National Observatory of Athens to make same analysis for Greece earthquakes [9].

Finally, we analyzed 9 large earthquakes that occurred in California between 1987 and 2003 with magnitudes equal to or greater than $m_{ms} \geq 5.5$. This analysis was made by Shcherbakov and Turcotte in 2004. We repeated exactly the same process to test our method for finding the aftershock sequence.

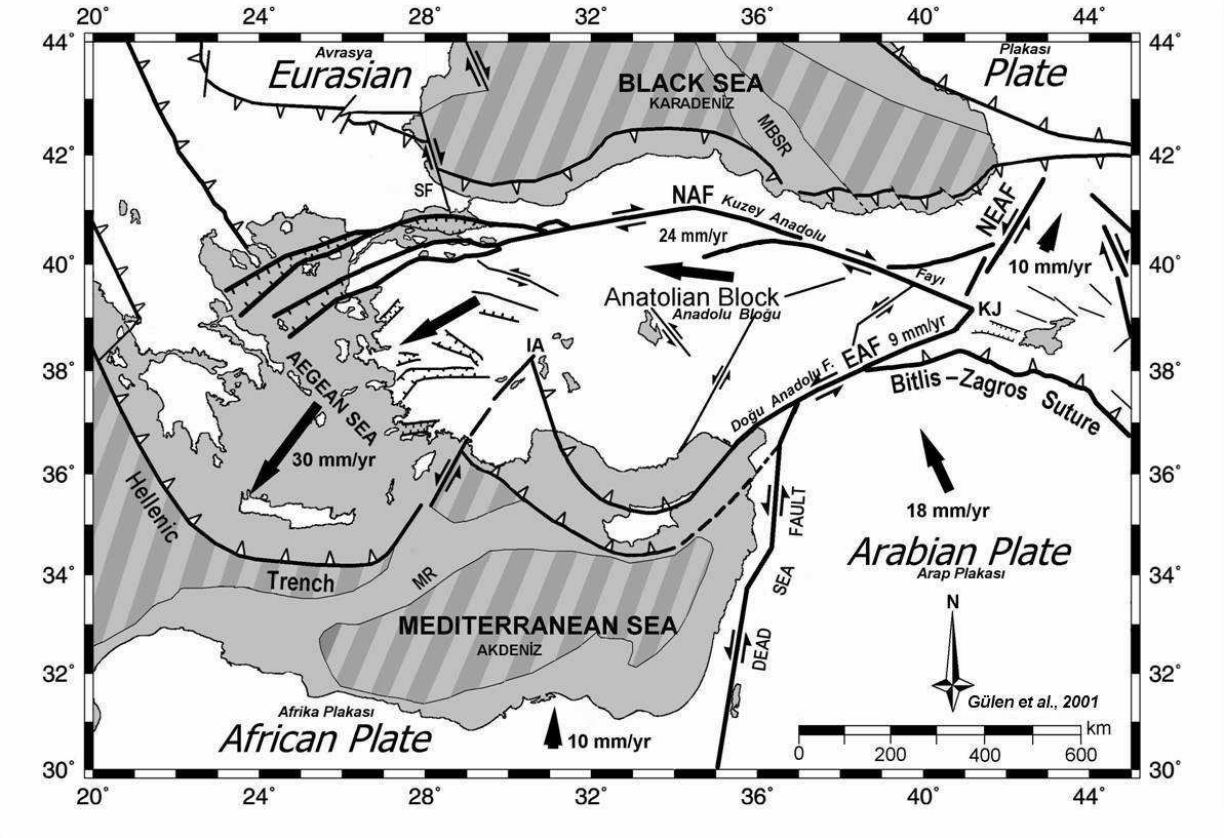

Figure 1.1. Plate interactions of Arabia, Eurasia and Africa [10].

2. THEORY

2.1. Earthquake

An earthquake is the sudden release of strain energy in the Earth's crust resulting in waves of shaking that radiate outwards from the earthquake source [11]. The Earth's crust, that is, the lithosphere consists of rigid blocks or plates of rock in different size in slow but constant motion caused by the convection currents in the mantle they float on. These convection currents, in term, are part of the mechanism of the transfer to the outside of heat in the Earth's mantle and core. That heat is partially left over from the formation of Earth, partially released by the decay of radioactive elements. The moving plates catch their neighbors and stop moving for a time but they are still being pulled or pushed. They flex a little until they finally become unstuck and spring very rapidly past each other up to many meters in only a few seconds. Plate boundaries lock as the plates move past each other, creating frictional stress. When a stress in the crust is more than the strength of the rock, it breaks along lines of weakness, either a pre-existing or new fault plane. The boundary of tectonic plates along which failure occurs is called the fault plane. The point where an earthquake starts is called the focus or hypocenter, the point at the surface directly above the focus is called the earthquake epicenter. Most naturally occurring earthquakes are related to the tectonic nature of the Earth. Such earthquakes are called tectonic earthquakes. The earthquakes in Turkey are generally tectonic earthquakes. Earthquakes are caused mostly by rupture of geological faults, but also by volcanic activity, landslides, mine blasts, and nuclear experiments.

When a rupture of the fault plane causes a big displacement of the Earth's crust, energy is released as a radiation of elastic strain seismic waves. If these resulting seismic waves pass by a point on the earth the ground rapidly moves either up and down or from side to side before returning to its initial position. The earthquakes whose intensity is large

can be felt by animals and people. However the most of earthquakes are so small that can not be noticed by people or animals. They can only be detected by seismographs. The energy that is released during an earthquake radiates from the focus, so that people close to the epicenter will be more likely to feel ground movement than people further away. Since the waves travel between 4-8 kilometers in one second people at different distances from the focus will feel the earthquake at different times.

2.2. Seismic Waves

When an earthquake occurs, it releases energy in the form of seismic waves that radiate from the earthquake focus in all directions. They are the energy that travels through the earth and is recorded on seismographs. The different types of energy waves shake the ground in different ways and also travel through the earth at different velocities. Because of the wave action of an earthquake, earthquakes can also be felt a long distance from the fault plane. As waves radiate outward from their source, they weaken. The character of wave can be changed by the medium that it travels through. For example, sandy soils increase the damage of an earthquake. There are different kinds of seismic waves, and they all move in different ways. The two main types of waves are body waves and surface waves. Earthquakes radiate seismic energy as both body and surface waves.

2.2.1. Body Waves

Body waves travel through the interior of the Earth. Body waves arrive before the surface waves emitted by an earthquake. These waves are of a higher frequency than surface waves. There are two kinds of body waves: primary waves and secondary waves.

2.2.1.1. P-Waves. P waves which are also named primary waves are longitudinal or compressional waves. P waves compress and dilate the ground in the direction of propagation.

They do not change the structure of the material. P waves are actually sound waves and can propagate through all layers of the earth. They travel through any type of material, solids, liquids or gases. They are the fastest waves and, as a result of this they arrive first at a seismic station. In solids, they travel almost twice as fast as S waves. In air, these waves take the form of sound waves; hence they travel at the speed of sound. Typical speeds are 330 m/s in air, 1450 m/s in water and about 5000 m/s in granite. Because of their smaller amplitude, P waves are less destructive than the S waves and surface waves that follow them. The velocity of a wave depends on the elastic properties and density of the material. If we let κ represent the bulk modulus of a material, μ the shear-modulus, and ρ the density, then the P-wave velocity, which we represent by α, is given by:

$$\alpha = \sqrt{\frac{\kappa + \frac{4}{3}\mu}{\rho}} \tag{2.1}$$

2.2.1.2. S-Waves. S waves which are also named secondary waves are transverse or shear waves. S waves' motion is perpendicular to the direction of propagation. Its name, secondary, comes from the fact that it is the second arrival on a seismic station. An S wave is slower than a P wave and can only travel through solid rock, not through any liquid medium since μ=0 in a fluid. S waves move rock particles up and down, or side-to-side perpendicular to the direction of wave propagation. Their speed is about 60% of that of P waves in a given material. S waves are several times larger in amplitude than P waves for earthquake sources. The S-wave speed β depends on μ represent shear modulus and ρ the density, and is given by:

$$\beta = \sqrt{\frac{\mu}{\rho}} \tag{2.2}$$

P waves move faster than the S waves, so far away from the focus difference of the arrival times of the two wave's increases. Distance to the epicenter can be found from this difference.

2.2.2. Surface Waves

Surface waves can only travel just under the Earth's surface and they are like water waves. They travel more slowly than body waves. Because of their low frequency, long duration, and large amplitude, they can be the most destructive type of seismic wave. There are three types of surface waves: Rayleigh waves, Love waves and Lg waves.

2.2.2.1. Rayleigh Waves. The Rayleigh wave is named after John William Strutt, Lord Rayleigh, who mathematically predicted the existence of this kind of wave in 1885. As it passes, a surface particle moves in a circle or ellipse in the direction of propagation. A Rayleigh wave rolls along the ground just like a water wave rolls across a lake or an ocean. They shake the ground much more than the other waves, so they are felt most from an earthquake. They are slower than body waves, roughly 70% of the velocity of S waves. Rayleigh waves travel along the surface of the earth at about 10 times the speed of sound in air. The particular speed at which they travel depends on the wave period and the geologic structure near the surface .

2.2.2.2. Love Waves. The Love wave is named after A.E.H. Love, a British mathematician who worked out the mathematical model for this kind of wave in 1911. Love waves are

surface waves that cause horizontal shearing of the ground during an earthquake. It is the fastest surface wave and moves the ground from side to side. Love waves produce entirely horizontal motion. They usually travel slightly faster than Rayleigh waves, about 90% of the S wave velocity. The speed at which a Love wave travels depends on the wave's period.

2.2.2.3. Lg Waves. Lg wave is a surface wave which travels through the continental crust with almost no dispersion. The regional phase Lg is a characteristics feature of high-frequency seismograms recorded in continental regions. It is observed at epicentral distances ranging from 150 km up to several thousand kilometers. The Lg-wave group is not a pure continental Love wave but rather a complex guided crustal wave. It is caused by superposition of multiple S-wave reverberations between the surface and the Moho and SV to P and/or P to SV conversions as well as by scattering of these waves at lateral heterogeneities in the crust.

2.3. Fault Types

2.3.1. Dip-Slip Faults

Dip-slip faults are faults on which the movement is parallel to the dip of the fault surface.

2.3.1.1. Normal Fault. In a normal fault, the block above the fault moves down relative to the block below the fault. This fault motion is caused by tensional forces (Figure 2.1a).

A downthrown block between two normal faults dipping towards each other is called a graben. An upthrown block between two normal faults dipping away from each other is called a horst. In Turkey Aegean Graben system consists of several grabens and horsts (Figure 2.1b). Where the dip of a normal fault's surface is very gentle or almost flat, it is

referred to as a detachment fault or low-angle normal fault. Detachment faults are common in the desert areas of California (Figure 2.1c).

2.3.1.2. Reverse Fault. In a reverse fault, the block above the fault moves up relative to the block below the fault. This fault motion is caused by compression forces that push rocks together and results in shortening. The Sierra Madre fault zone of southern California is an example of reverse-fault movement (Figure 2.1d). A thrust fault has the same sense of motion as a reverse fault, but with the dip of the fault plane at less than 45°. Thrust faults are very common in the Klamath Mountains of northern California (Figure 2.1e). South East Anatolian fault zone is a thrust fault.

2.3.2. Strike-Slip Fault

In a strike-slip fault, the movement of blocks along a fault is horizontal. The movement along a strike-slip fault is approximately parallel to the strike of the fault, meaning the rocks move past each other horizontally. If the block on the far side of the fault moves to the left, the fault is called left-lateral. If the block on the far side moves to the right, the fault is called right-lateral. The fault motion of a strike-slip fault is caused by shearing forces (Figure 2.1f). North Anatolian fault zone is a right-lateral and East Anatolian fault zone is a left-lateral strike-slip fault. The San Andreas fault zone is also a strike-slip fault that has displaced rocks hundreds of miles.

2.3.3. Oblique-Slip Fault

Oblique-slip fault has a component of both dip-slip fault and strike-slip fault. It is caused by a combination of shearing and tension of compression forces (Figure 2.1g).

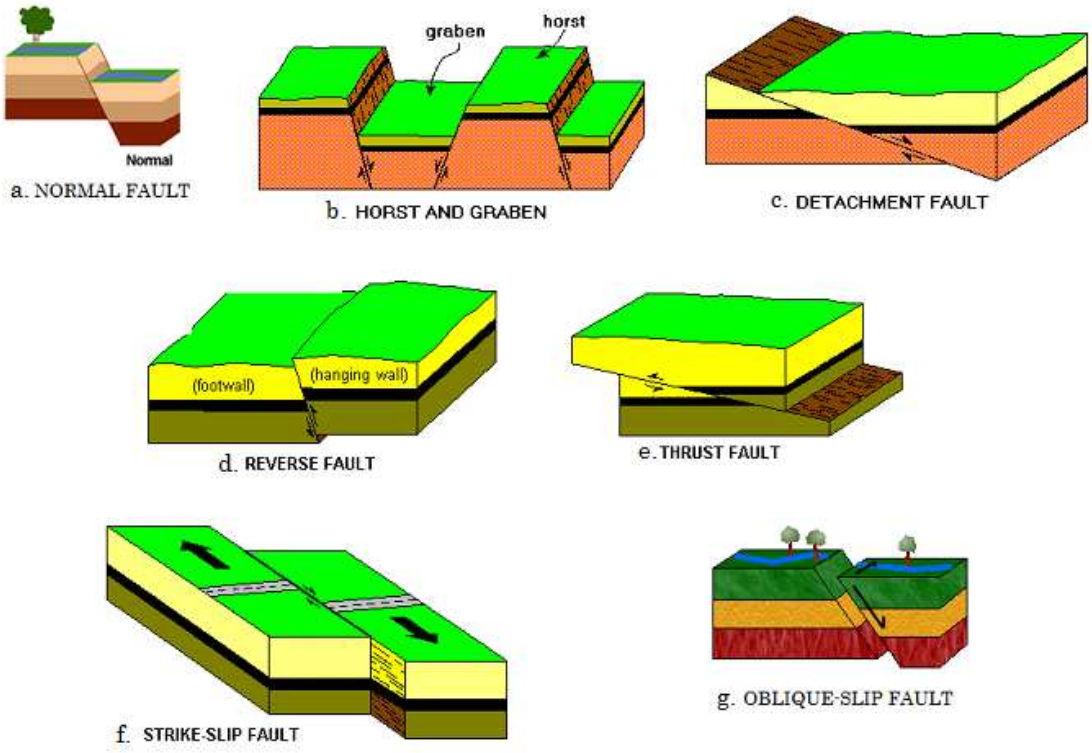

Figure 2.1. Fault Types

2.4. Magnitude

Earthquake size is expressed by its magnitude. Charles Richter introduced the earthquake magnitude in the 1930's. They defined the magnitude of earthquake in terms of the amplitude of ground velocity and distance from seismograph to the earthquake. This magnitude scale was referred to as M_L. As the number of seismograph stations increase around the world, it is understood that Richter's method is valid only for certain frequency and distance ranges. Then, new magnitude scales that are an extension of Richter's original magnitude scale were developed. These are body-wave magnitude m_b, surface-wave magnitude m_s and duration magnitude m_d. In recent years, seismologists have developed a new scale called moment magnitude m_w. In principle, all methods provide the similar value but calculation of these methods differs and this sometimes results in difference in

magnitudes.

2.4.1. M_L Richter Magnitude (Local Magnitude)

The Richter magnitude of an earthquake is determined from the logarithm of the amplitude of waves recorded by seismographs. The Richter magnitude scale assigns a single number to quantify the amount of seismic energy released by an earthquake. A difference in magnitude of 1.0 is equivalent to a factor of 31.6 in the energy released; a difference of magnitude of 2.0 is equivalent to a factor of 1000 in the energy released.

$$M_L = \log_{10} A(mm) + B \tag{2.3}$$

A: is the amplitude, in millimeters.
B: is distance correction factor.

2.4.2. m_b Body Wave Magnitude

The body-wave magnitude m_b is usually used for earthquakes that occurred more than about 2000 kilometers away from the station. It can be computed relatively fast, because its value relies on the amplitude of the P waves of an earthquake. For the earthquakes whose magnitude is larger than 6, m_b value saturates, meaning that although the actual size of the earthquake increase, the value of m_b does not increase any more. In such cases, seismologists have to rely on other magnitude types. The standard body-wave magnitude formula is

$$m_b = \log_{10}(A/T) + Q(D, h) \tag{2.4}$$

A: the amplitude of the ground motion (in microns)

T: the corresponding period (in seconds)

$Q(D, h)$: correction factor

D: distance between epicenter and station (in geocentric degrees)

h: focal depth (in kilometers)

2.4.3. m_s Surface Wave Magnitude

The surface wave magnitude is measured from surface waves. As a result of this, it can not be computed as fast as body wave magnitude m_b. It may take up to 1 or 2 hours until surface waves arrive depending on the distance, while body waves arrive at most in 20 minutes. Saturation of the surface wave magnitude starts only at magnitudes larger than 8. A high m_s value compared to the m_b value thus indicates that strong damage might have occurred. The standard surface-wave magnitude formula is

$$m_s = \log_{10}(A/T) + 1.66 \log_{10}(D) + 3.30 \tag{2.5}$$

2.4.4. m_w Moment Magnitude

The moment magnitude m_w is based on a physical quantity, called moment. Quantitative measure of the size and strength of a seismic shear source is the scalar seismic moment M_o (for its derivation see (2.6)):

$$M_o = \mu D A \tag{2.6}$$

with μ - rigidity or shear modulus of the medium, D - average final displacement after the rupture, A - the surface area of the rupture. M_o is a measure of the irreversible inelastic deformation in the rupture area.

The seismic moment is related to the final static displacement after an earthquake and consequently, the moment magnitude, m_w, is more closely related to the tectonic effects of an earthquake. Seismic moment magnitude developed by Kanamori (1977). It is tied to M_s but does not saturate for big events because it is based on seismic moment M_o, which is made from the measurement of the (constant) level of low-frequency spectral displacement amplitudes for f $\ll f_c$. This level increases linearly with M_o. M_o is proportional to the average static displacement and the area of the fault rupture and is so a good measure of the total deformation in the source region.

Moment magnitude has advantages over other magnitude scales. It does not saturate, allowing us to measure the largest earthquakes. It can be determined by instrumentally or from geology, so we can measure the size of old earthquakes and compare them to instrumentally recorded data. The procedures are more time consuming than other magnitude scales and m_w for larger earthquake can be found in several hours after an earthquake.

$$m_w = \frac{2}{3}\log_{10}(M_o) - 10.7 \tag{2.7}$$

2.4.5. m_d Duration Magnitude

The duration magnitude based on the duration of shaking as measured by the time decay of the amplitude of the seismogram. Applicable magnitude range is less than 4 magnitude and distance range is from 0 to 400 km.

2.5. Aftershocks

In an earthquake cluster, the one with the largest magnitude is called the mainshock; anything before the mainshock is a foreshock and anything after the mainshock is an aftershock. Aftershocks are a result of a readjustment of the crust around a major fault

movement. Aftershocks usually occur near the fault where the mainshock takes place. The stress on the mainshock's fault changes drastically during the mainshock and that fault produces most of the aftershocks. Sometimes the change in stress caused by the main shock is so great that it is enough to trigger aftershocks on other, nearby faults, and for a very large mainshock sometimes even farther away. Aftershocks usually occur within a few days of the mainshock, becoming less and less serious over time. The rate of aftershocks decreases quickly. The decrease is proportional to the inverse of time since the mainshock. Thus, an aftershock can occur weeks or decades after a mainshock. Bigger earthquakes have more and larger aftershocks. The bigger the main shock the bigger the largest aftershock will be, on average. The difference in magnitude between the mainshock and the largest aftershock ranges from 0.1 to 3 or more, but averages 1.2. There are more small aftershocks than large ones. In seismology, the statistical properties of aftershock sequence are associated with three empirical relations.

2.5.1. Gutenberg Richter Frequency Magnitude Law

Aftershocks satisfy Gutenberg-Richter frequency-magnitude scaling just as all earthquakes do. In seismology, the Gutenberg-Richter law expresses the relationship between the magnitude and total number of earthquake in any given region and time period [1]. That is

$$\log_{10} N(\geq m) = a - bm \tag{2.8}$$

where N($\geq m$) is the cumulative number of earthquakes with magnitude larger than m, m is the magnitude range, a and b are constant. The b value changes from region to region, but is generally in the range of $0.8 < b < 1.2$. The a value simply indicates the total seismicity rate of the region. The relationship is surprisingly strong and does not vary significantly from region to region or over time.

2.5.2. Omori's Law

Omori's law is an empirical relation for the temporal decay of aftershock rates [2]. Omori stated that aftershock frequency decreases by roughly the reciprocal of time after the main shock, in 1894.

$$n(t) = \frac{K}{c+t} \tag{2.9}$$

where:
$n(t)$ is the number of earthquakes n measured in a certain time t
K is the amplitude; and
c is the "time offset" parameter, it is almost always found to be positive and typically ranges from 0.5 to 20 hr in empirical studies.
Then Utsu proposed the modified version of the Omori's law that now commonly used in 1961.

$$n(t) = \frac{K}{(c+t)^p} \tag{2.10}$$

where p modifies the decay rate and typically in the range 0.7 - 1.5.

Omori's equation and its modified form explain us that the rate of aftershocks decreases quickly with time. The rate of aftershocks is proportional to the inverse of time since the mainshock. Thus if p is equal to 1, the number of aftershocks that occur on the second day is half of the number of aftershocks that occur on the first day and the number of aftershocks that occur on the tenth day is 1/10th of the number of aftershocks that occur on the first day. These patterns describe only the mass behavior of aftershocks; the actual times, numbers and locations of the aftershocks are random.

2.5.3. Båth's Law

The other main empirical law describing aftershocks is known as Båth's Law and this says that the difference between a mainshock magnitude and the largest aftershock magnitude is 1.2, independent of the mainshock magnitude [3]. That is

$$\Delta m = m_{ms} - m_{as}^{max} \tag{2.11}$$

Where m_{ms} is the mainshock magnitude, m_{as}^{max} is the largest aftershock and Δm is approximately constant which is 1.2. Aftershock sequences also follow Guttenberg-Richter scaling.

2.5.4. Modified Form of Båth's Law

A number of studies about the statistical variability of Δm have been carried out. Despite some progress in understanding the nature of Båth's law, its validity still remains an open question. Vere-Jones offered a statistical interpretation, which states that events in an aftershock sequence are drawn from the negative exponential distribution and are distributed independently of each other [12]. He showed that the distribution of the difference between the first and second largest event is the same negative exponential distribution. Using this result he obtained the value of $\Delta m = \frac{1}{b} ln10$. Recently, Helmstetter and Sornette pointed out that the selection process of aftershock sequence plays a significant role in calculating the Δm [13]. They argue that this difference is also controlled by the aftershock productivity.

A modified form of Båth's law has been proposed by Shcherbakov and Turcotte and says that the largest aftershock is inferred from an extrapolation of the Gutenberg-Richter frequency- magnitude statistics for a given mainshock-aftershock sequence [4][14]. It also assumes that the difference between the mainshock magnitude and inferred largest

aftershock magnitude is approximately constant.

Aftershock sequences also satisfy the Gutenberg-Richter scaling. In this case $N(\geq m)$ is the cumulative number of the aftershocks with magnitudes greater than m. Magnitude of inferred largest aftershock is found by taking $N(\geq m^*) = 1$. Substituting it into the GR equation, we obtain

$$a = bm^* \tag{2.12}$$

The inferred values of largest aftershock m^* is also satisfy Båth's law, and then we can write

$$\Delta m^* = m_{ms} - m^* \tag{2.13}$$

where m_{ms} is the mainshock magnitude, Δm^* is approximately constant. If we substitute equations (2.12) and (2.13) into equation (2.8), we get

$$\log_{10}[N(\geq m)] = b(m_{ms} - \Delta m^* - m) \tag{2.14}$$

which is the frequency-magnitude relation of aftershock sequence. Equation (2.14) is the modified form of Båth's law. In this approach, we get the inferred largest aftershock magnitude by analyzing many aftershocks instead of looking one largest aftershock.

3. THE APPLICATION OF THE MODIFIED FORM OF BÅTH'S LAW

3.1. The Application of The Modified Form of Båth's Law to Turkey

We applied the modified form of Båths law to fault zones in Turkey by considering 41 earthquakes that occurred between 1900 and 2005 with magnitude equal to or greater than $m_{ms} \geq 5.7$. Locations of these earthquakes are shown in Figure 3.1. These 41 earthquakes aftershock sequences do not overlap since they were separated in time and coordinates. We used the earthquake catalog that is provided by Boğaziçi University Kandilli Observatory and Earthquake Research Institute [5]. In this catalog, there are all earthquakes occuring in and near Turkey between 1900 and 2007. It contains the information about the earthquakes such as date, latitude, longitude, magnitude and depth. We were not interested in depth parameter of an earthquake because we did not use depth values in our calculations. There are more than one type of magnitude values in this catalog, including local, body-wave, surface-wave, duration and moment magnitude. In general, for magnitudes between 2.0 and 4.0 we used m_d duration magnitude, for magnitudes between 4.0 and 6.0 we used M_L local magnitude, for magnitudes between 6.0 and 7.0 we used m_s surface-wave or m_w moment magnitude, for magnitudes greater than 7.0 we used m_w moment magnitude. We used latitude and longitude values in determining the aftershocks of the mainshock.

There are approximately 200 earthquakes in the catalog which occurred between 1900 and 2005 with magnitude equal to or greater than $m_{ms} \geq 5.7$. We took 41 of them according to some criteria. Dates and mainshock magnitudes of earthquakes are given in Table 3.1 and 3.2. We did not take the earthquakes whose number of aftershocks is less than 5, because it has no statistical meaning. Then we plotted the graph of the cumulative number of aftershocks with magnitudes greater than m versus magnitude m. We eliminated

the earthquakes whose graphs r-square value is less than 0.95.

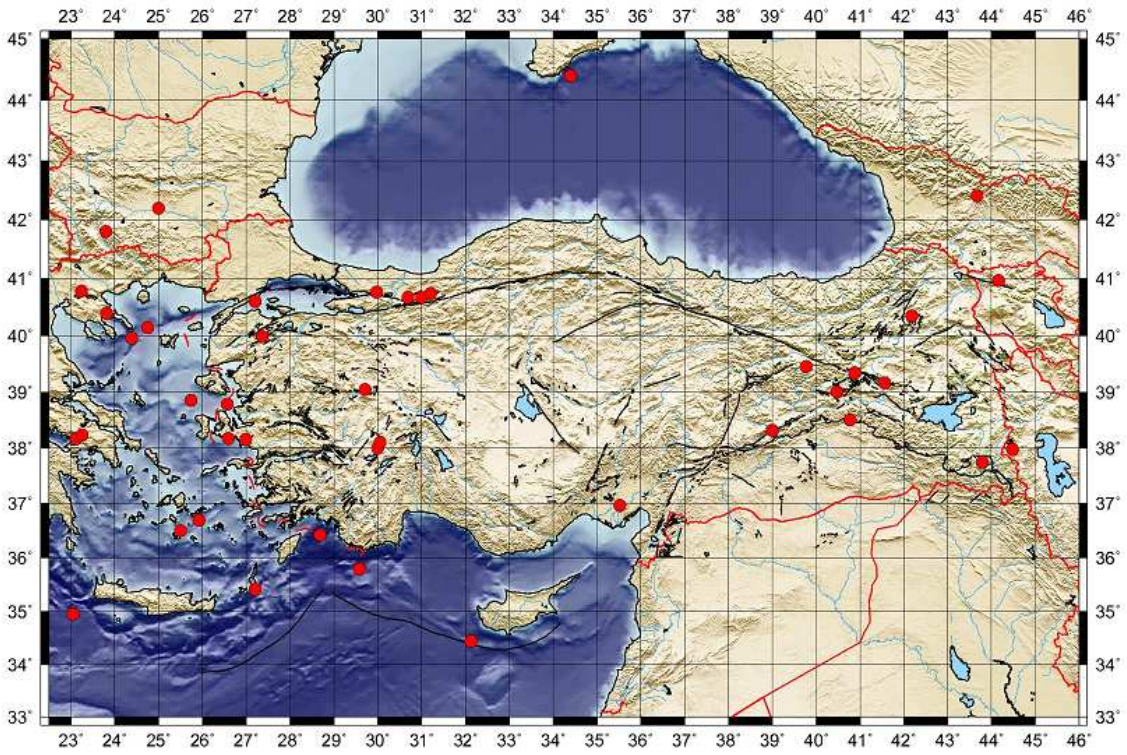

Figure 3.1. Map of earthquake locations [5].

Table 3.1. Dates and mainshock magnitudes of earthquakes.

Earthquake	**Date**	m_{ms}
Bulgaria	04-Apr-1904 10:25:00	7.8
Mürefte-Şarköy	09-Aug-1912 01:29:00	7.3
Burdur	03-Oct-1914 22:07:00	6.9
Aegean-12 Islands	25-Oct-1919 17:10:00	5.9
Ukraine-Crimea	26-Jun-1927 11:20:00	6.0
Plovdiv	18-Apr-1928 19:22:00	7.0
Turkey-Iran Border	06-May-1930 22:34:00	7.6
Gomati	26-Sep-1932 19:20:00	7.1
Karpathos-12 Islands	09-Feb-1948 12:58:00	7.1
Yenice-Gönen	18-Mar-1953 19:06:00	7.2
Aegean Sea	09-Jul-1956 03:11:00	7.4
Fethiye-Rodos	25-Apr-1957 02:25:00	7.1
Bolu-Abant	26-May-1957 06:33:00	7.1
Muş-Varto	19-Aug-1966 12:22:00	6.9
Adapazarı-Mudurnusuyu Valley	22-Jul-1967 16:56:00	7.2
Kütahya-Çavdarhisar	25-May-1971 05:43:00	5.7
Diyarbakır-Lice	06-Sep-1975 09:20:00	7.8
Mediterranean Sea-Crete Island	11-Sep-1977 23:19:00	5.8
Thessaloniki	20-Jun-1978 20:03:00	6.1
Karaburun-İzmir	14-Jun-1979 11:44:00	5.9
Greece-Athens	25-Feb-1981 02:35:00	5.7

To identify aftershocks of earthquakes, we defined space and time windows for each sequence. In each case we considered a square area centered on the mainshock epicenter.

Table 3.2. Continuation of Table 3.1.

Earthquake	**Date**	m_{ms}
Greece-Athens-2	04-Mar-1981 21:58:00	5.8
Greece-Mount Athos	18-Jan-1982 19:27:00	5.8
North Aegean Sea	06-Aug-1983 15:43:00	6.0
Narman-Erzurum	30-Oct-1983 04:12:00	6.0
Armenia-Spitak	07-Dec-1988 07:41:00	6.0
Racha	29-Apr-1991 09:12:00	6.2
Doğanbey-İzmir	06-Nov-1992 19:08:00	5.7
Afyon-Dinar	01-Oct-1995 15:57:00	6.0
Cyprus	09-Oct-1996 13:10:00	6.8
Middle Aegean Sea	14-Nov-1997 21:38:00	5.8
Adana-Ceyhan	27-Jun-1998 13:55:00	6.3
Kocaeli-Gölcük	17-Aug-1999 00:01:00	7.4
Düzce	12-Nov-1999 16:57:00	7.2
Pülümür-Tunceli	27-Jan-2003 05:26:22	6.2
Bingöl	01-May-2003 00:27:00	6.4
Pötürge-Malatya	13-Jul-2003 01:48:20	5.7
Kaş-Antalya	23-Jan-2005 22:36:05	5.8
Karlıova-Bingöl	25-Jan-2005 16:44:09	5.8
Karlıova-Bingöl2	14-Mar-2005 01:55:00	5.9
Sığacık-Seferihisar	20-Oct-2005 21:40:01	5.9

The linear size of the box L is given by Yan Y. Kagan [15] as

$$L = 0.02 \times 10^{(0.5 m_{ms})} \text{ km} \tag{3.1}$$

For example Bolu-Abant earthquakes mainshock magnitude is 7.1, latitude degree 40.67N and longitude degree is 31E. From equation L linear size of the square is 70.96 km. Then we transform this value into degrees. First, we need the half of L value. We find

$$35.48/6378 = 5.5629 \times 10^{-3} \text{ radian} \tag{3.2}$$

We take the Earths radius 6378 km. By multiplying with $180/\pi$, we convert this value to degrees. Finally, we find the $L_y = 0.32$ which is the linear extent in North-South direction. To find the L_x value, we take cosine of the latitude degree.

$$L_x = \frac{35.48}{6378} \cos 40.67 \text{ radian} \tag{3.3}$$

By multiplying with $180/\pi$, we convert this value to degree. Finally we find the $L_x = 0.42$ which is the linear extent in East-West direction. We made this calculation for all 41 earthquakes individually. The results are given in Table 3.3 and 3.4.

Time intervals of 92, 183, 365, 730 and 1095 days are taken except for the Kaş-Antalya, Karlıova-Bingöl, Karlıova-Bingöl2 and Sığacık-Seferihisar earthquakes where we did not use 1095 days because the data were not available. We used Matlab 7.1 to find aftershocks of mainshocks. Necessary codes are in the Appendix A. After defining what is and what is not an aftershock, we plot the graph of the cumulative number of earthquakes with magnitudes greater than m versus magnitude m. We draw these figures with Sigma Plot version 9.0. Then we found the possible best fits to the data. From the graph of the cumulative number of earthquakes with magnitudes greater than m versus magnitude m, we found a and b values using Sigma Plot version 9.0. Our b values are in the range $0.28 < b < 1.47$ and a values are in the range $1.90 < a < 6.69$.

The Bulgaria earthquake with mainshock magnitude $m_{ms} = 7.8$ had the largest detected aftershock of magnitude ${m_{as}}^{max}$= 5.9. From equation (2.11) the magnitude differ-

Table 3.3. Latitude, Longitude, L(km), L_y and L_x values of each earthquake

Earthquake	Latitude(N)	Longitude(E)	L (km)	L_y	L_x
Bulgaria-Strouma	41.8	23.8	158.87	0.71	0.96
Mürefte-Şarköy	40.6	27.2	89.34	0.40	0.53
Burdur	38	30	56.37	0.25	0.32
Aegean-12 Islands	36.5	25.5	17.83	0.08	0.10
Ukraine-Crimea	44.4	34.4	20.00	0.09	0.13
Plovdiv	42.2	25	63.25	0.28	0.38
Turkey-Iran Border	37.98	44.48	126.19	0.57	0.72
Gomati	40.39	23.81	70.96	0.32	0.42
Karpathos-12 Islands	35.41	27.2	70.96	0.32	0.39
Yenice-Gönen	39.99	27.36	79.62	0.36	0.47
Aegean Sea	36.69	25.92	100.24	0.45	0.56
Fethiye-Rodos	36.42	28.68	70.96	0.32	0.40
Bolu-Abant	40.67	31	70.96	0.32	0.42
Muş-Varto	39.17	41.56	56.37	0.25	0.33
Adapazarı-Mudurnusuyu Valley	40.67	30.69	79.62	0.36	0.47
Kütahya-Çavdarhisar	39.05	29.71	14.16	0.06	0.08
Diyarbakır-Lice	38.51	40.77	158.87	0.71	0.91
Mediterranean Sea-Crete Island	34.95	23.05	15.89	0.07	0.09
Thessaloniki	40.78	23.24	22.44	0.10	0.13
Karaburun-İzmir	38.79	26.57	17.83	0.08	0.10

ence between the mainshock and the largest aftershock is Δm=1.9. We found b = 0.45 $\pm$0.03 and a = 3.26 $\pm$0.13 from correlation of the aftershock frequency magnitude data given in Figure 3.2 with G-R scaling. From equation (2.12) the inferred magnitude of the largest aftershock is $m^* = 7.32 \pm 0.54$. From equation (2.13) the magnitude difference

Table 3.4. Continuation of Table 3.3.

Earthquake	Latitude (N)	Longitude (E)	L (km)	L_y	L_x
Greece-Athens	38.17	23.12	14.16	0.06	0.08
Greece-Athens-2	38.24	23.26	15.89	0.07	0.09
Greece-Mount Athos	39.96	24.39	15.89	0.07	0.09
North Aegean Sea	40.14	24.75	20.00	0.09	0.12
Narman-Erzurum	40.35	42.18	20.00	0.09	0.12
Armenia-Spitak	40.96	44.16	20.00	0.09	0.12
Racha	42.41	43.67	25.18	0.11	0.15
Doğanbey-İzmir	38.16	26.99	14.16	0.06	0.08
Afyon-Dinar	38.11	30.05	20.00	0.09	0.11
Cyprus	34.44	32.13	50.24	0.23	0.27
Middle Aegean Sea	38.86	25.74	15.89	0.07	0.09
Adana-Ceyhan	36.96	35.52	28.25	0.13	0.16
Kocaeli-Gölcük	40.76	29.97	100.24	0.45	0.59
Düzce	40.74	31.21	79.62	0.36	0.47
Pülümür-Tunceli	39.46	39.77	25.18	0.11	0.15
Bingöl	39.01	40.47	31.70	0.14	0.18
Pötürge-Malatya	38.32	39	14.16	0.06	0.08
Kaş-Antalya	35.79	29.58	15.89	0.07	0.09
Karlıova-Bingöl	37.75	43.79	15.89	0.07	0.09
Karlıova-Bingöl2	39.35	40.88	17.83	0.08	0.10
Sığacık-Seferihisar	38.18	26.59	17.83	0.08	0.10

between the mainshock and the inferred largest aftershock is $\Delta m^* = 0.48 \pm 0.54$. The Bulgaria earthquake belongs to graben fault system.

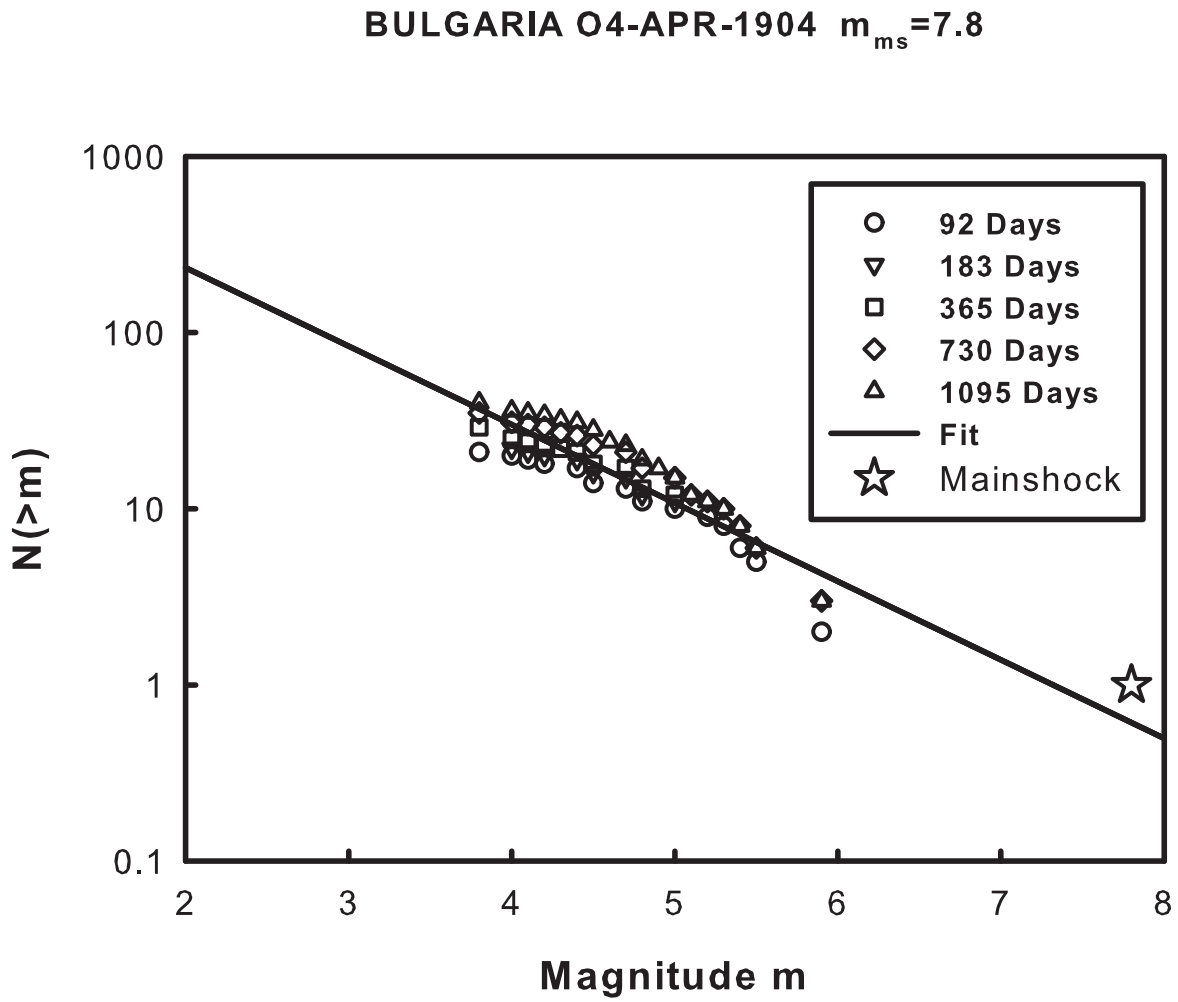

Figure 3.2. Frequency-magnitude distribution of Bulgaria earthquake

The Mürefte-Şarköy earthquake with mainshock magnitude $m_{ms} = 7.3$ had the largest detected aftershock of magnitude ${m_{as}}^{max}$=6.3. From equation (2.11) the magnitude difference between the mainshock and the largest aftershock is Δm=1.0. We found b = 0.28 $\pm$0.03 and a =2.05 $\pm$ 0.16 from correlation of the aftershock frequency magnitude data given in Figure 3.3 with G-R scaling. From equation (2.12) the inferred magnitude of the largest aftershock is $m^* = 7.22 \pm 0.96$. From equation (2.13) the magnitude difference between the mainshock and the inferred largest aftershock is $\Delta m^* = 0.08 \pm 0.96$. The Mürefte-Şarköy earthquake belongs to North Anatolian Fault Zone.

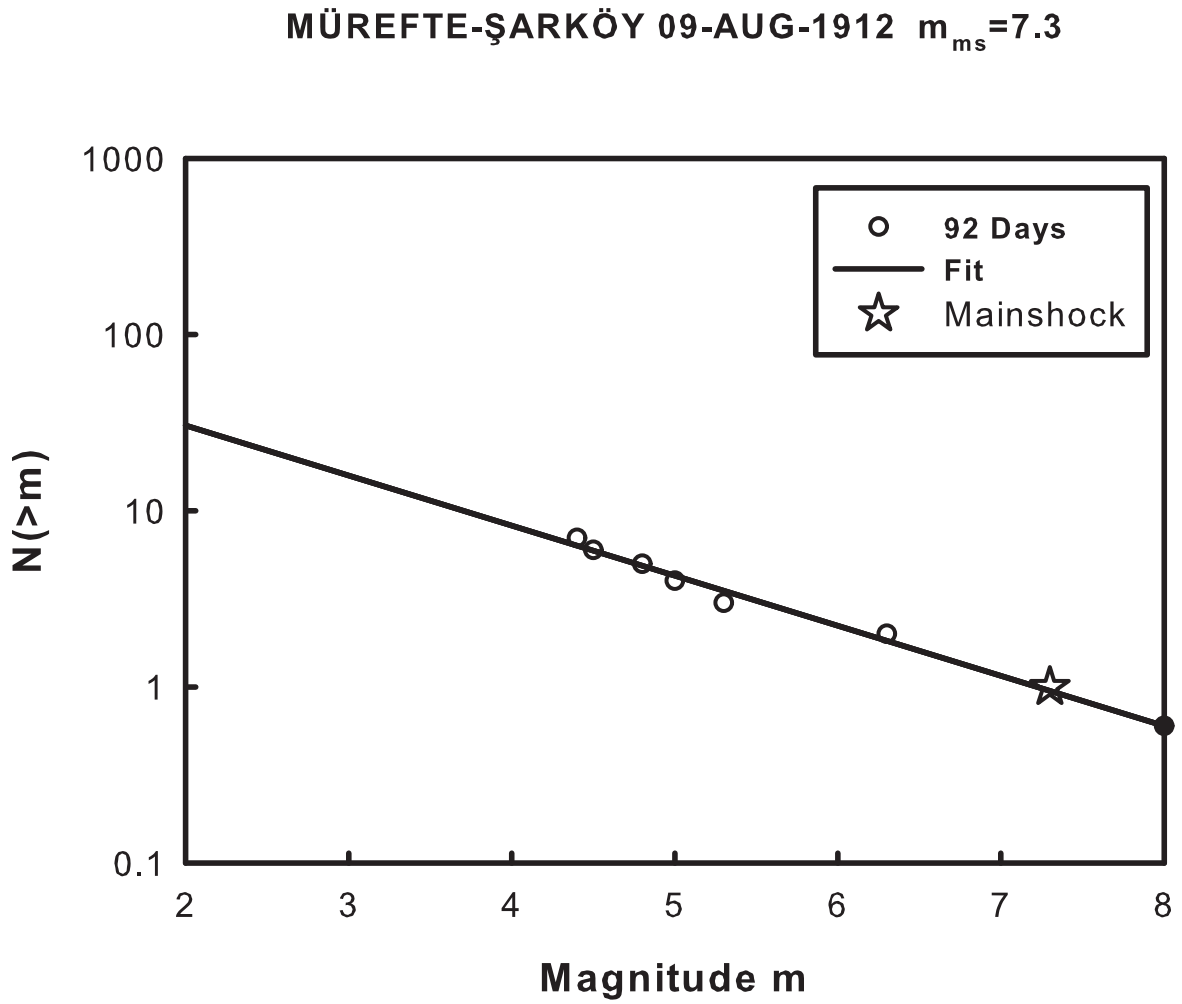

Figure 3.3. Frequency-magnitude distribution of Mürefte-Şarköy earthquake

The Burdur earthquake with mainshock magnitude m_{ms} = 6.9 had the largest detected aftershock of magnitude ${m_{as}}^{max}$= 5.2. From equation (2.11) the magnitude difference between the mainshock and the largest aftershock is Δm=1.7. We found b = 1.19 ±0.07 and a = 6.53 ±0.32 from correlation of the aftershock frequency magnitude data given in Figure 3.4 with G-R scaling. From equation (2.12) the inferred magnitude of the largest aftershock is m^* = 5.49 ±0.40. From equation (2.13) the magnitude difference between the mainshock and the inferred largest aftershock is $\Delta m^* = 1.41 \pm 0.40$. The Burdur earthquake belongs to graben fault system.

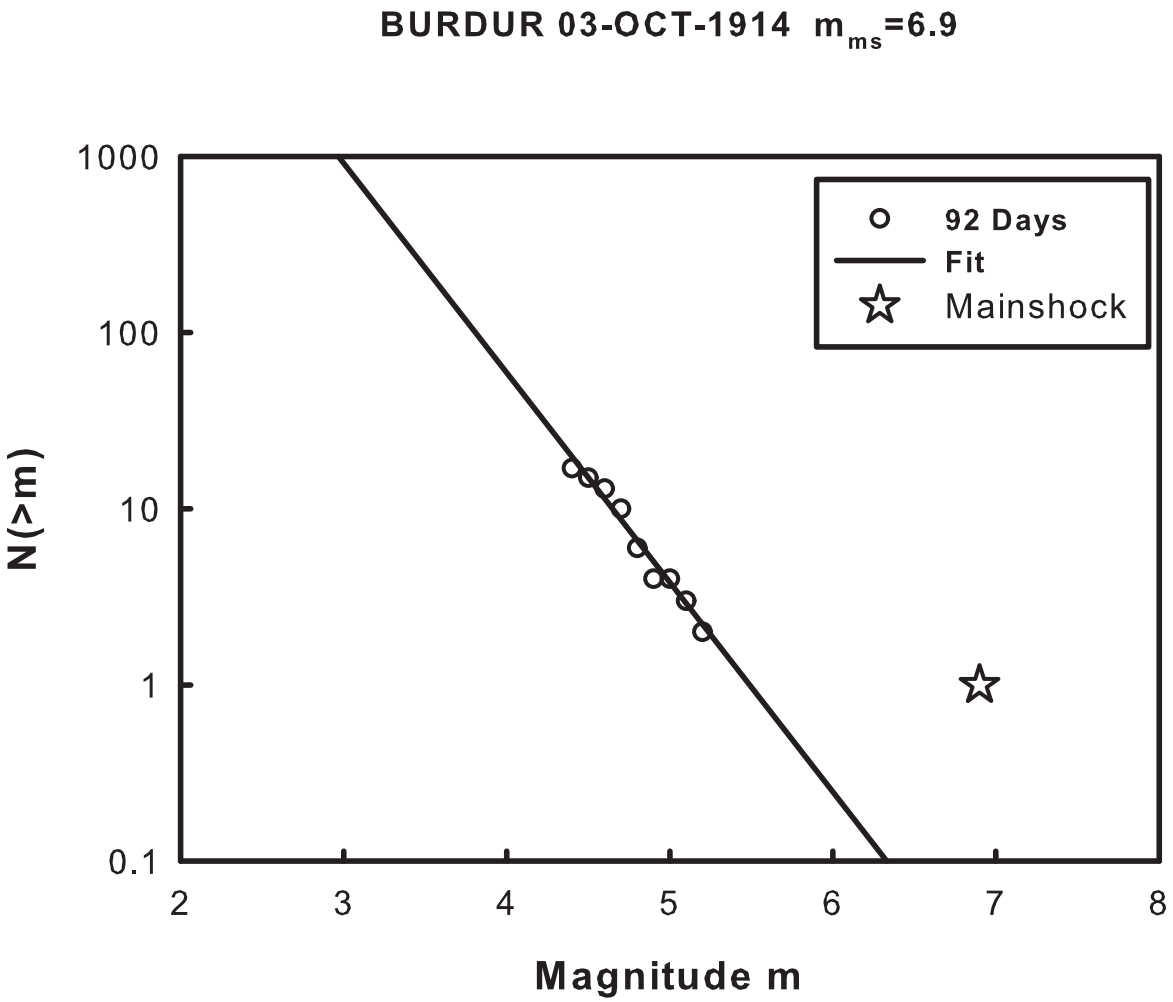

Figure 3.4. Frequency-magnitude distribution of Burdur earthquake

The Aegean-12 Islands earthquake with mainshock magnitude m_{ms} = 5.9 had the largest detected aftershock of magnitude ${m_{as}}^{max}$= 5.5. From equation (2.11) the magnitude difference between the mainshock and the largest aftershock is Δm= 0.4. We found b = 0.68 ±0.06 and a =3.98 ± 0.29 from correlation of the aftershock frequency magnitude data given in Figure 3.5 with G-R scaling. From equation (2.12) the inferred magnitude of the largest aftershock is m^* = 5.83 ±0.68. From equation (2.13) the magnitude difference between the mainshock and the inferred largest aftershock is Δm^* = 0.07 ± 0.68. The Aegean-12 Islands earthquake belongs to Cyprus Arc zone.

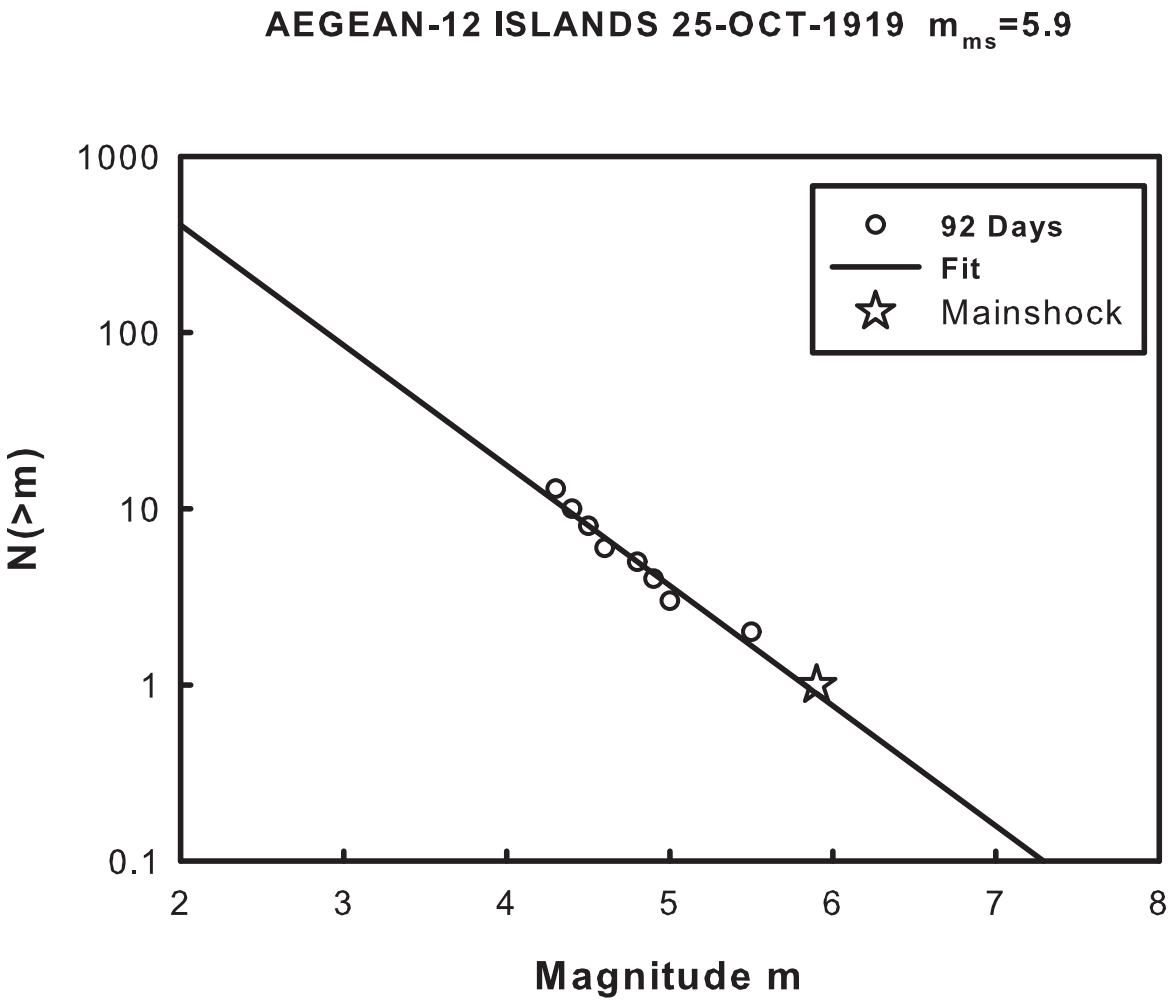

Figure 3.5. Frequency-magnitude distribution of Aegean-12 Islands earthquake

The Ukraine-Crimea earthquake with mainshock magnitude m_{ms} = 6.0 had the largest detected aftershock of magnitude ${m_{as}}^{max}$= 5.7. From equation (2.11) the magnitude difference between the mainshock and the largest aftershock is Δm=0.3. We found b = 0.42 ±0.05 and a = 2.50 ±0.22 from correlation of the aftershock frequency magnitude data given in Figure 3.6 with G-R scaling. From equation (2.12) the inferred magnitude of the largest aftershock is m^* = 5.89 ±0.91. From equation (2.13) the magnitude difference between the mainshock and the inferred largest aftershock is $\Delta m^* = 0.11 \pm 0.91$.

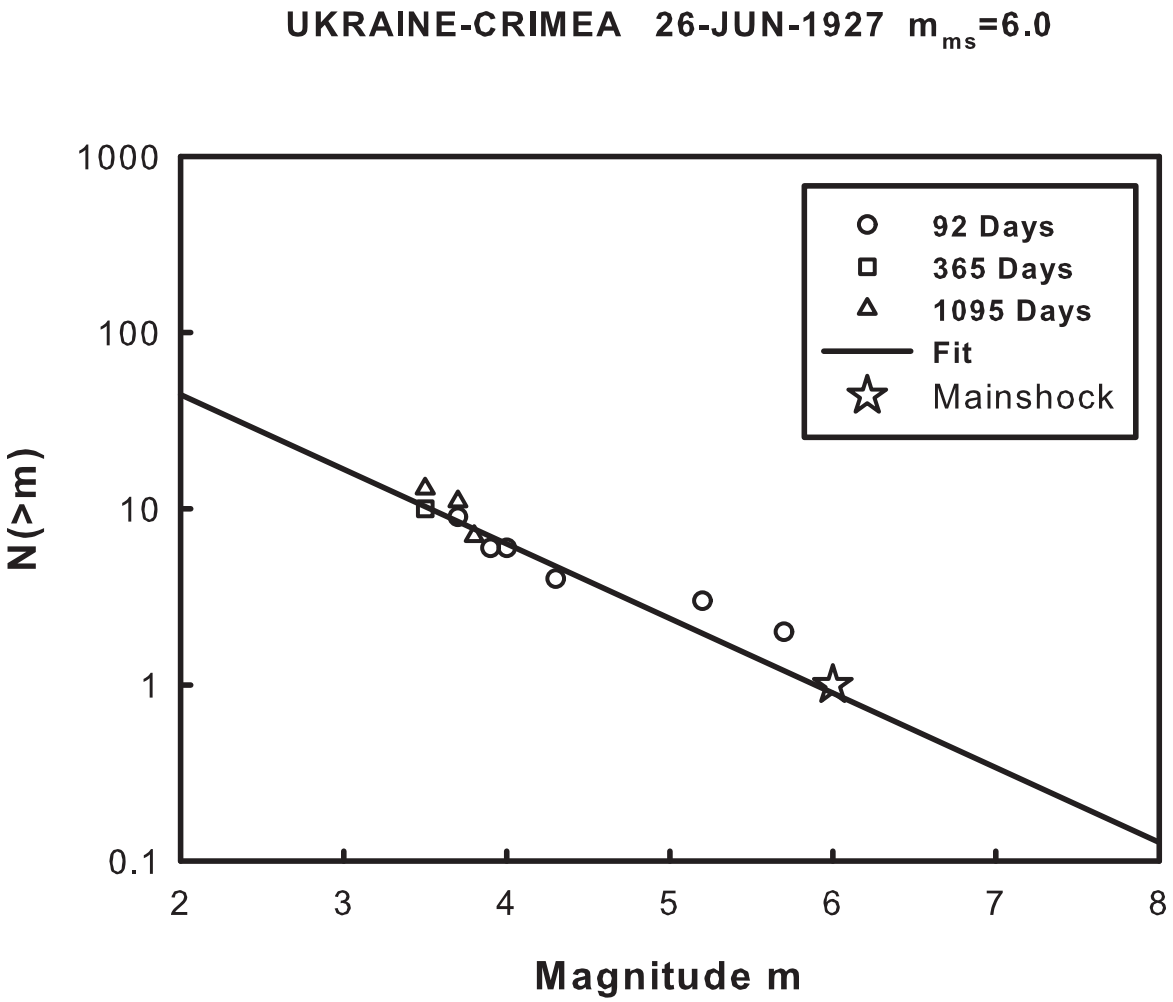

Figure 3.6. Frequency-magnitude distribution of Ukraine-Crimea earthquake

The Plovdiv earthquake with mainshock magnitude m_{ms} = 7.0 had the largest detected aftershock of magnitude ${m_{as}}^{max}$= 5.6. From equation (2.11) the magnitude difference between the mainshock and the largest aftershock is Δm= 1.4. We found b = 0.60 ±0.03 and a = 3.75 ±0.15 from correlation of the aftershock frequency magnitude data given in Figure 3.7 with G-R scaling. From equation (2.12) the inferred magnitude of the largest aftershock is m^* = 6.21±0.42. From equation (2.13) the magnitude difference between the mainshock and the inferred largest aftershock is Δm^* = 0.79 ± 0.42. The Plovdiv earthquake belongs to graben fault system.

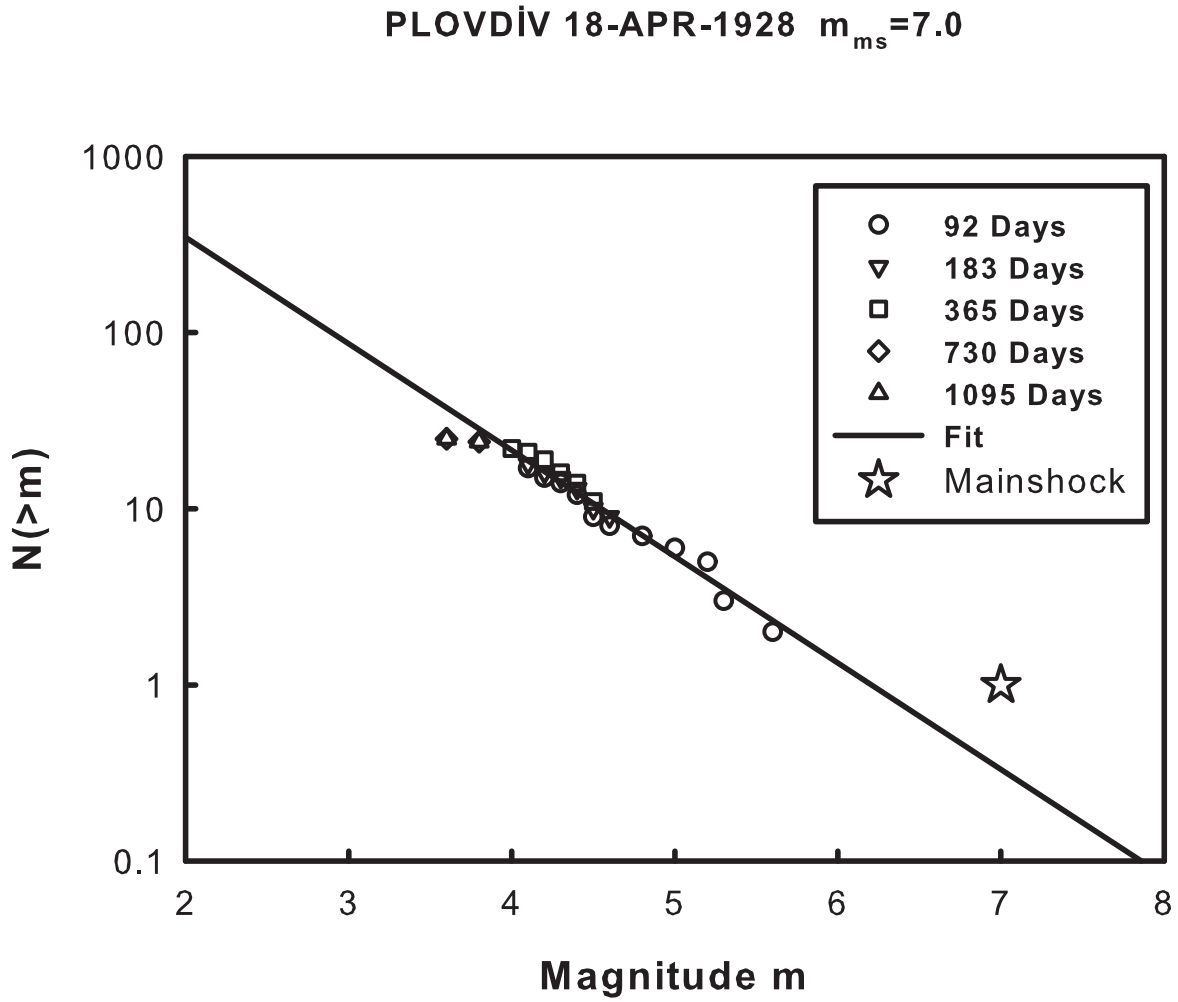

Figure 3.7. Frequency-magnitude distribution of Plovdiv earthquake

The Turkey-Iran Border earthquake with mainshock magnitude $m_{ms} = 7.6$ had the largest detected aftershock of magnitude $m_{as}{}^{max} = 6.3$. From equation (2.11) the magnitude difference between the mainshock and the largest aftershock is $\Delta m = 1.3$. We found b = 0.67 $\pm$0.04 and a =4.25 $\pm$0.21 from correlation of the aftershock frequency magnitude data given in Figure 3.8 with G-R scaling. From equation (2.12) the inferred magnitude of the largest aftershock is $m^* = 6.35 \pm 0.51$. From equation (2.13) the magnitude difference between the mainshock and the inferred largest aftershock is $\Delta m^* = 1.25 \pm 0.51$.

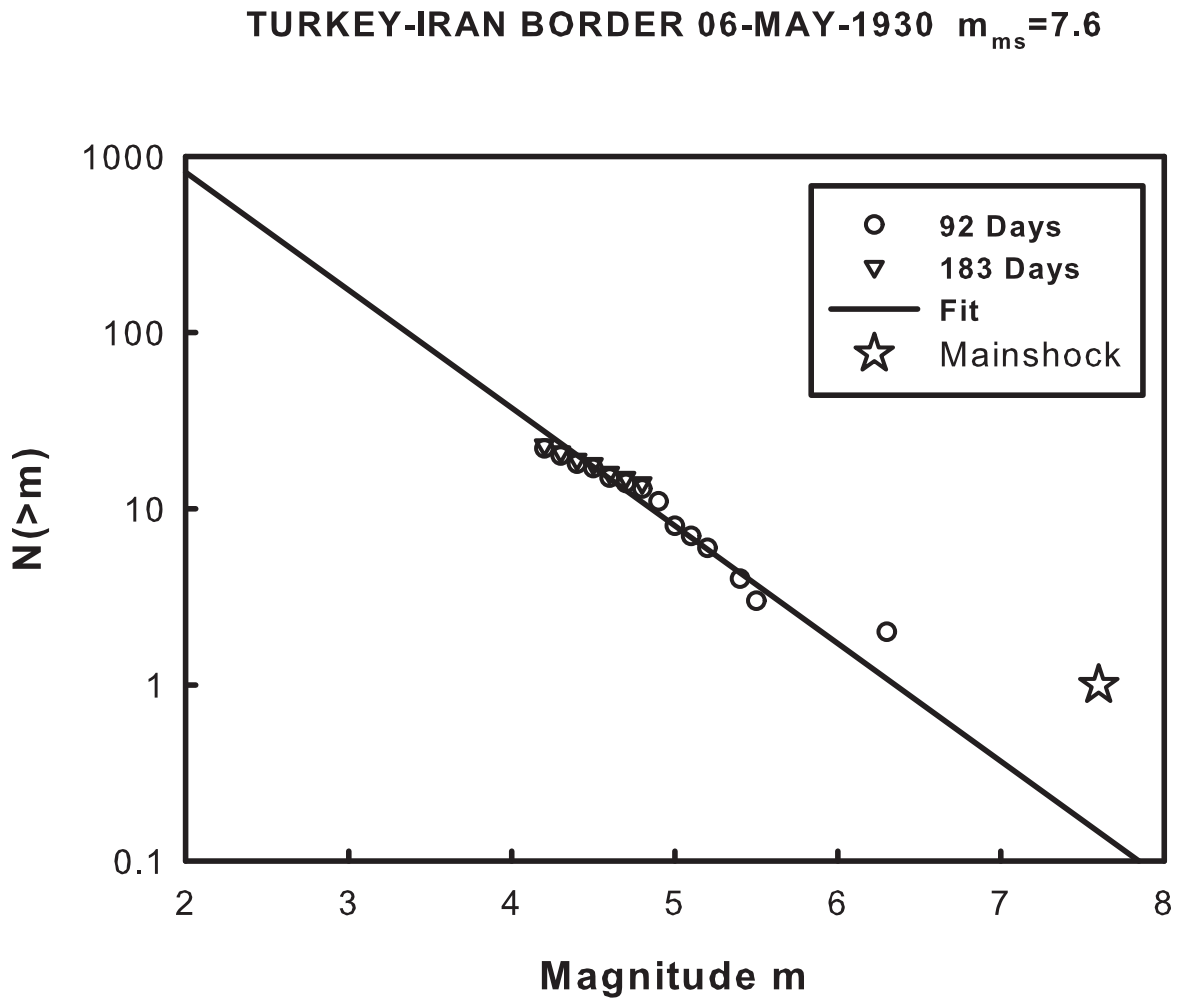

Figure 3.8. Frequency-magnitude distribution of Turkey-Iran Border earthquake

The Gomati earthquake with mainshock magnitude m_{ms} = 7.1 had the largest detected aftershock of magnitude ${m_{as}}^{max}$=5.9. From equation (2.11) the magnitude difference between the mainshock and the largest aftershock is Δm=1.2. We found b = 0.71 ±0.05 and a = 4.60 ±0.24 from correlation of the aftershock frequency magnitude data given in Figure 3.9 with G-R scaling. From equation (2.12) the inferred magnitude of the largest aftershock is m^* =6.48 ±0.54. From equation (2.13) the magnitude difference between the mainshock and the inferred largest aftershock is Δm^*= 0.62±0.54. The Gomati earthquake belongs to graben fault system.

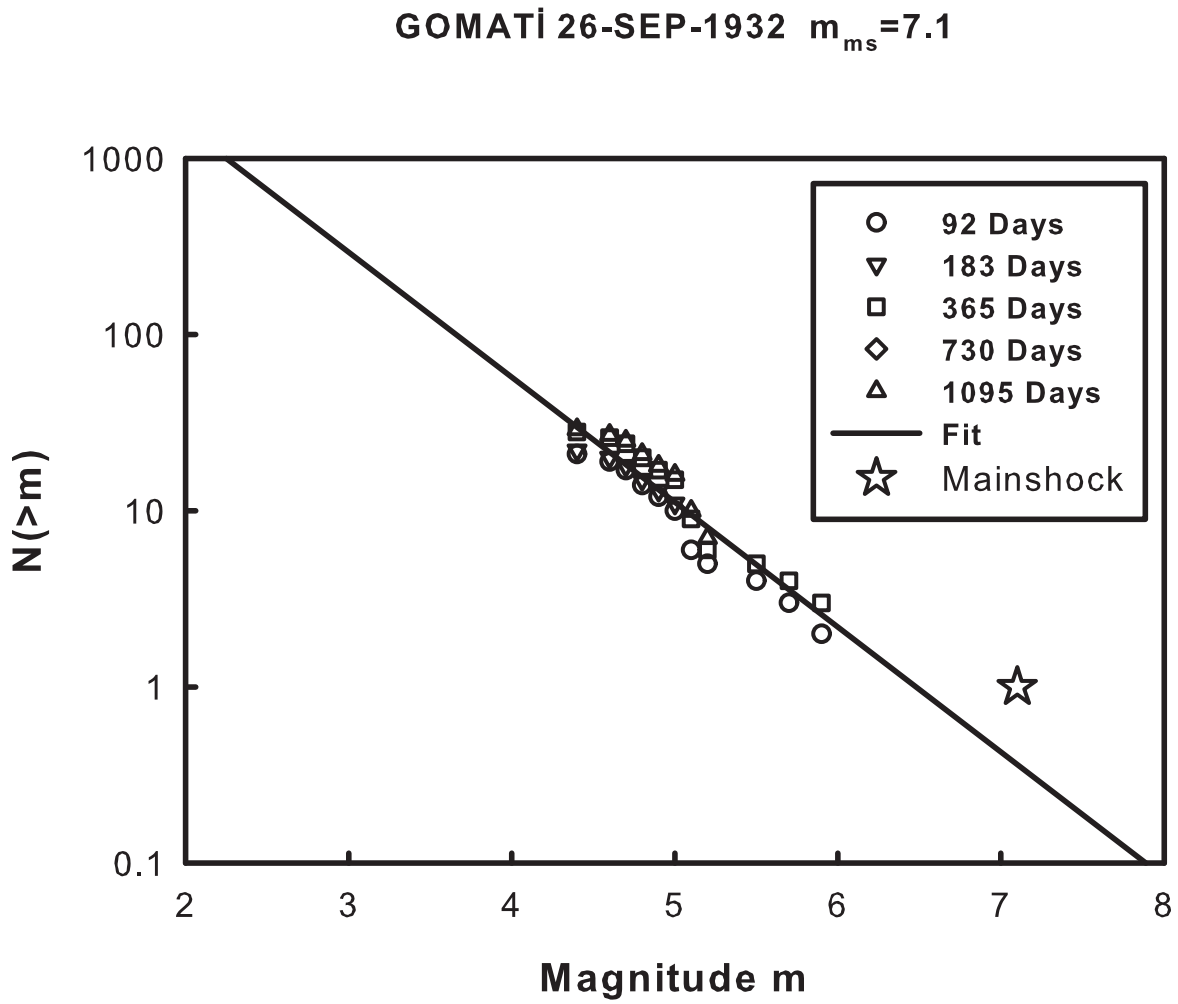

Figure 3.9. Frequency-magnitude distribution of Gomati earthquake

The Karpathos-12 Islands earthquake with mainshock magnitude m_{ms} =7.1 had the largest detected aftershock of magnitude ${m_{as}}^{max}$= 5.5. From equation (2.11) the magnitude difference between the mainshock and the largest aftershock is Δm=1.6. We found b = 0.97 ±0.12 and a = 5.61 ±0.60 from correlation of the aftershock frequency magnitude data given in Figure 3.10 with G-R scaling. From equation (2.12) the inferred magnitude of the largest aftershock is m^* =5.78 ±0.93. From equation (2.13) the magnitude difference between the mainshock and the inferred largest aftershock is Δm^*= 1.32±0.93. The Karpathos-12 Islands earthquake belongs to Cyprus Arc zone.

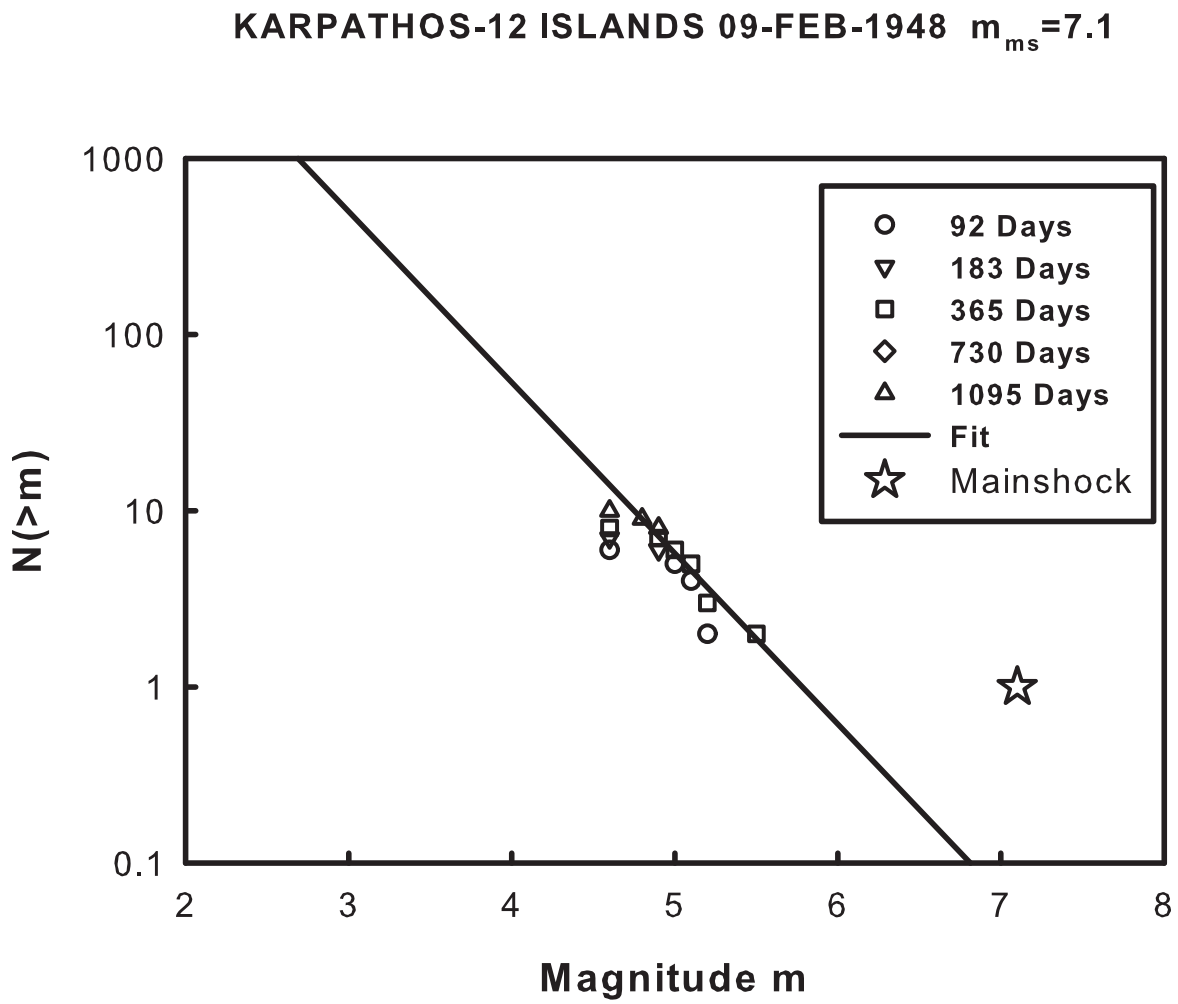

Figure 3.10. Frequency-magnitude distribution of Karpathos-12 Islands earthquake

The Yenice-Gönen earthquake with mainshock magnitude $m_{ms} = 7.2$ had the largest detected aftershock of magnitude $m_{as}{}^{max} = 5.4$. From equation (2.11) the magnitude difference between the mainshock and the largest aftershock is $\Delta m = 1.8$. We found b = 0.81 $\pm$0.06 and a = 4.72 $\pm$0.28 from correlation of the aftershock frequency magnitude data given in Figure 3.11 with G-R scaling. From equation (2.12) the inferred magnitude of the largest aftershock is $m^* = 5.84 \pm 0.54$. From equation (2.13) the magnitude difference between the mainshock and the inferred largest aftershock is $\Delta m^* = 1.36 \pm 0.54$. The Yenice-Gönen earthquake belongs to North Anatolian Fault zone.

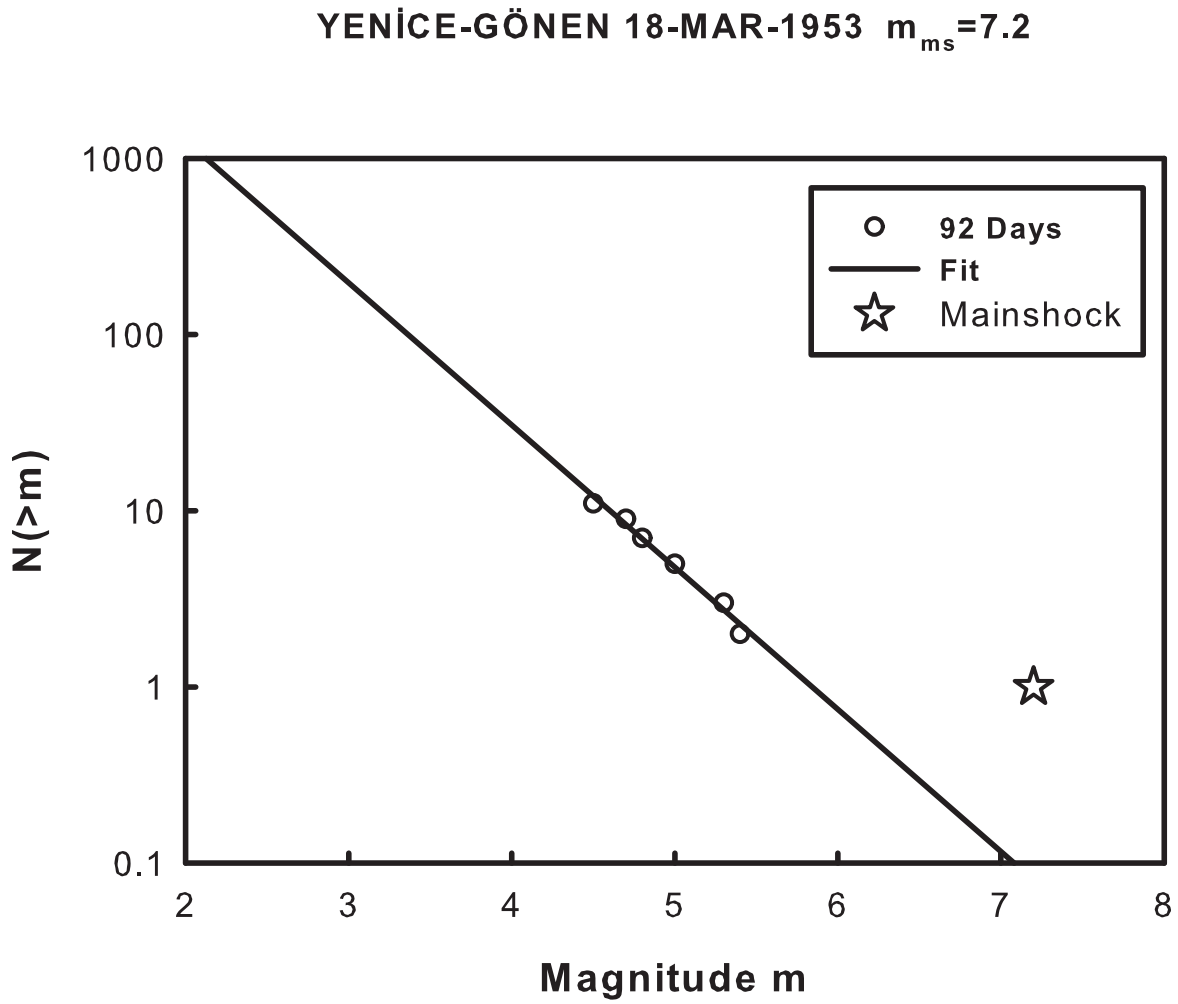

Figure 3.11. Frequency-magnitude distribution of Yenice-Gönen earthquake

The Aegean Sea earthquake with mainshock magnitude m_{ms} =7.4 had the largest detected aftershock of magnitude $m_{as}{}^{max}$= 6.5. From equation (2.11) the magnitude difference between the mainshock and the largest aftershock is Δm= 0.9. We found b = 1.03 ±0.09 and a = 6.00 ±0.44 from correlation of the aftershock frequency magnitude data given in Figure 3.12 with G-R scaling. From equation (2.12) the inferred magnitude of the largest aftershock is m^* = 5.80 ±0.65. From equation (2.13) the magnitude difference between the mainshock and the inferred largest aftershock is Δm^*= 1.60±0.65. The Aegean Sea earthquake belongs to Cyprus Arc zone.

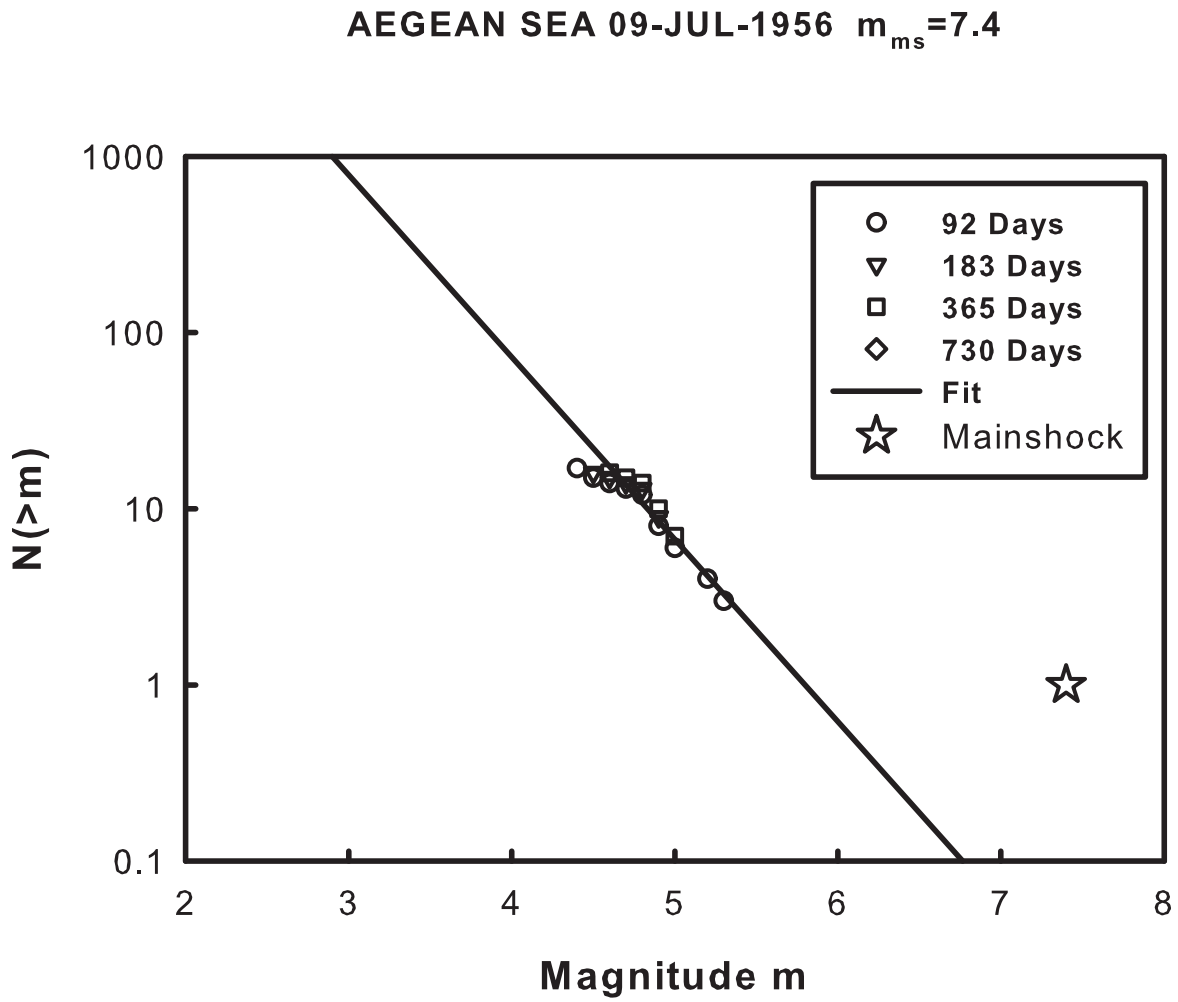

Figure 3.12. Frequency-magnitude distribution of Aegean Sea earthquake

The Fethiye-Rodos earthquake with mainshock magnitude $m_{ms} = 7.1$ had the largest detected aftershock of magnitude ${m_{as}}^{max}$=5.9. From equation (2.11) the magnitude difference between the mainshock and the largest aftershock is Δm= 1.2. We found b = 0.47 ±0.04 and a = 2.87 ±0.17 from correlation of the aftershock frequency magnitude data given in Figure 3.13 with G-R scaling. From equation (2.12) the inferred magnitude of the largest aftershock is m^* = 6.16 ±0.62. From equation (2.13) the magnitude difference between the mainshock and the inferred largest aftershock is Δm^*= 0.94±0.62. The Fethiye-Rodos earthquake belongs to Crete Rodos Arc zone.

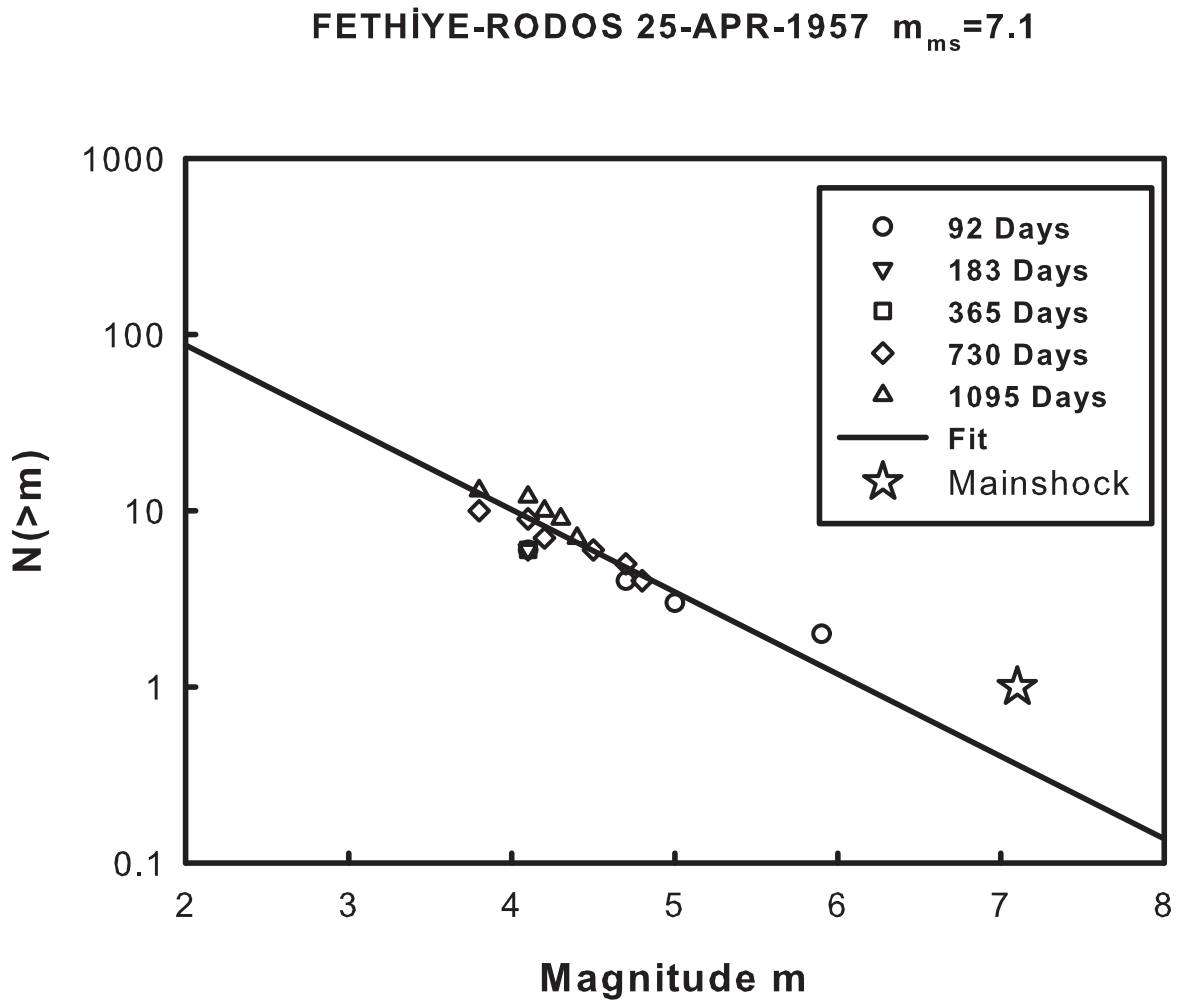

Figure 3.13. Frequency-magnitude distribution of Fethiye-Rodos earthquake

The Bolu-Abant earthquake with mainshock magnitude m_{ms} =7.1 had the largest detected aftershock of magnitude $m_{as}{}^{max}$= 5.9. From equation (2.11) the magnitude difference between the mainshock and the largest aftershock is Δm=1.2. We found b =0.47 ±0.04 and a = 3.14 ±0.21 from correlation of the aftershock frequency magnitude data given in Figure 3.14 with G-R scaling. From equation (2.12) the inferred magnitude of the largest aftershock is m^* = 6.66 ± 0.76. From equation (2.13) the magnitude difference between the mainshock and the inferred largest aftershock is Δm^*=0.44 ±0.76. The Bolu-Abant earthquake belongs to North Anatolian Fault Zone.

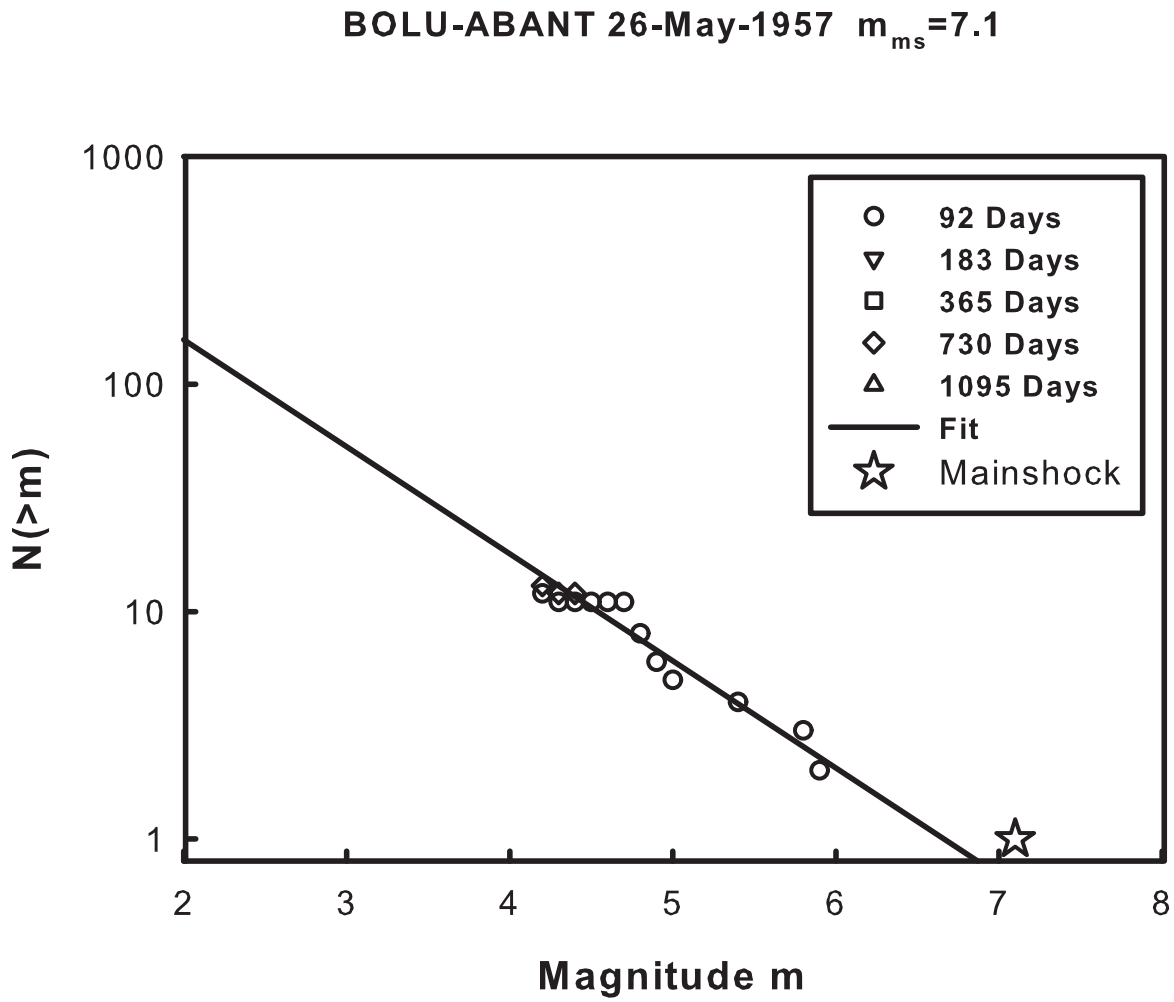

Figure 3.14. Frequency-magnitude distribution of Bolu-Abant earthquake

The Muş-Varto earthquake with mainshock magnitude m_{ms} = 6.9 had the largest detected aftershock of magnitude ${m_{as}}^{max}$=5.3. From equation (2.11) the magnitude difference between the mainshock and the largest aftershock is Δm= 1.6. We found b =1.01 ±0.14 and a = 5.60 ±0.67 from correlation of the aftershock frequency magnitude data given in Figure 3.15 with G-R scaling. From equation (2.12) the inferred magnitude of the largest aftershock is m^* = 5.56 ±1.01. From equation (2.13) the magnitude difference between the mainshock and the inferred largest aftershock is Δm^*= 1.34±1.01. The Muş-Varto earthquake belongs to South East Anatolian fault zone.

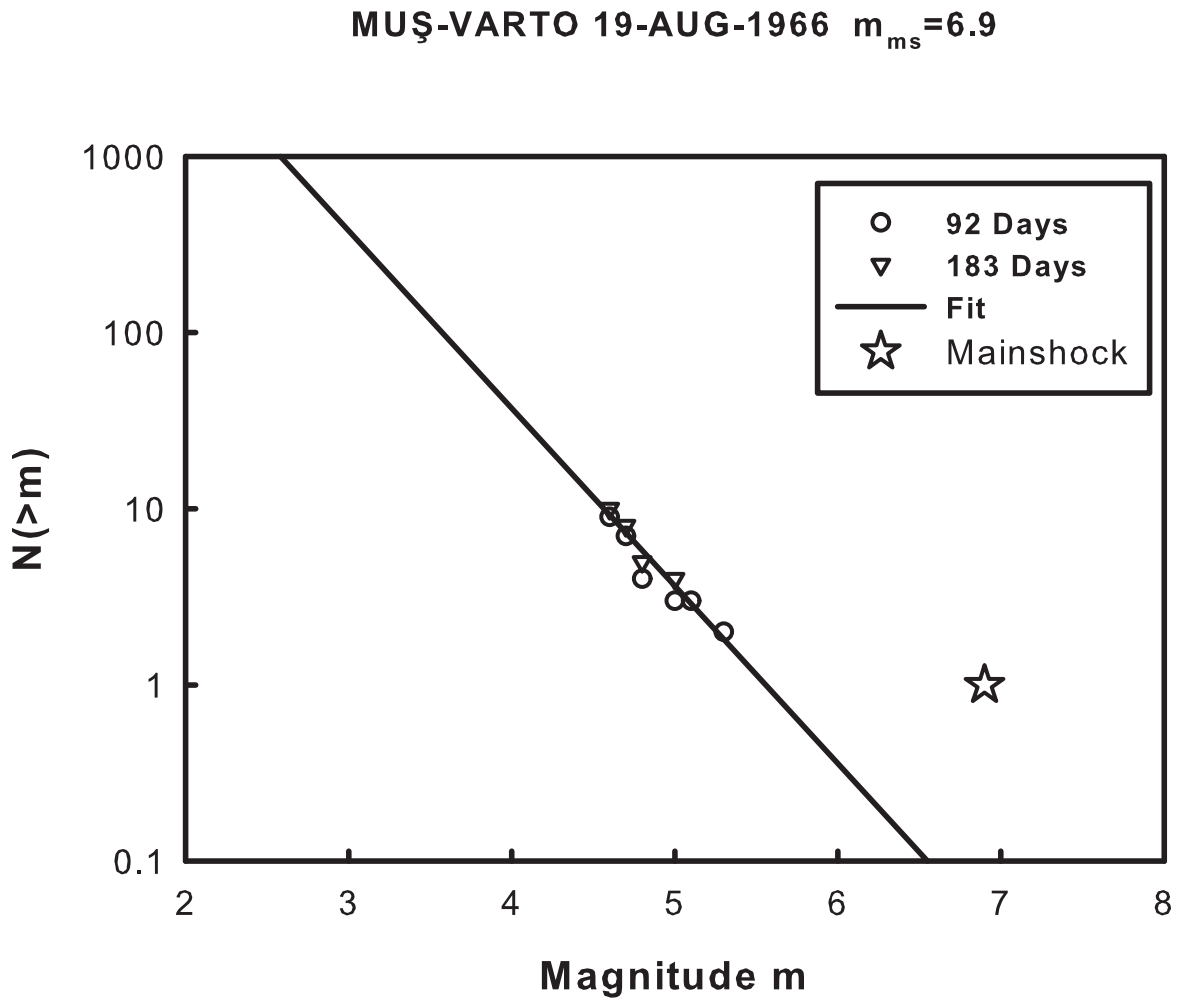

Figure 3.15. Frequency-magnitude distribution of Muş-Varto earthquake

The Adapazarı-Mudurnusuyu Valley earthquake with mainshock magnitude m_{ms} =7.2 had the largest detected aftershock of magnitude ${m_{as}}^{max}$= 5.4. From equation (2.11) the magnitude difference between the mainshock and the largest aftershock is Δm=1.8. We found b = 0.85 ±0.06 and a = 4.93 ±0.28 from correlation of the aftershock frequency magnitude data given in Figure 3.16 with G-R scaling. From equation (2.12) the inferred magnitude of the largest aftershock is m^* = 5.79±0.53. From equation (2.13) the magnitude difference between the mainshock and the inferred largest aftershock is Δm^*=1.41 ±0.53. The Adapazarı-Mudurnusuyu Valley earthquake belongs to North Anatolian Fault

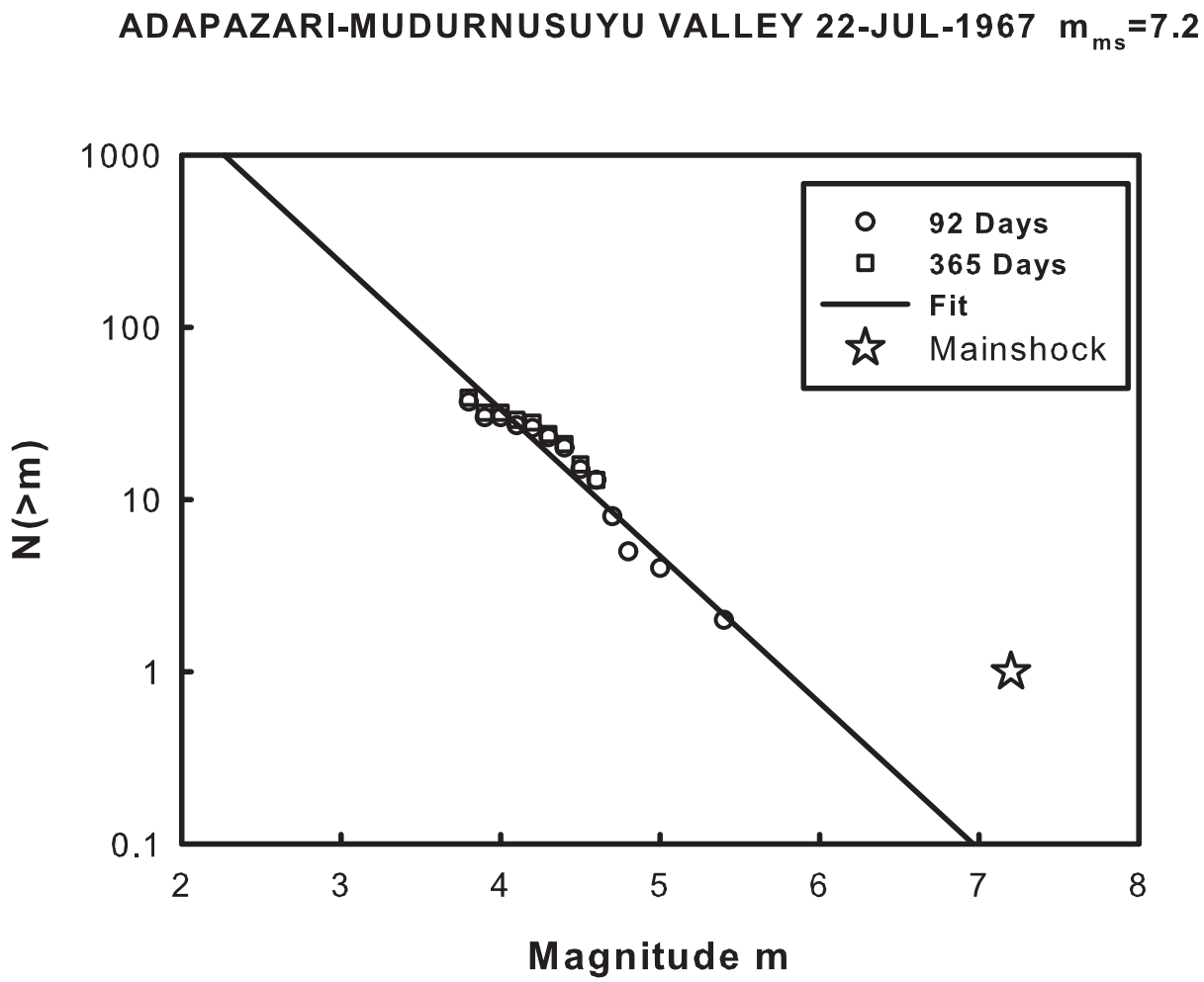

Figure 3.16. Frequency-magnitude distribution of Adapazarı Mudurnusuyu Valley earthquake

Zone.

The Kütahya-Çavdarhisar earthquake with mainshock magnitude m_{ms} =5.7 had the largest detected aftershock of magnitude ${m_{as}}^{max}$= 5.0. From equation (2.11) the magnitude difference between the mainshock and the largest aftershock is Δm= 0.7. We found b =0.38 ±0.03 and a = 1.98 ±0.09 from correlation of the aftershock frequency magnitude data given in Figure 3.17 with G-R scaling. From equation (2.12) the inferred magnitude of the largest aftershock is m^* = 5.15 ± 0.46. From equation (2.13) the magnitude differ-

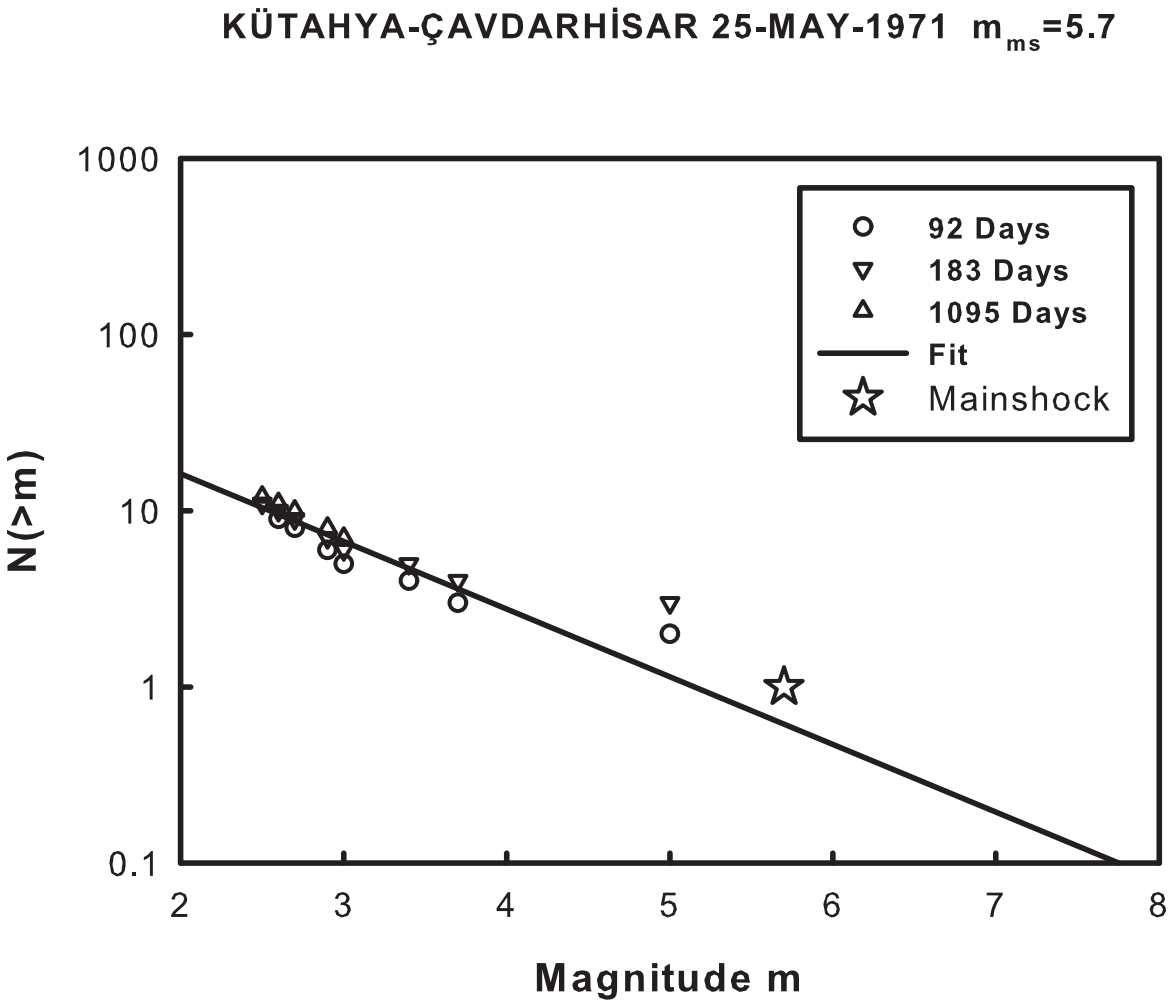

Figure 3.17. Frequency-magnitude distribution of Kütahya-Çavdarhisar earthquake

ence between the mainshock and the inferred largest aftershock is Δm^*=0.55 ±0.46. The Kütahya-Çavdarhisar earthquake belongs to graben fault system.

The Diyarbakır-Lice earthquake with mainshock magnitude m_{ms} =7.8 had the largest detected aftershock of magnitude ${m_{as}}^{max}$= 5.2. From equation (2.11) the magnitude difference between the mainshock and the largest aftershock is Δm= 2.6. We found b = 1.08 ±0.06 and a = 5.98 ±0.27 from correlation of the aftershock frequency magnitude data given in Figure 3.18 with G-R scaling. From equation (2.12) the inferred magnitude

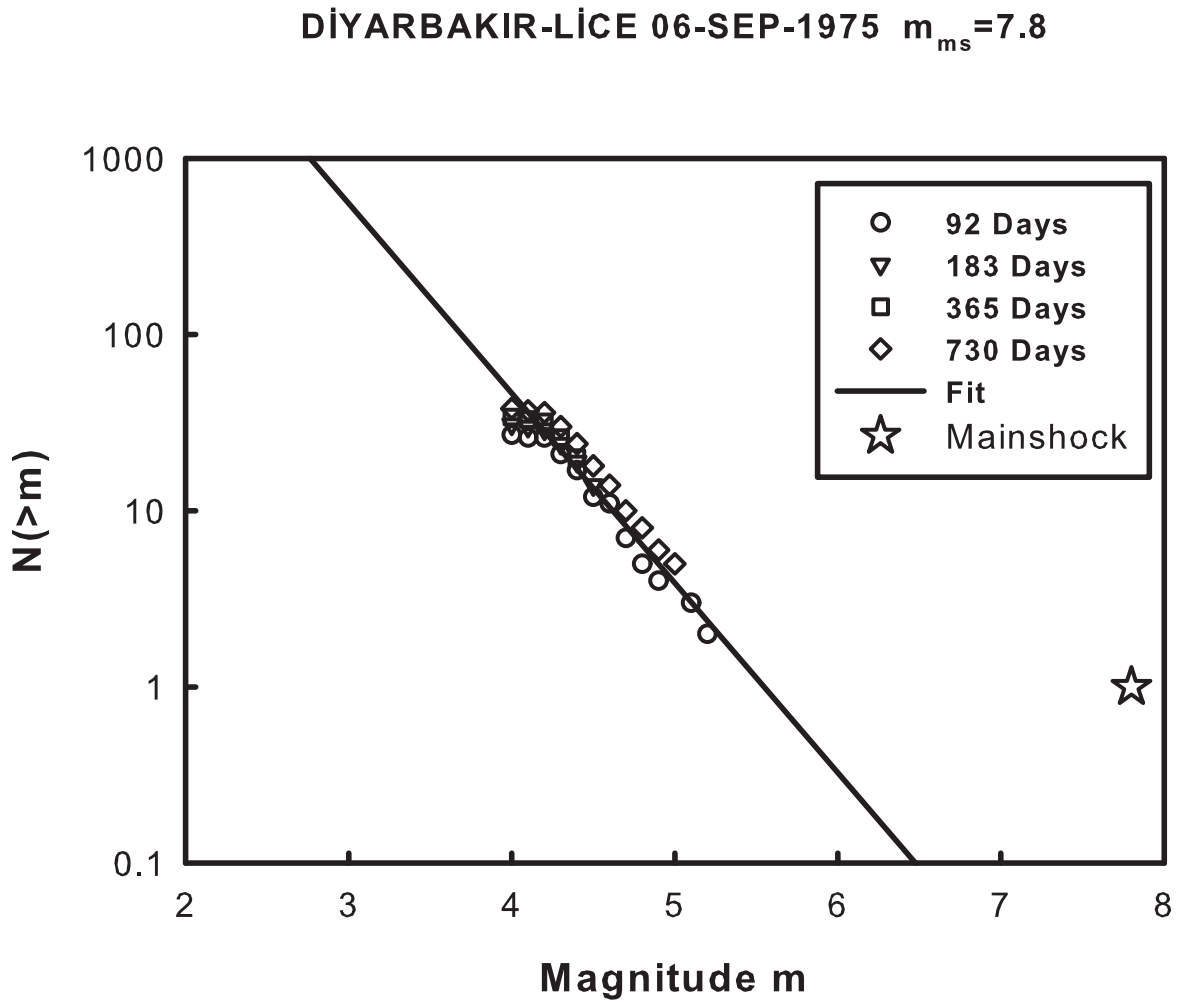

Figure 3.18. Frequency-magnitude distribution of Diyarbakır-Lice earthquake

of the largest aftershock is m^* =5.55 ±0.39. From equation (2.13) the magnitude difference between the mainshock and the inferred largest aftershock is Δm^*=2.25 ±0.39. The Diyarbakır-Lice earthquake belongs to South East Anatolian Fault zone.

The Mediterranean Sea-Crete Island earthquake with mainshock magnitude m_{ms} =5.8 had the largest detected aftershock of magnitude ${m_{as}}^{max}$= 4.9. From equation (2.11) the magnitude difference between the mainshock and the largest aftershock is Δm=0.9. We found b = 0.64 ±0.04 and a = 3.44±0.17 from correlation of the aftershock frequency

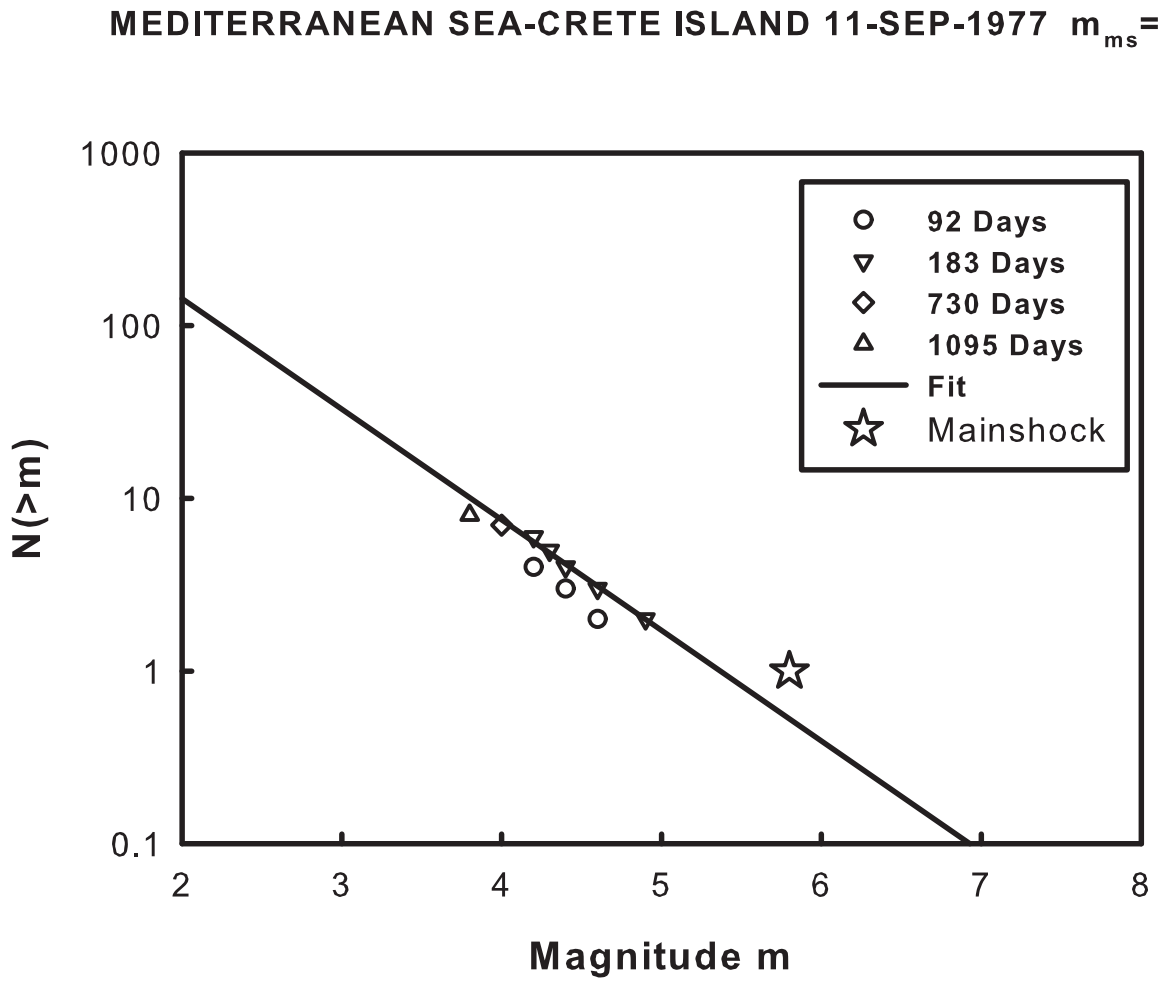

Figure 3.19. Frequency-magnitude distribution of Mediterranean Sea-Crete earthquake

magnitude data given in Figure 3.32 with G-R scaling. From equation (2.12) the inferred magnitude of the largest aftershock is $m^* = 5.37 \pm 0.41$. From equation (2.13) the magnitude difference between the mainshock and the inferred largest aftershock is Δm^*=0.43 ±0.41. The Mediterranean Sea-Crete Island earthquake belongs to Cyprus Arc Zone.

The Thessaloniki earthquake with mainshock magnitude m_{ms} =6.1 had the largest detected aftershock of magnitude $m_{as}{}^{max}$= 4.7. From equation (2.11) the magnitude difference between the mainshock and the largest aftershock is Δm= 1.4. We found b =0.77 ±0.04 and a = 4.19 ±0.15 from correlation of the aftershock frequency magnitude data

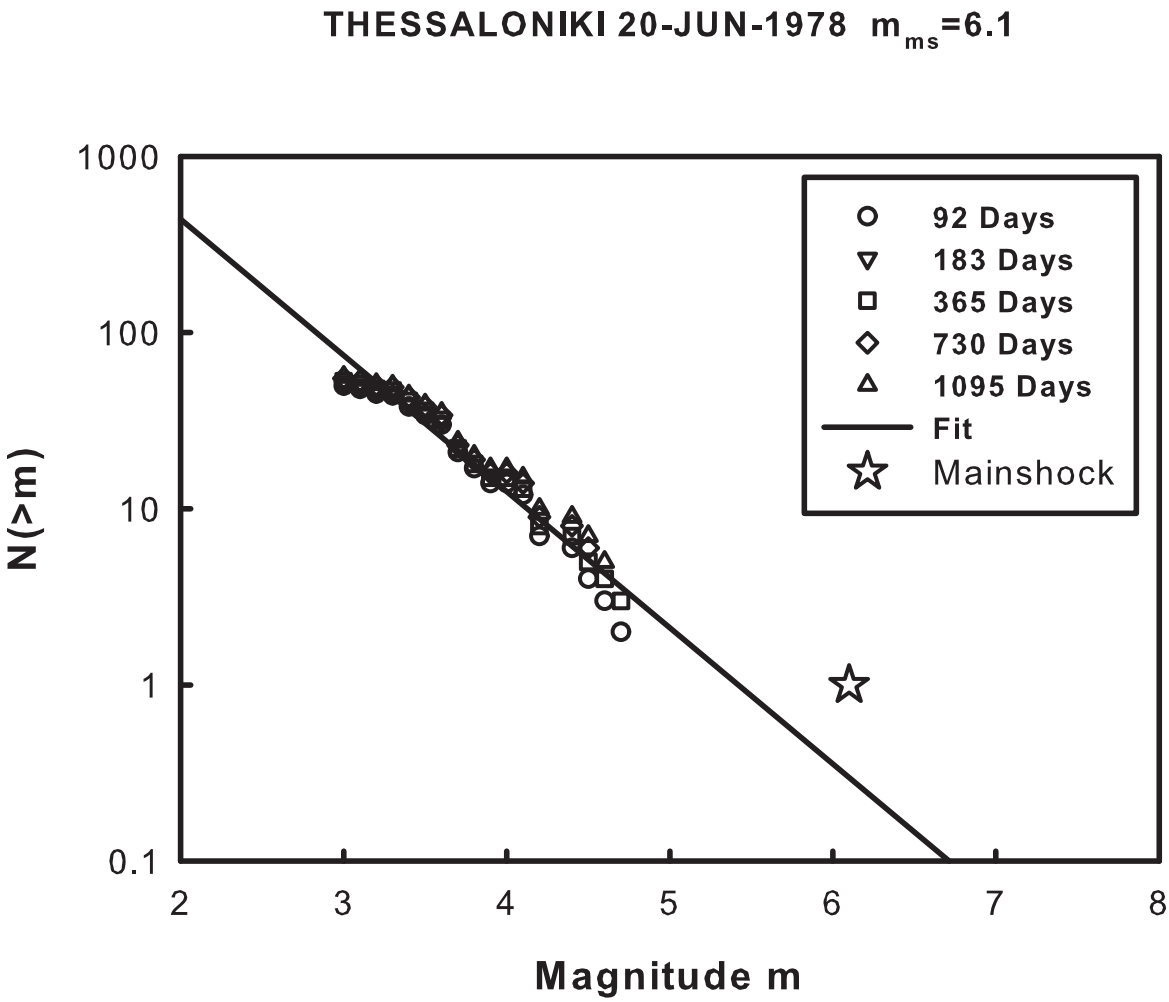

Figure 3.20. Frequency-magnitude distribution of Thessaloniki earthquake

given in Figure 3.20 with G-R scaling. From equation (2.12) the inferred magnitude of the largest aftershock is m^* =5.42 ±0.34. From equation (2.13) the magnitude difference between the mainshock and the inferred largest aftershock is Δm^*= 0.68±0.34. The Thessaloniki earthquake belongs to graben fault system.

The Karaburun-İzmir earthquake with mainshock magnitude m_{ms} = 5.9 had the largest detected aftershock of magnitude ${m_{as}}^{max}$= 4.9. From equation (2.11) the magnitude difference between the mainshock and the largest aftershock is Δm= 1.0. We found

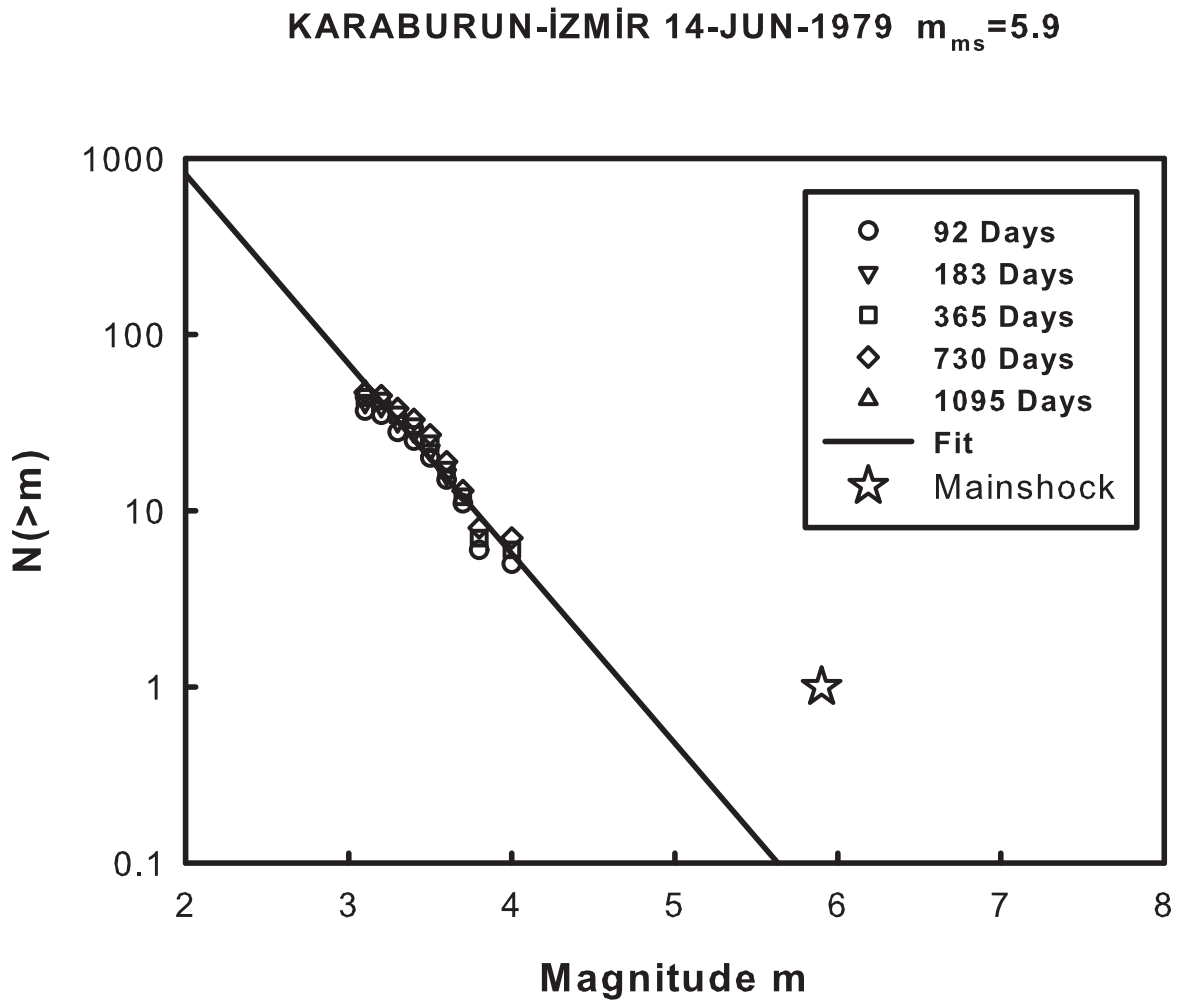

Figure 3.21. Frequency-magnitude distribution of Karaburun-İzmir earthquake

b =1.08 ±0.09 and a = 5.07 ±0.32 from correlation of the aftershock frequency magnitude data given in Figure 3.21 with G-R scaling. From equation (2.12) the inferred magnitude of the largest aftershock is $m^* = 4.70 \pm 0.50$. From equation (2.13) the magnitude difference between the mainshock and the inferred largest aftershock is Δm^*=1.20 ±0.50. The Karaburun-İzmir earthquake belongs to graben fault system.

The Greece-Athens earthquake with mainshock magnitude $m_{ms} = 5.7$ had the largest detected aftershock of magnitude ${m_{as}}^{max}$= 5.3. From equation (2.11) the magnitude dif-

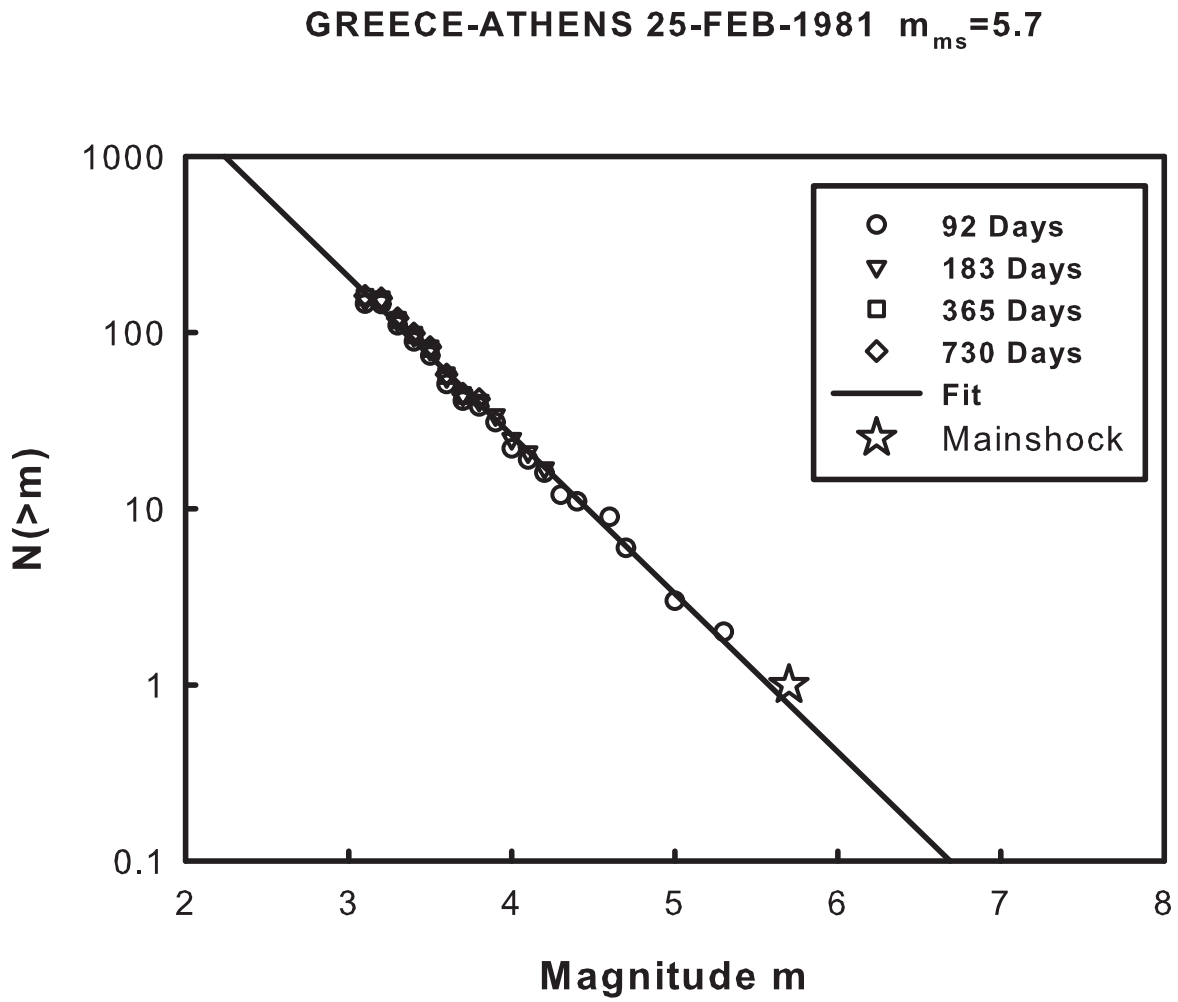

Figure 3.22. Frequency-magnitude distribution of Greece-Athens earthquake

ference between the mainshock and the largest aftershock is Δm=0.4. We found b = 0.90 $\pm$0.02 and a = 5.01 $\pm$0.06 from correlation of the aftershock frequency magnitude data given in Figure 3.22 with G-R scaling. From equation (2.12) the inferred magnitude of the largest aftershock is m^* =5.58 $\pm$ 0.12. From equation (2.13) the magnitude difference between the mainshock and the inferred largest aftershock is Δm^*=0.12 $\pm$0.12. The Greece-Athens earthquake belongs to graben fault system.

The Greece-Athens-2 earthquake with mainshock magnitude m_{ms} = 5.8 had the

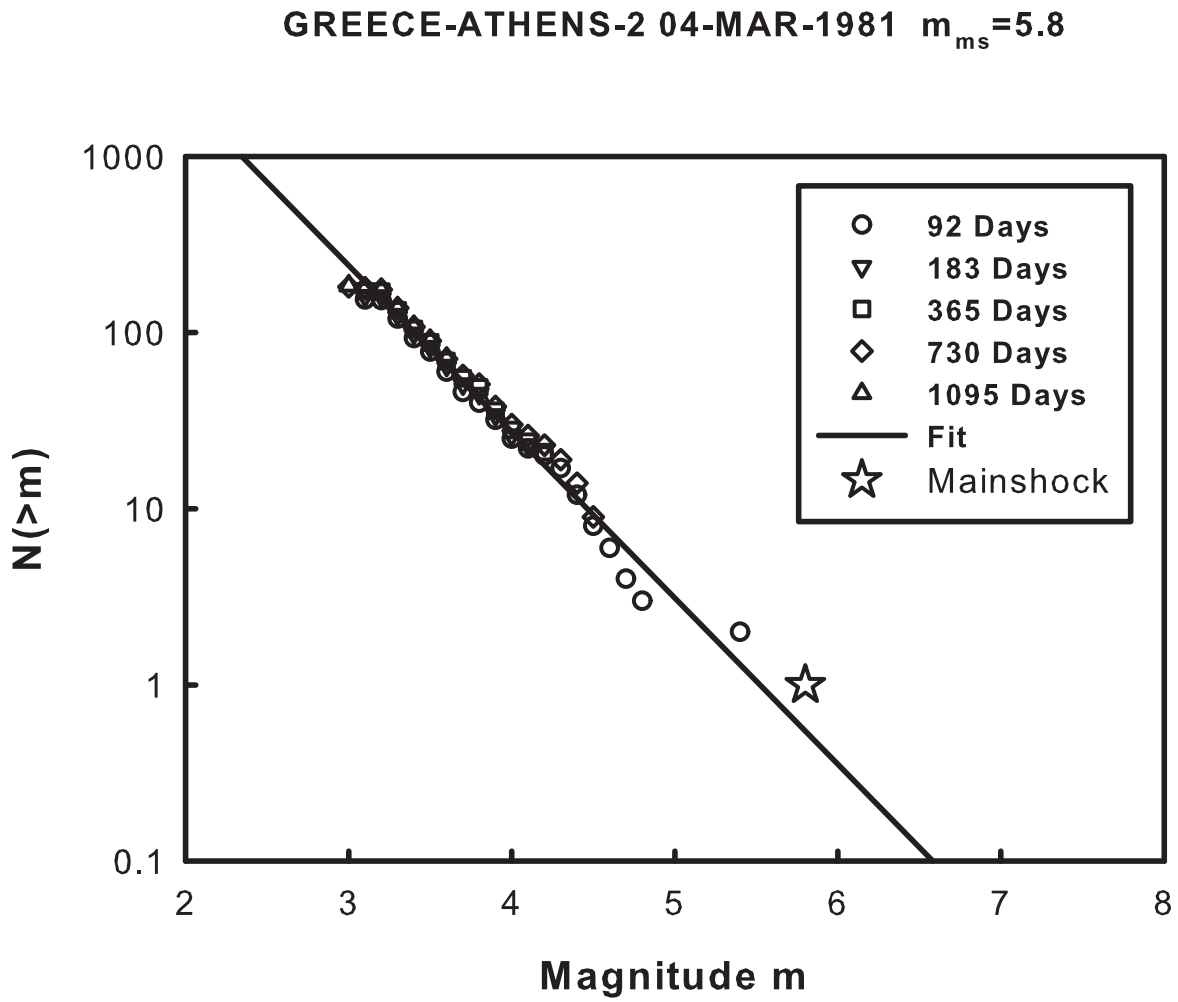

Figure 3.23. Frequency-magnitude distribution of Greece-Athens2 earthquake

largest detected aftershock of magnitude $m_{as}{}^{max}$= 5.4. From equation (2.11) the magnitude difference between the mainshock and the largest aftershock is Δm= 0.4. We found b =0.89 ±0.04 and a = 4.99 ±0.15 from correlation of the aftershock frequency magnitude data given in Figure 3.23 with G-R scaling. From equation (2.12) the inferred magnitude of the largest aftershock is m^* =5.59 ±0.29. From equation (2.13) the magnitude difference between the mainshock and the inferred largest aftershock is Δm^*= 0.21±0.29. The Greece-Athens-2 earthquake belongs to graben fault system.

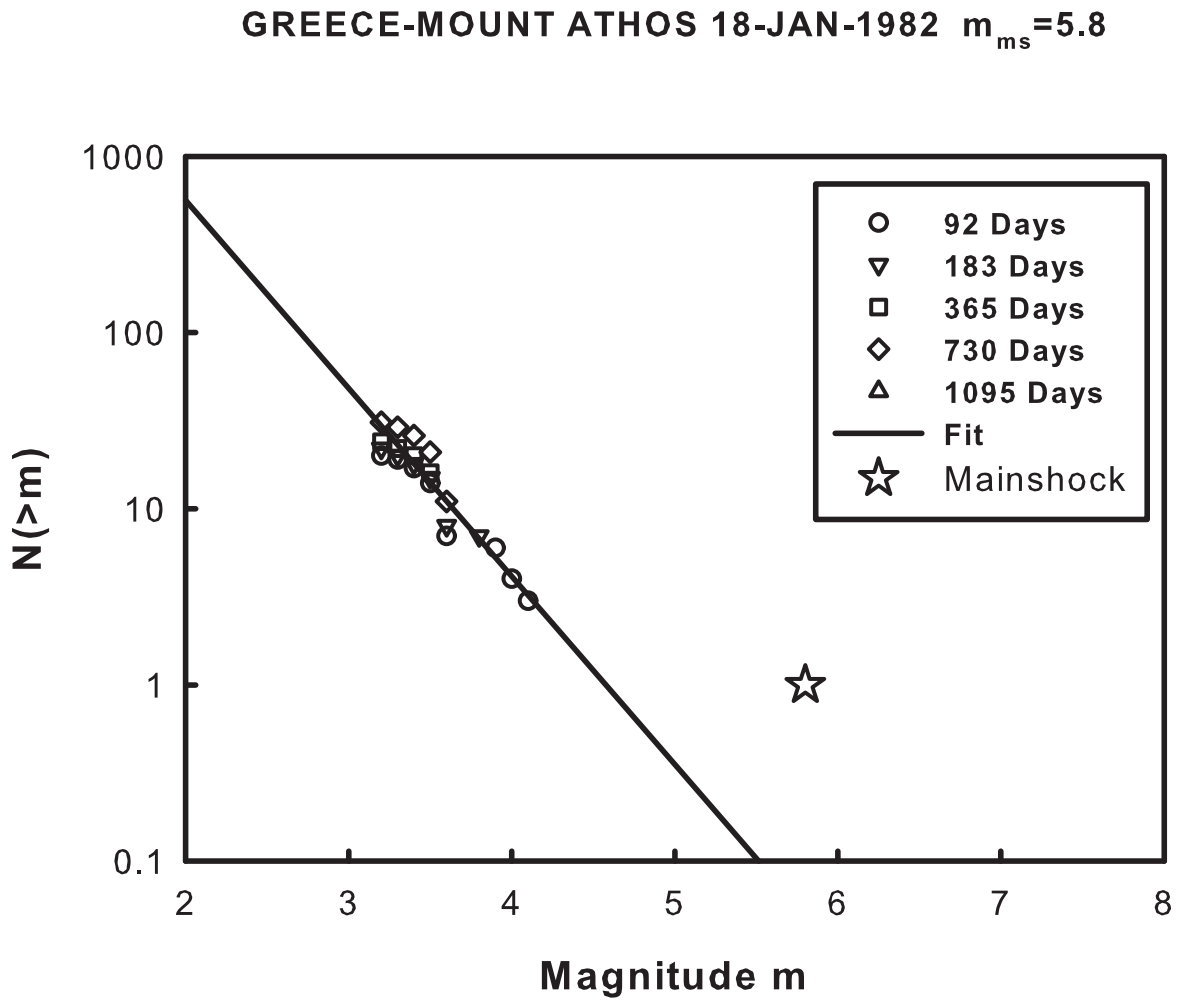

Figure 3.24. Frequency-magnitude distribution of Greece-Mount Athos earthquake

The Greece-Mount Athos earthquake with mainshock magnitude $m_{ms} = 5.8$ had the largest detected aftershock of magnitude ${m_{as}}^{max}= 4.1$. From equation (2.11) the magnitude difference between the mainshock and the largest aftershock is Δm=1.7. We found b = 1.07 ±0.08 and a = 4.89 ±0.28 from correlation of the aftershock frequency magnitude data given in Figure 3.24 with G-R scaling. From equation (2.12) the inferred magnitude of the largest aftershock is $m^* = 4.58$ ±0.42. From equation (2.13) the magnitude difference between the mainshock and the inferred largest aftershock is $\Delta m^*= 1.22\pm0.42$. The Greece-Mount Athos earthquake belongs to graben fault system.

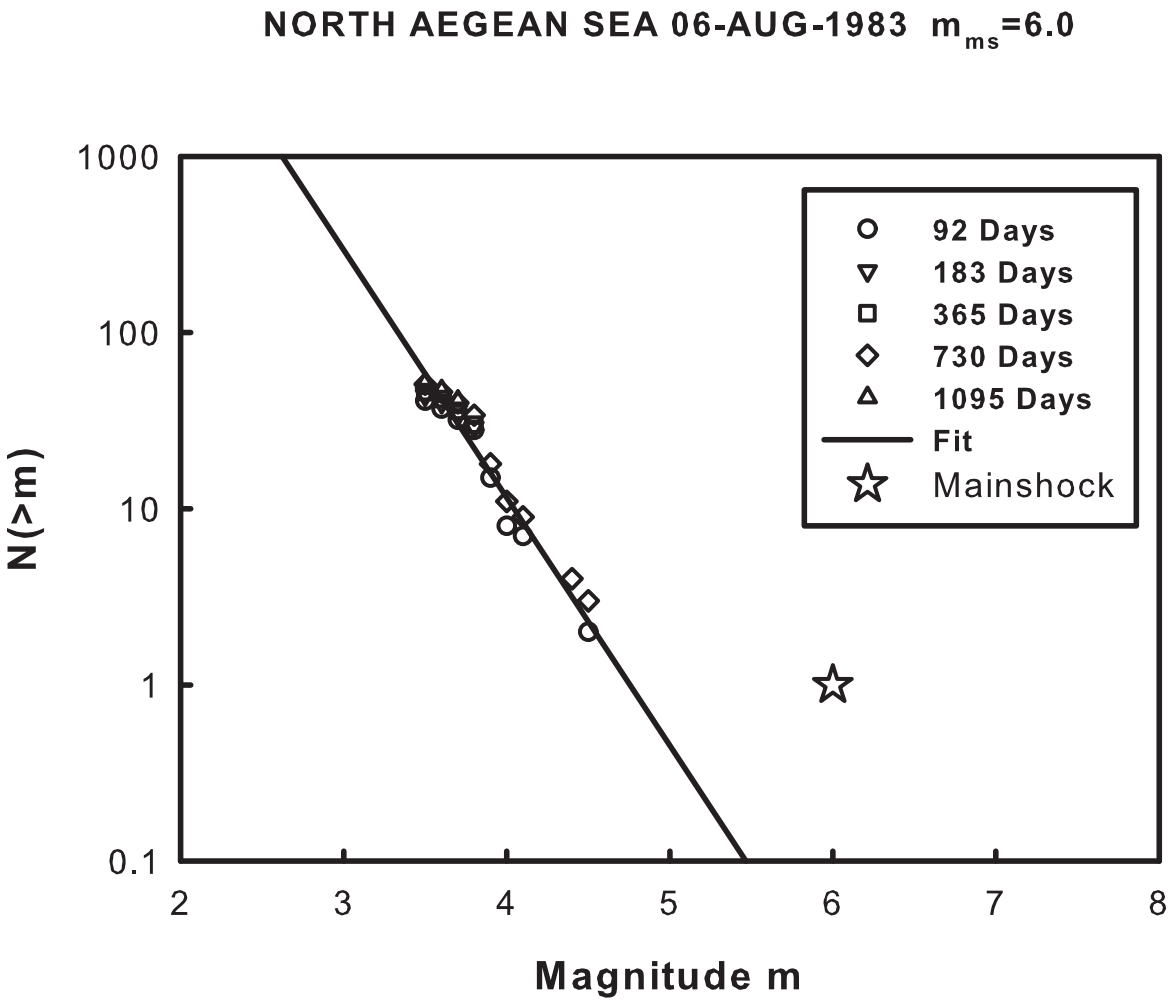

Figure 3.25. Frequency-magnitude distribution of North Aegean Sea earthquake

The North Aegean Sea earthquake with mainshock magnitude m_{ms} =6.0 had the largest detected aftershock of magnitude ${m_{as}}^{max}$=4.5. From equation (2.11) the magnitude difference between the mainshock and the largest aftershock is Δm=1.5. We found b =1.41 ±0.10 and a = 6.69±0.39 from correlation of the aftershock frequency magnitude data given in Figure 3.25 with G-R scaling. From equation (2.12) the inferred magnitude of the largest aftershock is m^* = 4.76 ±0.44. From equation (2.13) the magnitude difference between the mainshock and the inferred largest aftershock is Δm^*= 1.24±0.44. The North Aegean Sea earthquake belongs to graben fault system.

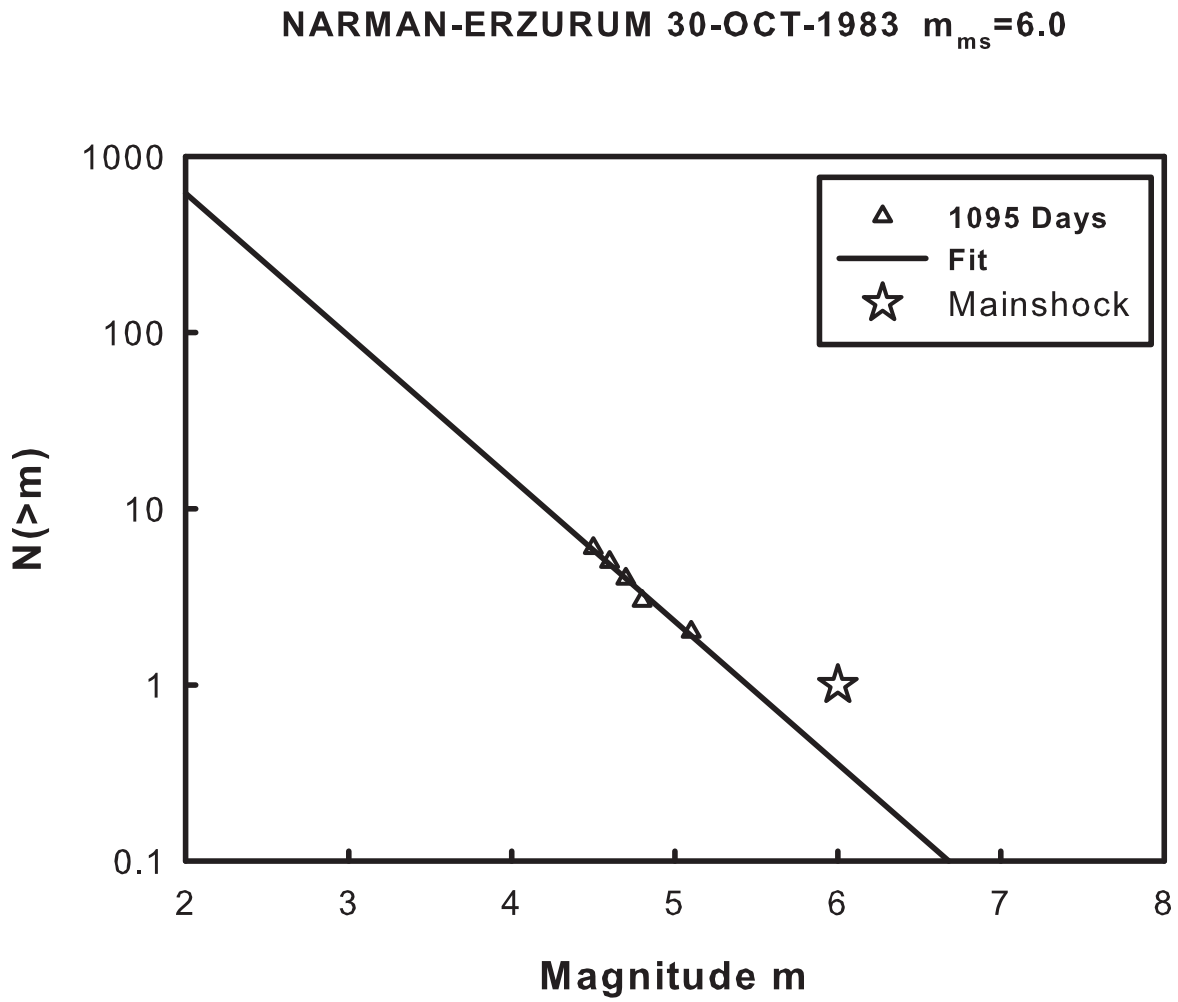

Figure 3.26. Frequency-magnitude distribution of Narman-Erzurum earthquake

The Narman-Erzurum earthquake with mainshock magnitude m_{ms} =6.0 had the largest detected aftershock of magnitude ${m_{as}}^{max}$=5.1. From equation (2.11) the magnitude difference between the mainshock and the largest aftershock is Δm=0.9. We found b = 0.81 ±0.07 and a =4.41 ±0.32 from correlation of the aftershock frequency magnitude data given in Figure 3.26 with G-R scaling. From equation (2.12) the inferred magnitude of the largest aftershock is m^* = 5.45 ±0.60. From equation (2.13) the magnitude difference between the mainshock and the inferred largest aftershock is Δm^*= 0.55±0.60. The Narman-Erzurum earthquake belongs to Erzurum Fault zone.

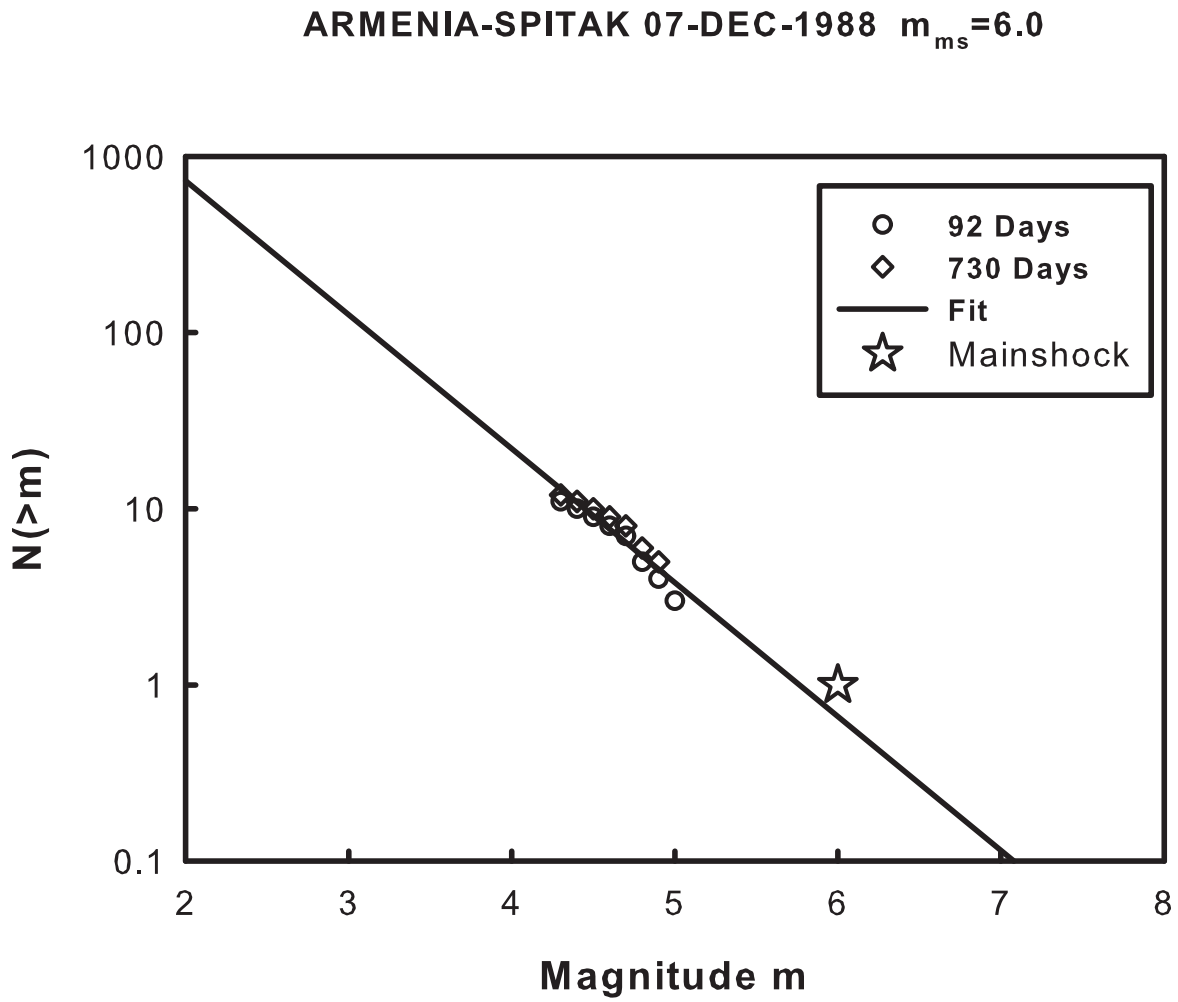

Figure 3.27. Frequency-magnitude distribution of Armenia-Spitak earthquake

The Armenia-Spitak earthquake with mainshock magnitude m_{ms} = 6.0 had the largest detected aftershock of magnitude ${m_{as}}^{max}$= 5.8. From equation (2.11) the magnitude difference between the mainshock and the largest aftershock is Δm=0.2. We found b = 0.76 ±0.07 and a = 4.38 ±0.35 from correlation of the aftershock frequency magnitude data given in Figure 3.27 with G-R scaling. From equation (2.12) the inferred magnitude of the largest aftershock is m^* =5.76 ±0.73. From equation (2.13) the magnitude difference between the mainshock and the inferred largest aftershock is Δm^*=0.24 ±0.73. The Armenia-Spitak earthquake belongs to Caucasians fault system.

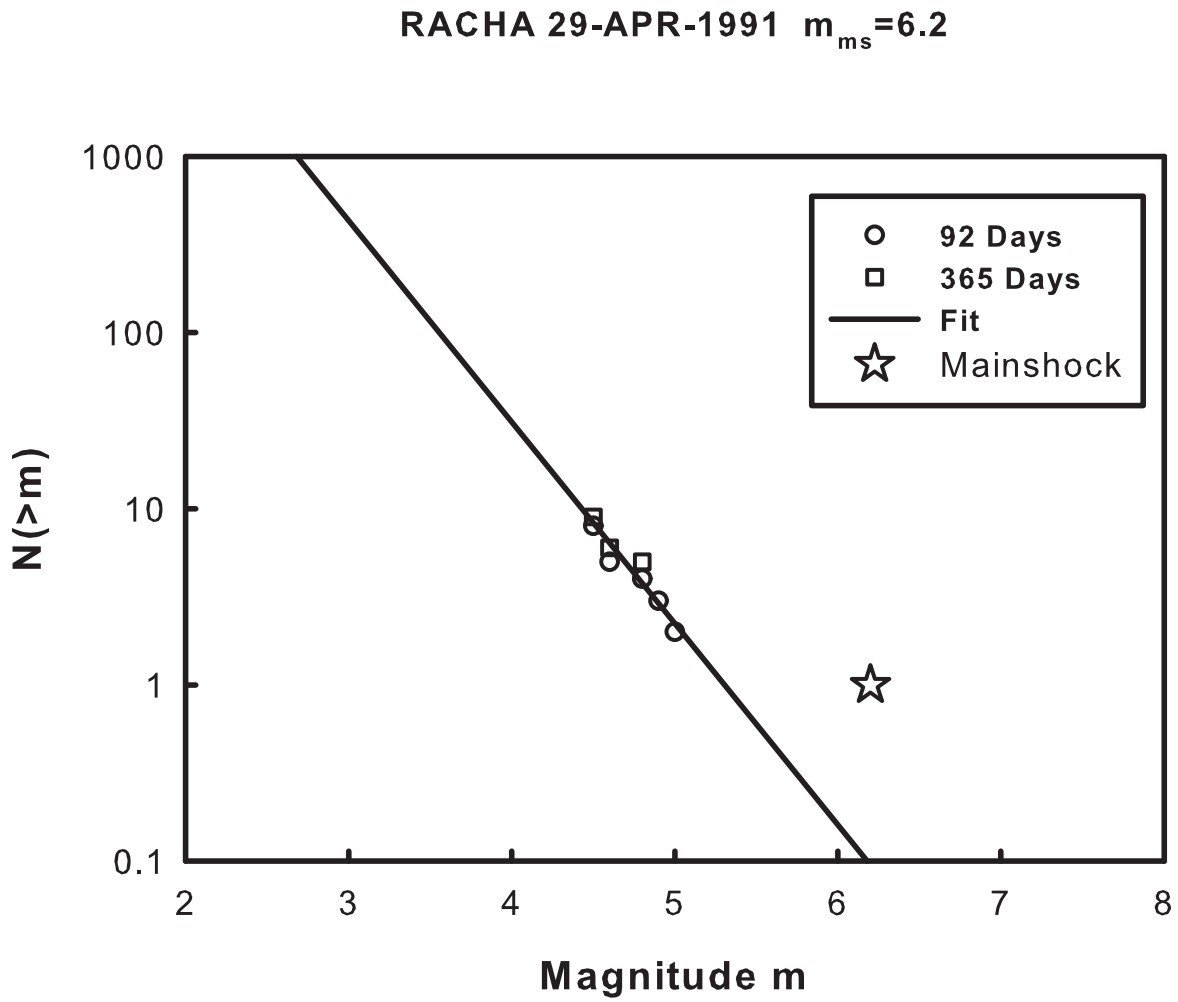

Figure 3.28. Frequency-magnitude distribution of Racha earthquake

The Racha earthquake with mainshock magnitude $m_{ms} = 6.2$ had the largest detected aftershock of magnitude ${m_{as}}^{max}$=5.0. From equation (2.11) the magnitude difference between the mainshock and the largest aftershock is Δm=1.2. We found b = 1.14 ±0.07 and a = 6.07 ±0.79 from correlation of the aftershock frequency magnitude data given in Figure 3.28 with G-R scaling. From equation (2.12) the inferred magnitude of the largest aftershock is m^* =5.31 ±1.03. From equation (2.13) the magnitude difference between the mainshock and the inferred largest aftershock is Δm^*=0.89 ±1.03. The Racha earthquake belongs to Caucasians fault system.

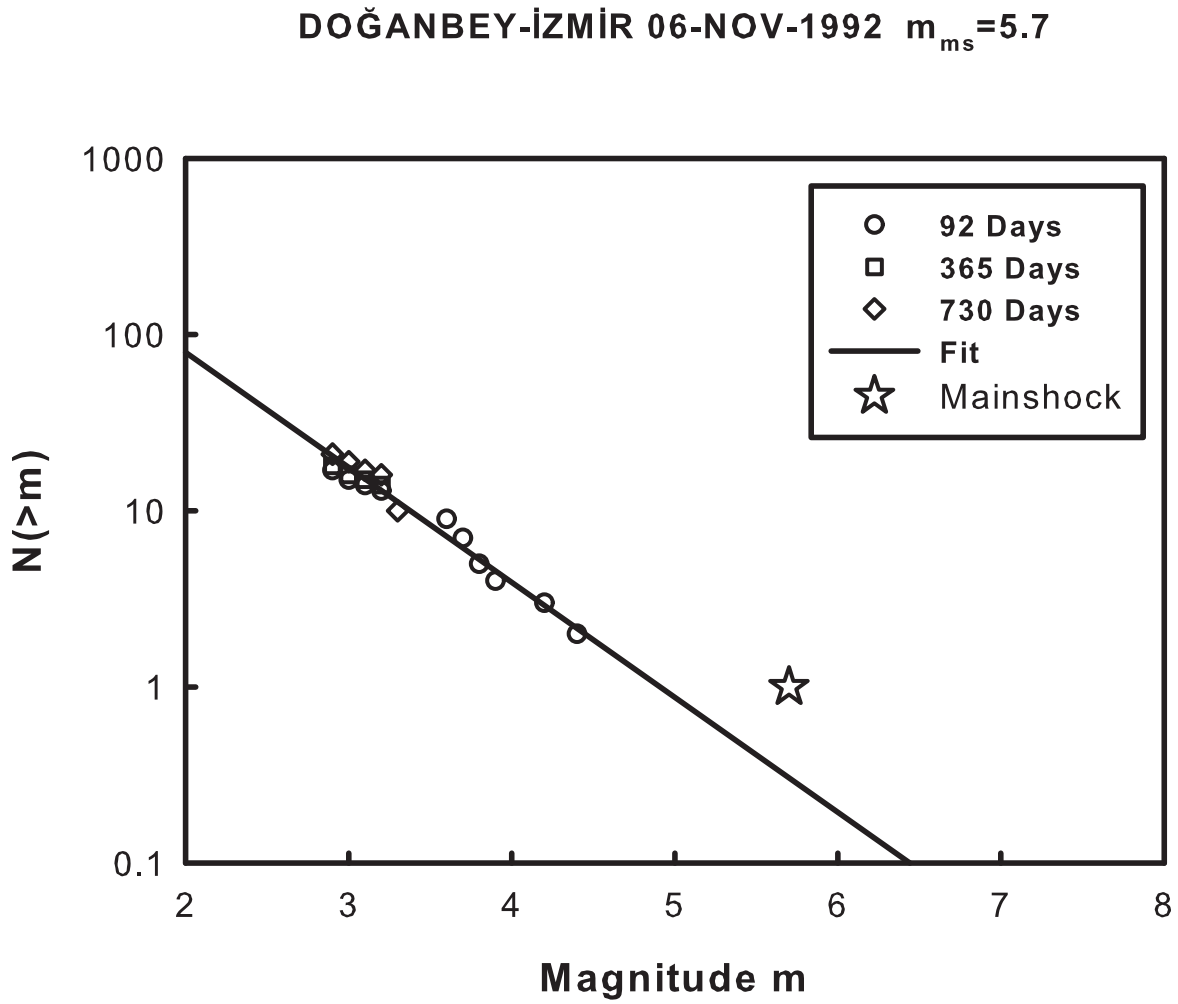

Figure 3.29. Frequency-magnitude distribution of Doğanbey-İzmir earthquake

The Doğanbey-İzmir earthquake with mainshock magnitude m_{ms} = 5.7 had the largest detected aftershock of magnitude ${m_{as}}^{max}$= 4.4. From equation (2.11) the magnitude difference between the mainshock and the largest aftershock is Δm=1.3. We found b =0.65 ± 0.04and a = 3.21 ±0.13 from correlation of the aftershock frequency magnitude data given in Figure 3.29 with G-R scaling. From equation (2.12) the inferred magnitude of the largest aftershock is m^* = 4.91 ±0.33. From equation (2.13) the magnitude difference between the mainshock and the inferred largest aftershock is Δm^*= 0.79±0.33. The Doğanbey-İzmir earthquake belongs to graben fault system.

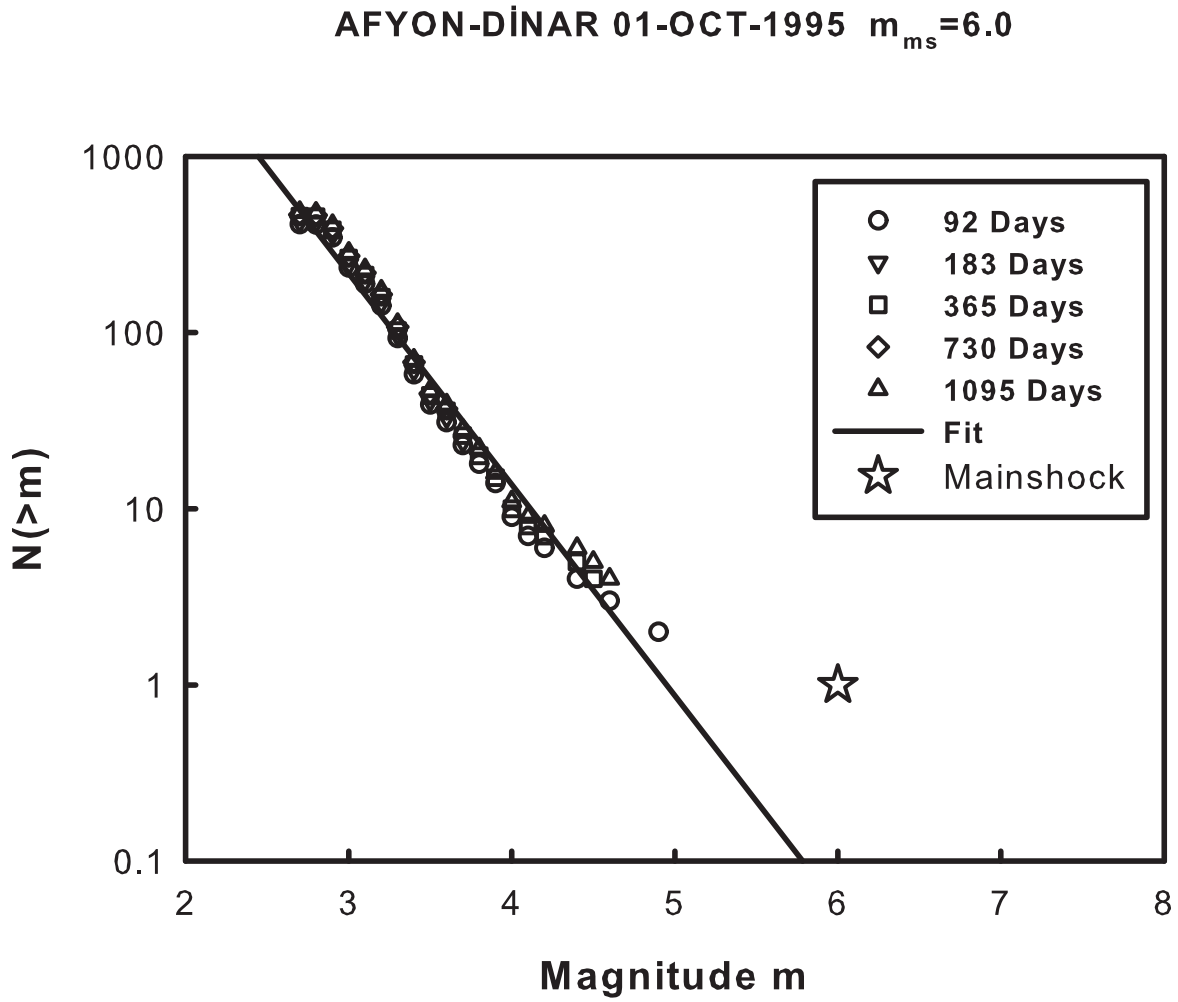

Figure 3.30. Frequency-magnitude distribution of Afyon-Dinar earthquake

The Afyon-Dinar earthquake with mainshock magnitude m_{ms} =6.0 had the largest detected aftershock of magnitude $m_{as}{}^{max}$= 4.9. From equation (2.11) the magnitude difference between the mainshock and the largest aftershock is Δm=1.1. We found b =1.20 ±0.04 and a = 5.93 ±0.15 from correlation of the aftershock frequency magnitude data given in Figure 3.30 with G-R scaling. From equation (2.12) the inferred magnitude of the largest aftershock is m^* = 4.95 ±0.20. From equation (2.13) the magnitude difference between the mainshock and the inferred largest aftershock is Δm^*= 1.05±0.20. The Afyon-Dinar earthquake belongs to graben fault system.

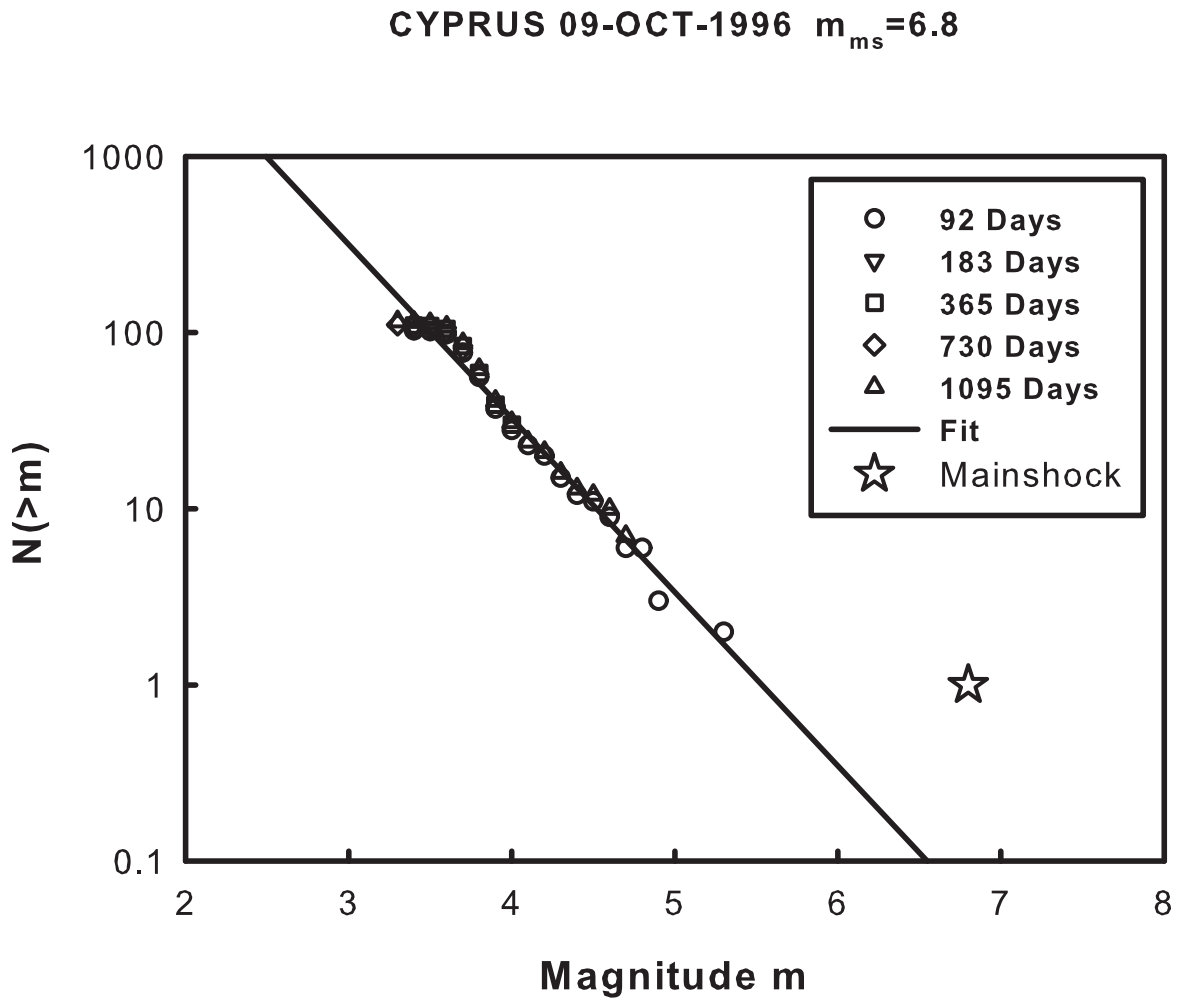

Figure 3.31. Frequency-magnitude distribution of Cyprus earthquake

The Cyprus earthquake with mainshock magnitude m_{ms} =6.8 had the largest detected aftershock of magnitude ${m_{as}}^{max}$=5.3. From equation (2.11) the magnitude difference between the mainshock and the largest aftershock is Δm=1.5. We found b = 0.99 ±0.03 and a = 5.46 ±0.14 from correlation of the aftershock frequency magnitude data given in Figure 3.31 with G-R scaling. From equation (2.12) the inferred magnitude of the largest aftershock is m^* =5.53 ±0.24. From equation (2.13) the magnitude difference between the mainshock and the inferred largest aftershock is Δm^*=1.27 ±0.24. The Cyprus earthquake belongs to Cyprus Arc Zone.

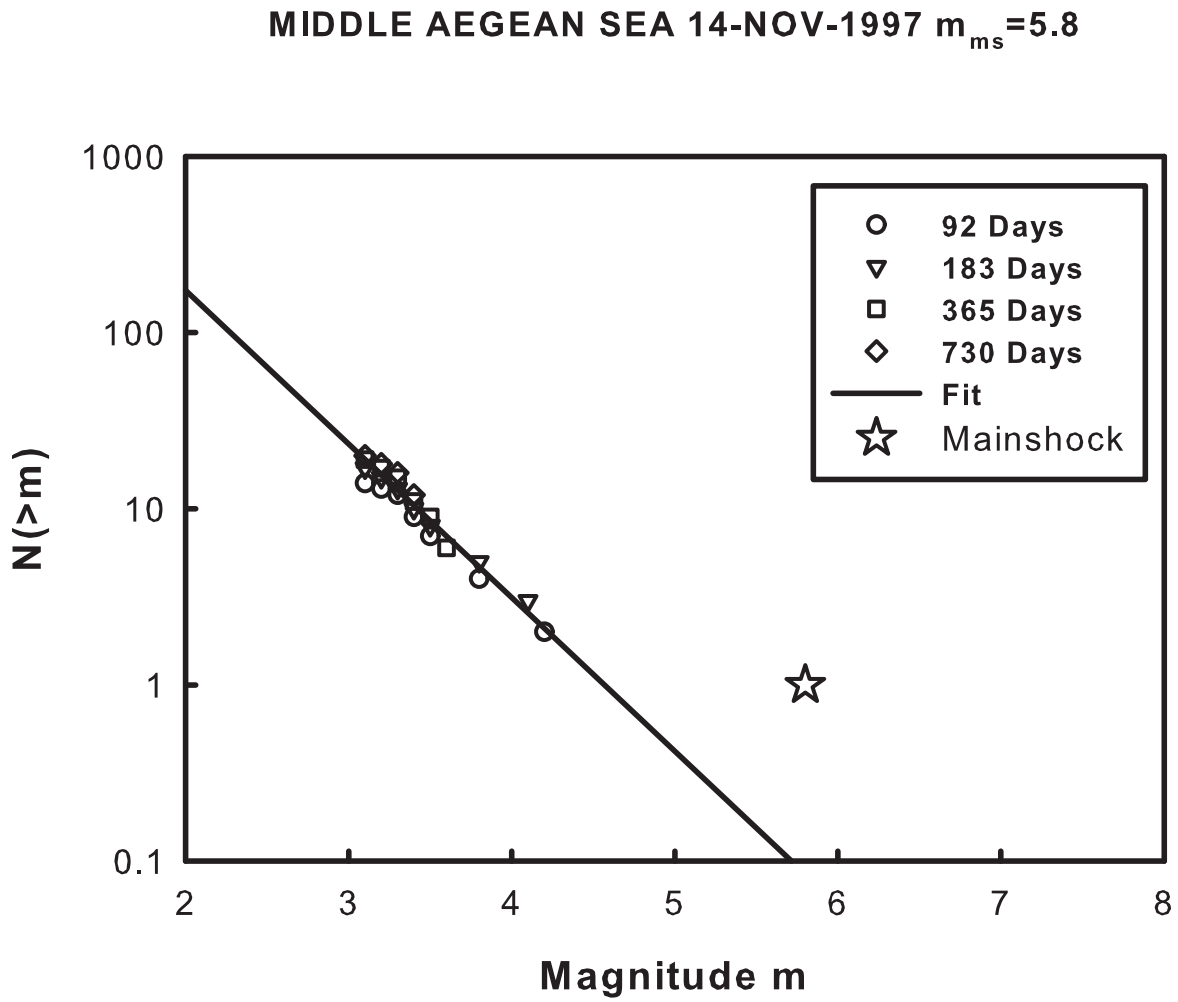

Figure 3.32. Frequency-magnitude distribution of Middle Aegean Sea earthquake

The Middle Aegean Sea earthquake with mainshock magnitude m_{ms} = 5.8 had the largest detected aftershock of magnitude ${m_{as}}^{max}$=4.2. From equation (2.11) the magnitude difference between the mainshock and the largest aftershock is Δm=1.6. We found b =0.87 ±0.04 and a = 3.99±0.14 from correlation of the aftershock frequency magnitude data given in Figure 3.32 with G-R scaling. From equation (2.12) the inferred magnitude of the largest aftershock is m^* = 4.57 ±0.27. From equation (2.13) the magnitude difference between the mainshock and the inferred largest aftershock is Δm^*=1.23 ±0.27. The Middle Aegean Sea earthquake belongs to graben fault system.

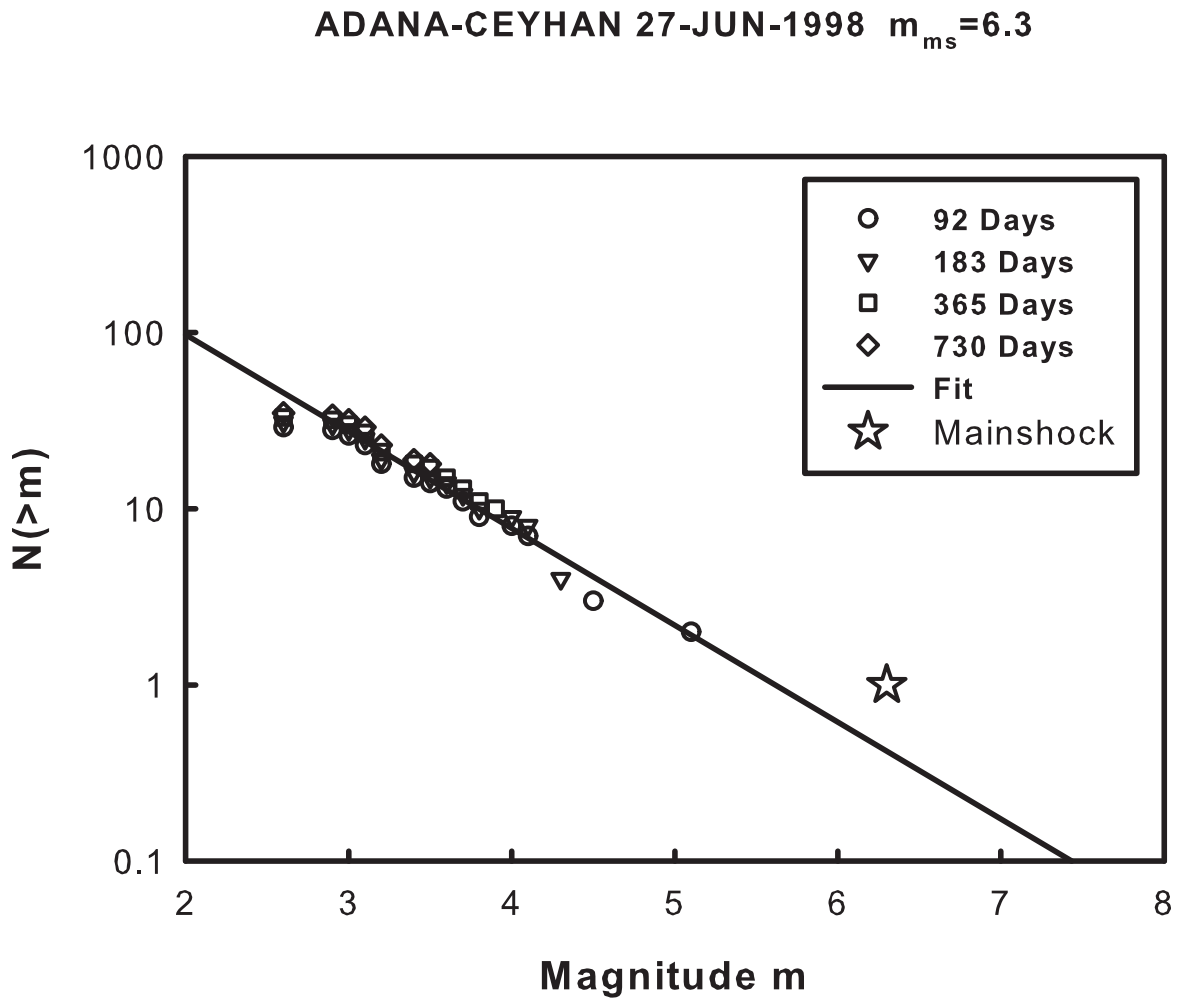

Figure 3.33. Frequency-magnitude distribution of Adana-Ceyhan earthquake

The Adana-Ceyhan earthquake with mainshock magnitude $m_{ms} = 6.3$ had the largest detected aftershock of magnitude ${m_{as}}^{max}$= 5.1. From equation (2.11) the magnitude difference between the mainshock and the largest aftershock is Δm=1.2. We found b = 0.55 $\pm$0.03 and a = 3.09 $\pm$0.11 from correlation of the aftershock frequency magnitude data given in Figure 3.33 with G-R scaling. From equation (2.12) the inferred magnitude of the largest aftershock is m^* = 5.62 $\pm$0.36. From equation (2.13) the magnitude difference between the mainshock and the inferred largest aftershock is Δm^*= 0.68$\pm$0.36. The Adana-Ceyhan earthquake belongs to East Anatolian Fault Zone.

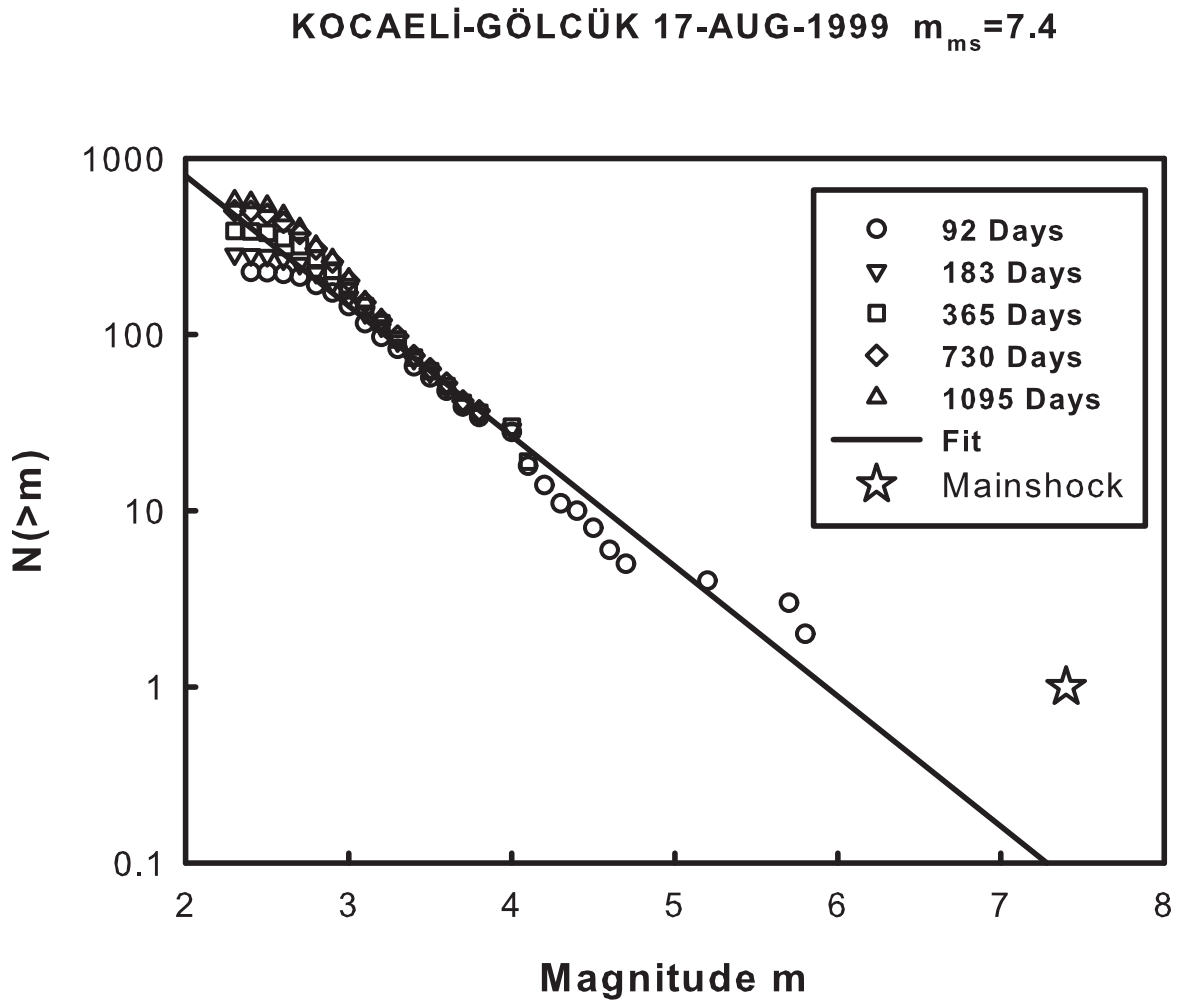

Figure 3.34. Frequency-magnitude distribution of Kocaeli-Gölcük earthquake

The Kocaeli-Gölcük earthquake with mainshock magnitude $m_{ms} = 7.4$ had the largest detected aftershock of magnitude ${m_{as}}^{max}$= 5.8. From equation (2.11) the magnitude difference between the mainshock and the largest aftershock is Δm=1.6. We found b = 0.74 ±0.03 and a = 4.38 ±0.10 from correlation of the aftershock frequency magnitude data given in Figure 3.34 with G-R scaling. From equation (2.12) the inferred magnitude of the largest aftershock is m^* =5.93 ±0.25. From equation (2.13) the magnitude difference between the mainshock and the inferred largest aftershock is Δm^*= 1.47±0.25. The Kocaeli-Gölcük earthquake belongs to North Anatolian Fault Zone.

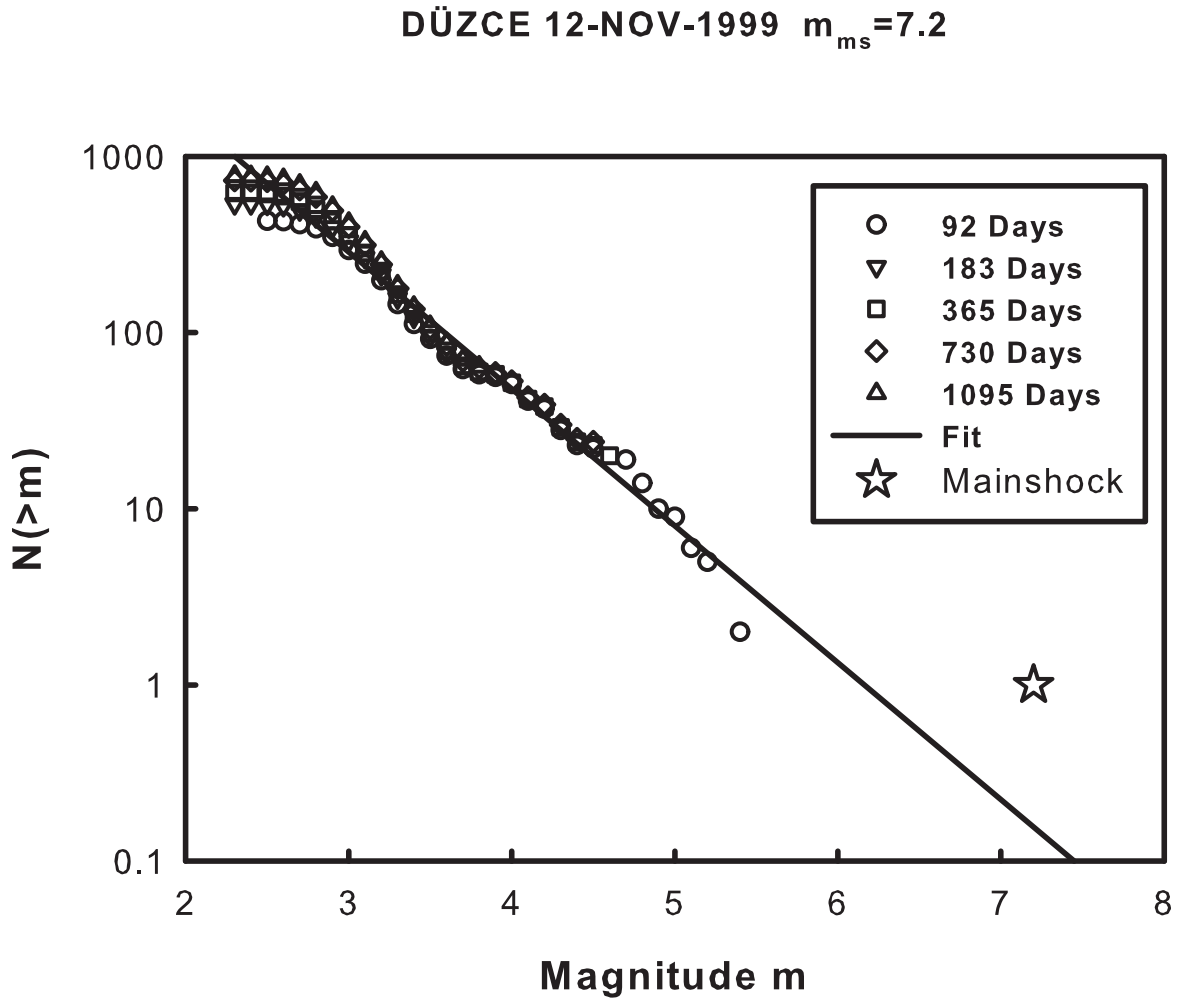

Figure 3.35. Frequency-magnitude distribution of Düzce earthquake

The Düzce earthquake with mainshock magnitude m_{ms} =7.2 had the largest detected aftershock of magnitude ${m_{as}}^{max}$= 5.4. From equation (2.11) the magnitude difference between the mainshock and the largest aftershock is Δm=1.8. We found b = 0.78±0.02 and a =4.79 ±0.08 from correlation of the aftershock frequency magnitude data given in Figure 3.35 with G-R scaling. From equation (2.12) the inferred magnitude of the largest aftershock is m^* = 6.16 ±0.18. From equation (2.13) the magnitude difference between the mainshock and the inferred largest aftershock is Δm^*=1.04 ±0.18. The Düzce earthquake belongs to North Anatolian Fault Zone.

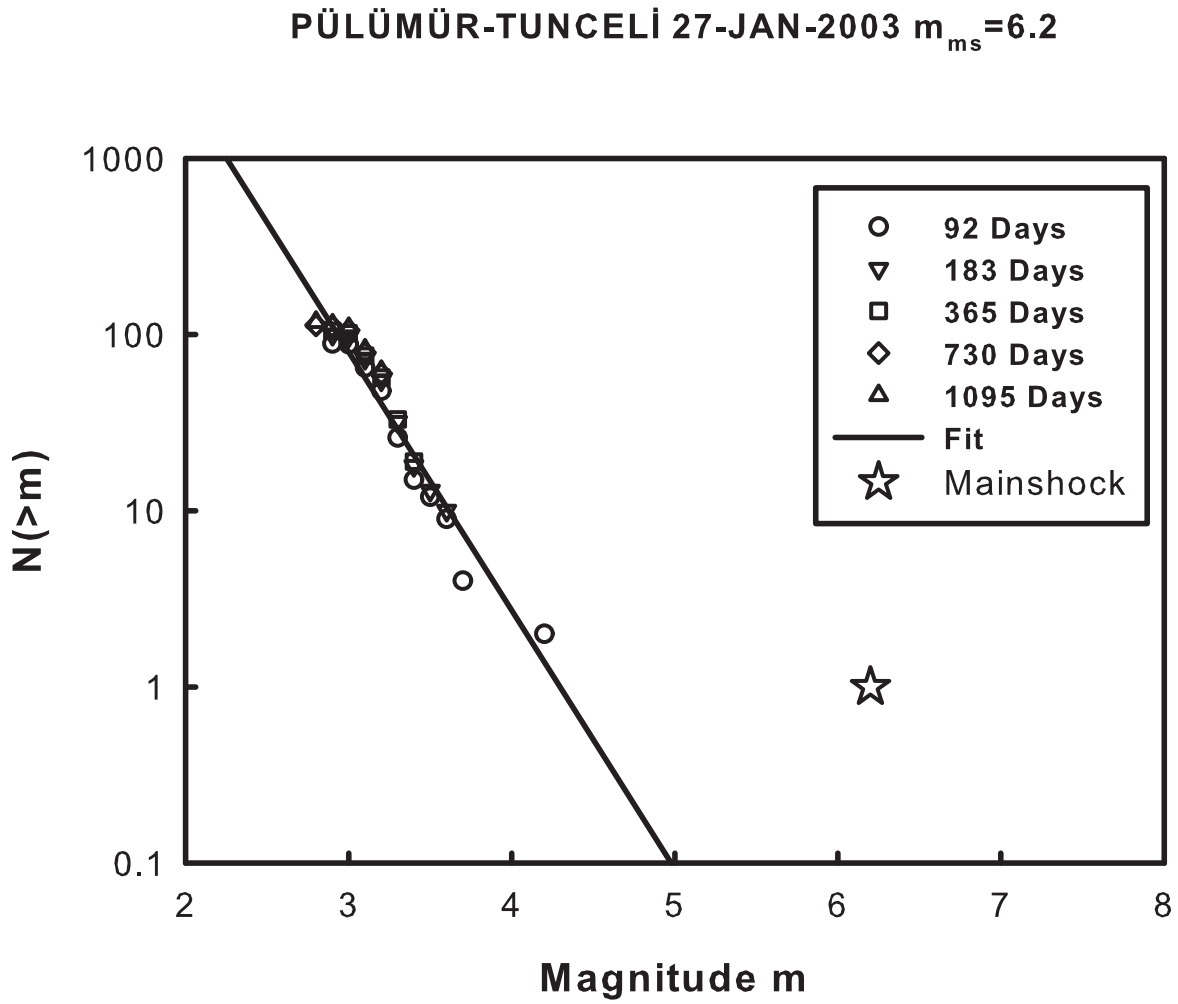

Figure 3.36. Frequency-magnitude distribution of Pülümür-Tunceli earthquake

The Pülümür-Tunceli earthquake with mainshock magnitude m_{ms} = 6.2 had the largest detected aftershock of magnitude ${m_{as}}^{max}$=4.2. From equation (2.11) the magnitude difference between the mainshock and the largest aftershock is Δm=2.0. We found b = 1.47 ±0.11 and a = 6.30±0.39 from correlation of the aftershock frequency magnitude data given in Figure 3.36 with G-R scaling. From equation (2.12) the inferred magnitude of the largest aftershock is m^* = 4.30 ±0.43. From equation (2.13) the magnitude difference between the mainshock and the inferred largest aftershock is Δm^*= 1.90±0.43. The Pülümür-Tunceli earthquake belongs to Pülümür Fault Zone.

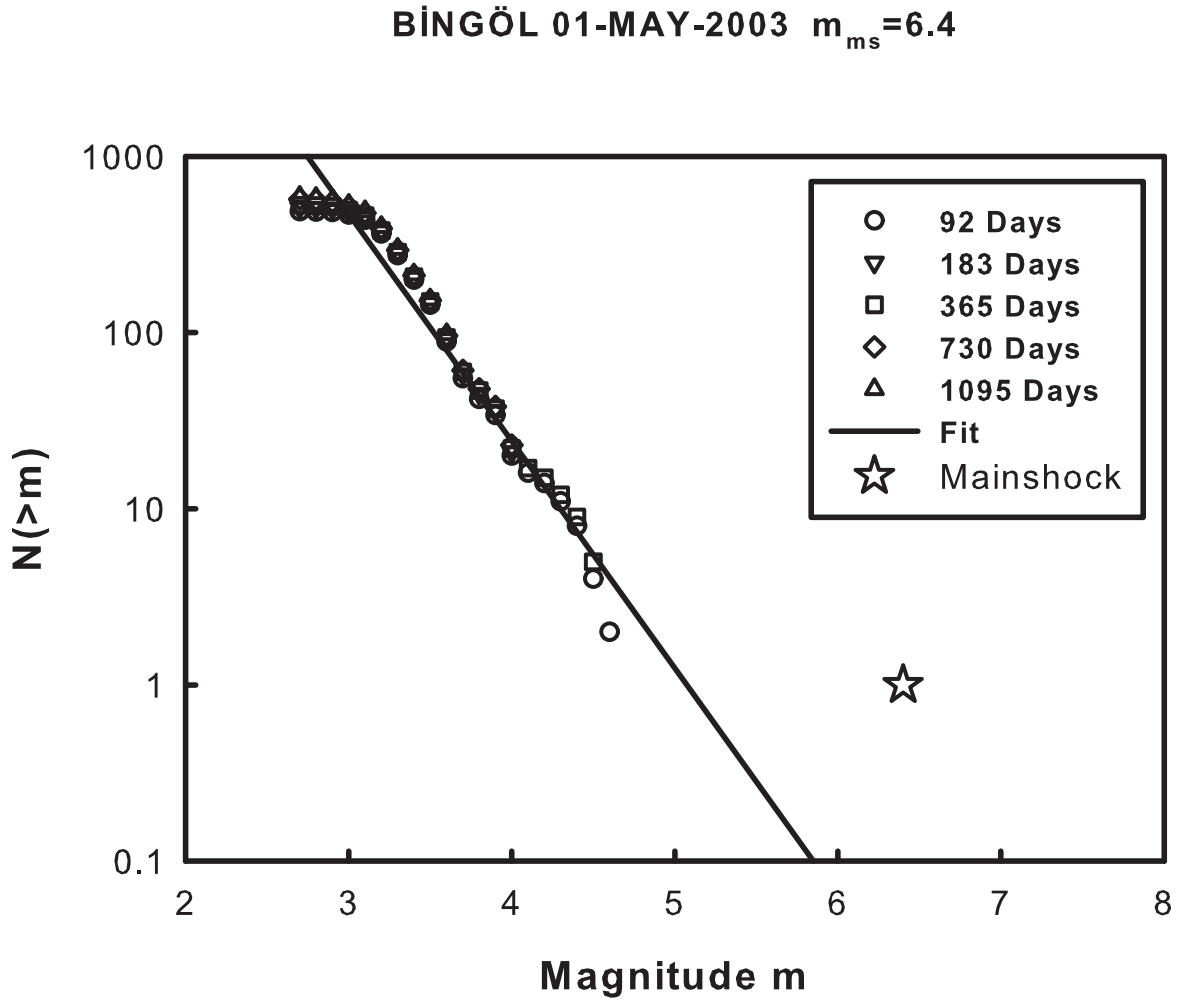

Figure 3.37. Frequency-magnitude distribution of Bingöl earthquake

The Bingöl earthquake with mainshock magnitude m_{ms} =6.4 had the largest detected aftershock of magnitude ${m_{as}}^{max}$= 4.6. From equation (2.11) the magnitude difference between the mainshock and the largest aftershock is Δm=1.8. We found b = 1.29 ±0.06 and a = 6.54 ±0.21 from correlation of the aftershock frequency magnitude data given in Figure 3.37 with G-R scaling. From equation (2.12) the inferred magnitude of the largest aftershock is m^* = 5.07±0.28. From equation (2.13) the magnitude difference between the mainshock and the inferred largest aftershock is Δm^*=1.33 ±0.28. The Bingöl earthquake belongs to Bingöl Hanoçayırı-Sudüğünü Fault Zone.

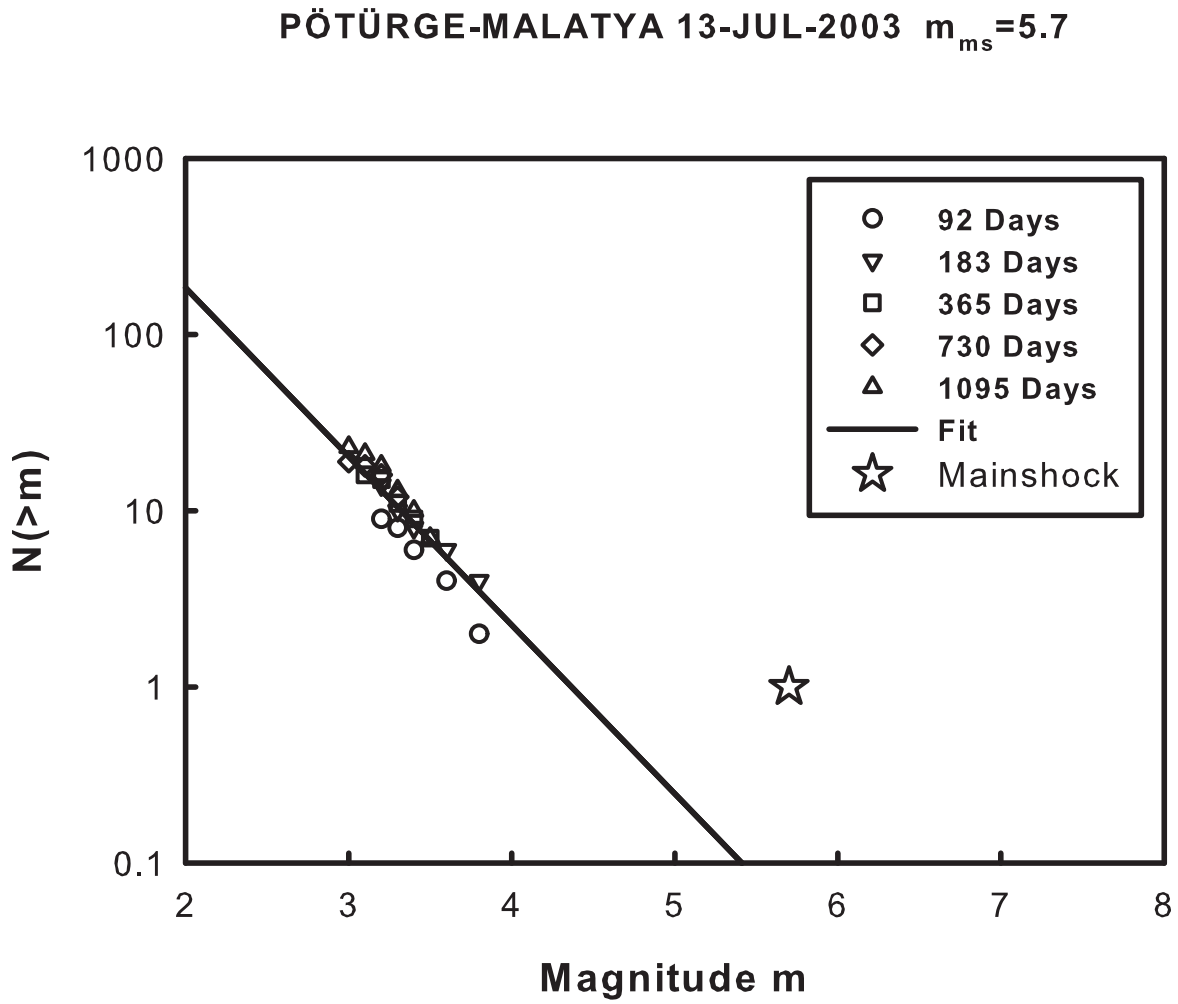

Figure 3.38. Frequency-magnitude distribution of Pötürge-Malatya earthquake

The Pötürge-Malatya earthquake with mainshock magnitude m_{ms} = 5.7 had the largest detected aftershock of magnitude ${m_{as}}^{max}$=4.8. From equation (2.11) the magnitude difference between the mainshock and the largest aftershock is Δm=0.9. We found b = 0.96 ±0.06 and a = 4.18 ±0.20 from correlation of the aftershock frequency magnitude data given in Figure 3.38 with G-R scaling. From equation (2.12) the inferred magnitude of the largest aftershock is m^* = 4.37 ±0.35. From equation (2.13) the magnitude difference between the mainshock and the inferred largest aftershock is Δm^*= 1.33±0.35. The Pötürge-Malatya earthquake belongs to Malatya-Pötürge Fault Zone.

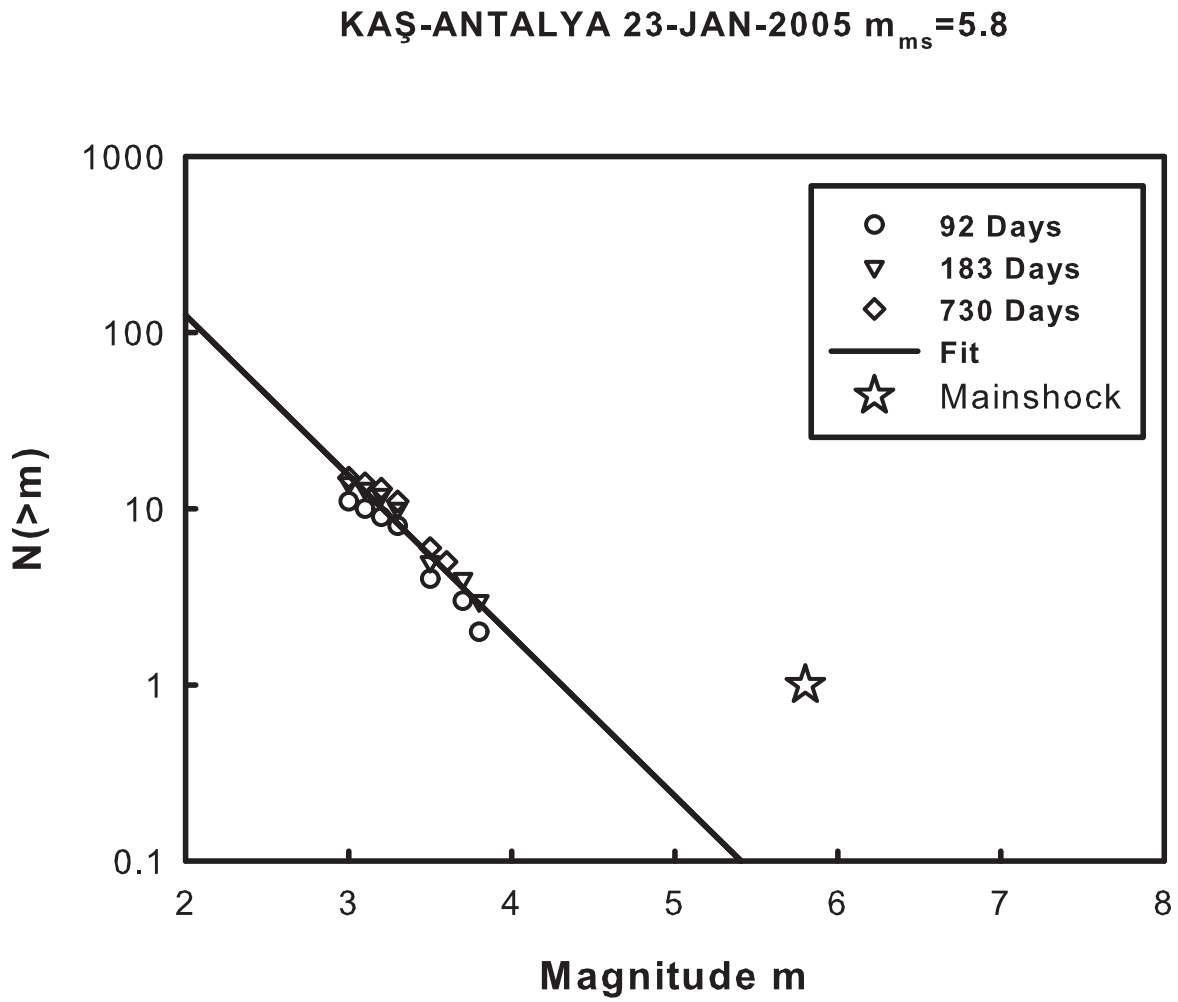

Figure 3.39. Frequency-magnitude distribution of Kaş-Antalya earthquake

The Kaş-Antalya earthquake with mainshock magnitude m_{ms} =5.8 had the largest detected aftershock of magnitude ${m_{as}}^{max}$= 4.3. From equation (2.11) the magnitude difference between the mainshock and the largest aftershock is Δm=1.5. We found b = 0.91 ±0.07 and a =3.92 ±0.24 from correlation of the aftershock frequency magnitude data given in Figure 3.39 with G-R scaling. From equation (2.12) the inferred magnitude of the largest aftershock is m^* = 4.31 ±0.43. From equation (2.13) the magnitude difference between the mainshock and the inferred largest aftershock is Δm^*=1.49 ±0.43. The Kaş-Antalya earthquake belongs to Crete-Rodos Arc Zone.

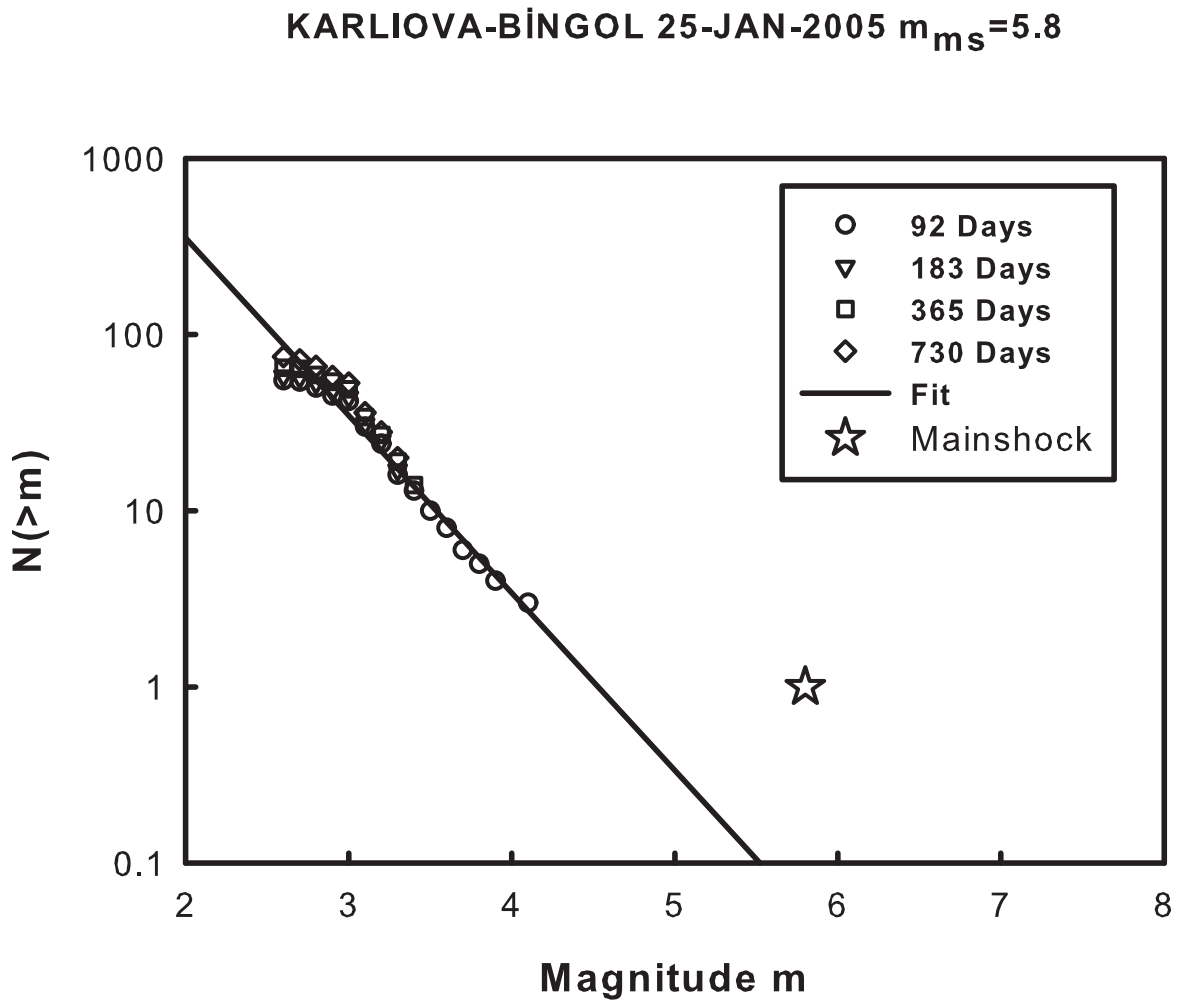

Figure 3.40. Frequency-magnitude distribution of Karlıova-Bingöl earthquake

The Karlıova-Bingöl earthquake with mainshock magnitude $m_{ms} = 5.8$ had the largest detected aftershock of magnitude ${m_{as}}^{max}$= 4.7. From equation (2.11) the magnitude difference between the mainshock and the largest aftershock is Δm= 1.1. We found b = 1.01±0.04 and a =4.56 ±0.14 from correlation of the aftershock frequency magnitude data given in Figure 3.40 with G-R scaling. From equation (2.12) the inferred magnitude of the largest aftershock is m^* = 4.53±0.23. From equation (2.13) the magnitude difference between the mainshock and the inferred largest aftershock is Δm^*=1.27 ±0.23. The Karlıova-Bingöl earthquake belongs to Çatak-Ilıpınar Fault Zone.

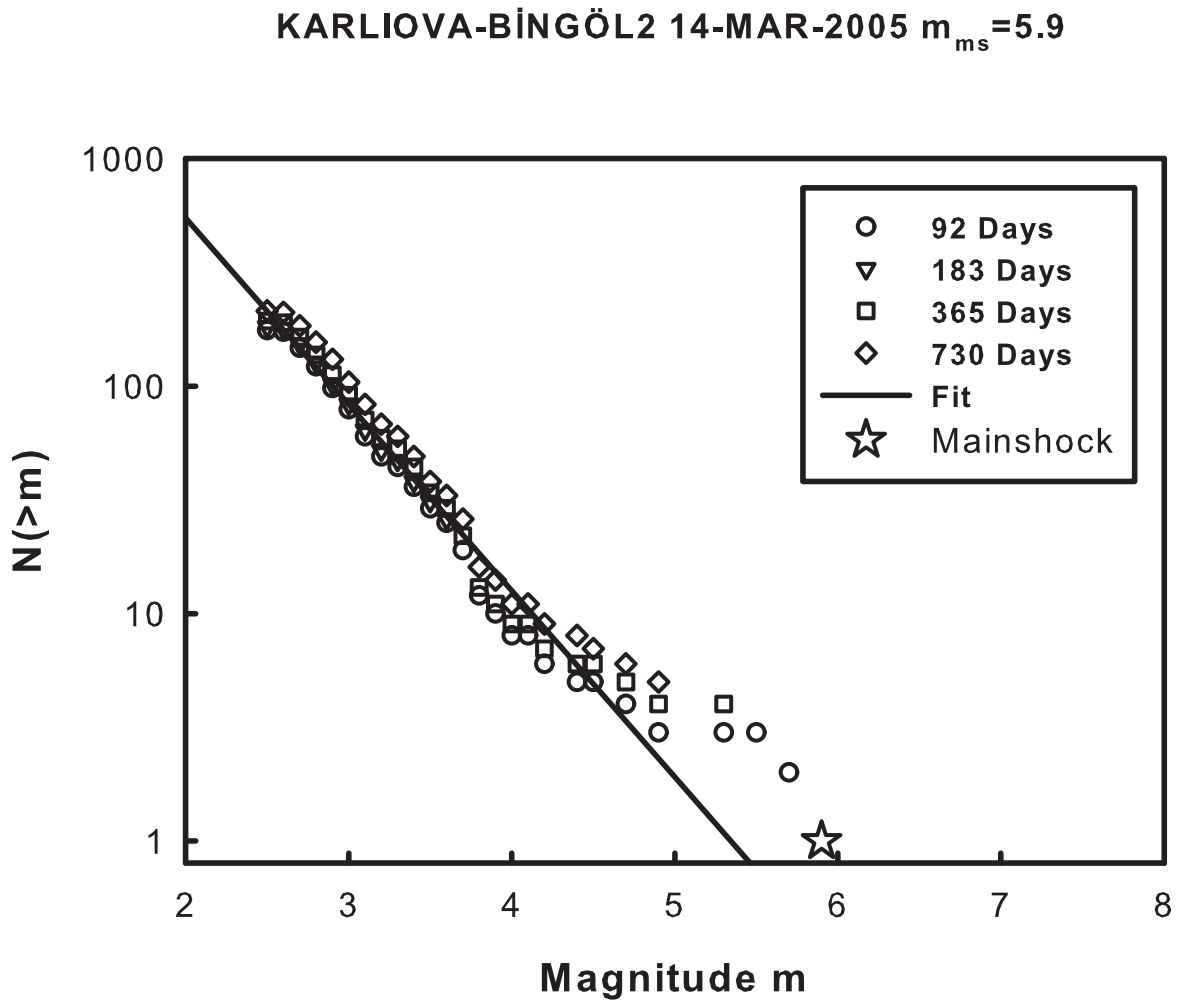

Figure 3.41. Frequency-magnitude distribution of Karlıova-Bingöl2 earthquake

The Karlıova-Bingöl2 earthquake with mainshock magnitude m_{ms} = 5.9 had the largest detected aftershock of magnitude $m_{as}{}^{max}$= 5.7. From equation (2.11) the magnitude difference between the mainshock and the largest aftershock is Δm= 0.2. We found b = 0.82 ±0.03 and a = 4.38 ±0.09 from correlation of the aftershock frequency magnitude data given in Figure 3.41 with G-R scaling. From equation (2.12) the inferred magnitude of the largest aftershock is m^* = 5.34 ±0.21. From equation (2.13) the magnitude difference between the mainshock and the inferred largest aftershock is Δm^*=0.56 ±0.21. The Karlıova-Bingöl2 earthquake belongs to Çatak-Ilıpınar Fault Zone.

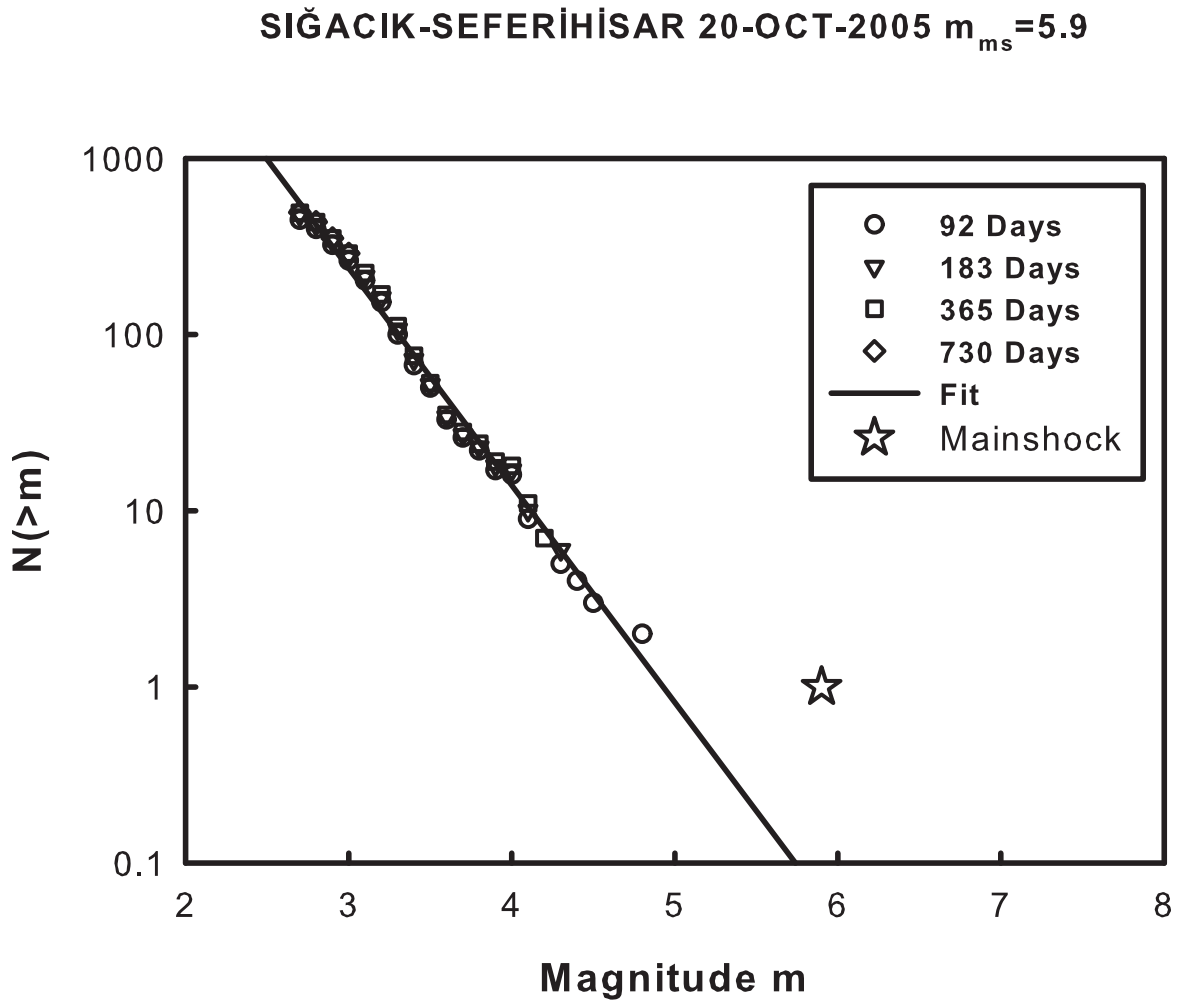

Figure 3.42. Frequency-magnitude distribution of Sığacık-Seferihisar earthquake

The Sığacık-Seferihisar earthquake with mainshock magnitude m_{ms} = 5.9 had the largest detected aftershock of magnitude ${m_{as}}^{max}$= 4.8. From equation (2.11) the magnitude difference between the mainshock and the largest aftershock is Δm= 1.1. We found b = 1.23 ±0.03 and a = 6.08 ±0.10 from correlation of the aftershock frequency magnitude data given in Figure 3.42 with G-R scaling. From equation (2.12) the inferred magnitude of the largest aftershock is m^* = 4.93 ± 0.13. From equation (2.13) the magnitude difference between the mainshock and the inferred largest aftershock is Δm^*=0.97 ±0.13. The Sığacık-Seferihisar earthquake belongs to Sığacık-Seferihisar Fault Zone.

The summary of our results are given in Table 3.5, 3.6, 3.7 and 3.8.

Table 3.5. a and b values of each earthquake

Earthquake	b	a
Bulgaria	0.45±0.03	3.26±0.13
Mürefte-Şarköy	0.28±0.03	2.05±0.16
Burdur	1.19±0.07	6.53±0.32
Aegean-12 Islands	0.68±0.06	3.98±0.29
Ukraine-Crimea	0.42±0.05	2.50±0.22
Plovdiv	0.60±0.03	3.75±0.15
Turkey-Iran Border	0.67±0.04	4.25±0.21
Gomati	0.71±0.05	4.60±0.24
Karpathos-12 Islands	0.97±0.12	5.61±0.60
Yenice-Gönen	0.81±0.06	4.72±0.28
Aegean Sea	1.03±0.09	6.00±0.44
Fethiye-Rodos	0.47±0.04	2.87±0.17
Bolu-Abant	0.47±0.04	3.14±0.21
Muş-Varto	1.01±0.14	5.60±0.67
Adapazarı-Mudurnusuyu Valley	0.85±0.06	4.93±0.28
Kütahya-Çavdarhisar	0.38±0.03	1.98±0.09
Diyarbakır-Lice	1.08±0.06	5.98±0.27
Mediterranean Sea-Crete Island	0.64±0.04	3.44±0.17
Thessaloniki	0.77±0.04	4.19±0.15
Karaburun-İzmir	1.08±0.09	5.07±0.32

Table 3.6. Continuation of Table 3.5.

Earthquake	b	a
Greece-Athens	0.90±0.02	5.01±0.06
Greece-Athens-2	0.94±0.03	5.21±0.14
Greece-Mount Athos	1.07±0.08	4.89±0.28
North Aegean Sea	1.41±0.10	6.69±0.39
Narman-Erzurum	0.81±0.07	4.41±0.32
Armenia-Spitak	0.76±0.07	4.38±0.35
Racha	1.14±0.17	6.07±0.79
Doğanbey-İzmir	0.65±0.04	3.21±0.13
Afyon-Dinar	1.20±0.04	5.93±0.15
Cyprus	0.99±0.03	5.46±0.14
Middle Aegean Sea	0.87±0.04	3.99±0.14
Adana-Ceyhan	0.55±0.03	3.09±0.11
Kocaeli-Gölcük	0.74±0.03	4.38±0.10
Düzce	0.78±0.02	4.79±0.08
Pülümür-Tunceli	1.47±0.11	6.30±0.39
Bingöl	1.29±0.06	6.54±0.21
Pötürge-Malatya	0.96±0.06	4.18±0.20
Kaş-Antalya	0.91±0.07	3.92±0.24
Karlıova-Bingöl	1.01±0.04	4.56±0.14
Karlıova-Bingöl2	0.82±0.03	4.38±0.09
Sığacık-Seferihisar	1.23±0.03	6.08±0.10

3.2. The Application of The Modified Form of Båth's Law to California

We analyzed 9 large earthquakes that occurred in California between 1987 and 2003 with magnitudes equal to or greater than $m_{ms} \geq 5.5$. We repeated exactly the same pro-

Table 3.7. m_{ms}, Δm, m^* and Δm^* values of each earthquake

Earthquake	m_{ms}	${m^{as}}_{max}$	Δm	m^*	Δm^*
Bulgaria	7.8	5.9	1.9	7.32±0.54	0.48±0.54
Mürefte-Şarköy	7.3	6.3	1.0	7.22±0.96	0.08±0.96
Burdur	6.9	5.2	1.7	5.49±0.40	1.41±0.40
Aegean-12 Islands	5.9	5.5	0.4	5.83±0.68	0.07±0.68
Ukraine-Crimea	6.0	5.7	0.3	5.89±0.91	0.11±0.91
Plovdiv	7.0	5.6	1.4	6.21±0.42	0.79±0.42
Turkey-Iran Border	7.6	6.3	1.3	6.35±0.51	1.25±0.51
Gomati	7.1	5.9	1.2	6.48±0.54	0.62±0.54
Karpathos-12 Islands	7.1	5.5	1.6	5.78±0.93	1.32±0.93
Yenice-Gönen	7.2	5.4	1.8	5.84±0.54	1.36±0.54
Aegean Sea	7.4	6.5	0.9	5.80±0.65	1.60±0.65
Fethiye-Rodos	7.1	5.9	1.2	6.16±0.62	0.94±0.62
Bolu-Abant	7.1	5.9	1.2	6.66±0.76	0.44±0.76
Muş-Varto	6.9	5.3	1.6	5.56±1.01	1.34±1.01
Adapazarı-Mudurnusuyu Valley	7.2	5.4	1.8	5.79±0.53	1.41±0.53
Kütahya-Çavdarhisar	5.7	5.0	0.7	5.15±0.46	0.55±0.46
Diyarbakır-Lice	7.8	5.2	2.6	5.55±0.39	2.25±0.39
Mediterranean Sea-Crete Island	5.8	4.9	0.9	5.37±0.41	0.43±0.41
Thessaloniki	6.1	4.7	1.4	5.42±0.34	0.68±0.34
Karaburun-İzmir	5.9	4.9	1.0	4.70±0.50	1.20±0.50

cess with Shcherbakov and Turcotte to test our method for finding the aftershock sequence. These are Superstition Hill earthquake with mainshock magnitude m_{ms}=6.6, Upland earthquake with mainshock magnitude m_{ms}=5.5, Sierra Madre earthquake with mainshock magnitude m_{ms}=5.8, Landers earthquake with mainshock magnitude m_{ms}=7.3, Northridge

Table 3.8. Continuation of Table 3.7.

Earthquake	m_{ms}	${m^{as}}_{max}$	Δm	m*	Δm*
Greece-Athens	5.7	5.3	0.4	5.58±0.12	0.12±0.12
Greece-Athens-2	5.8	5.4	0.4	5.52±0.25	0.28±0.25
Greece-Mount Athos	5.8	4.1	1.7	4.58±0.42	1.22±0.42
North Aegean Sea	6.0	4.5	1.5	4.76±0.44	1.24±0.44
Narman-Erzurum	6.0	5.1	0.9	5.45±0.60	0.55±0.60
Armenia-Spitak	6.0	5.8	0.2	5.76±0.73	0.24±0.73
Racha	6.2	5.0	1.2	5.31±1.03	0.89±1.03
Doğanbey-İzmir	5.7	4.4	1.3	4.91±0.33	0.79±0.33
Afyon-Dinar	6.0	4.9	1.1	4.95±0.20	1.05±0.20
Cyprus	6.8	5.3	1.5	5.53±0.24	1.27±0.24
Middle Aegean Sea	5.8	4.2	1.6	4.57±0.27	1.23±0.27
Adana-Ceyhan	6.3	5.1	1.2	5.62±0.36	0.68±0.36
Kocaeli-Gölcük	7.4	5.8	1.6	5.93±0.25	1.47±0.25
Düzce	7.2	5.4	1.8	6.16±0.18	1.04±0.18
Pülümür-Tunceli	6.2	4.2	2.0	4.30±0.43	1.90±0.43
Bingöl	6.4	4.6	1.8	5.07±0.28	1.33±0.28
Pötürge-Malatya	5.7	4.8	0.9	4.37±0.35	1.33±0.35
Kaş-Antalya	5.8	4.3	1.5	4.31±0.43	1.49±0.43
Karlıova-Bingöl	5.8	4.7	1.1	4.53±0.23	1.27±0.23
Karlıova-Bingöl2	5.9	5.7	0.2	5.34±0.21	0.56±0.21
Sığacık-Seferihisar	5.9	4.8	1.1	4.93±0.13	0.97±0.13

earthquake with mainshock magnitude m_{ms}=6.7, Ridgecrest earthquake with mainshock magnitude m_{ms}=5.8, Hector Mine earthquake with mainshock magnitude m_{ms}=7.1, Baja earthquake with mainshock magnitude m_{ms}=5.7, San Simeon earthquake with mainshock

magnitude m_{ms}=6.5. Summary of the data of California earthquake are given in Table 3.9, Table 3.10 and Table 3.11. Comparison of our data with Shcherbakov and Turcotte's data is given in Table 3.12.

Table 3.9. Date and m_{ms} values of California earthquakes

Earthquake	Date	m_{ms}
Superstition Hill	24-Nov-1987	6.60
Upland	28-Feb-1990	5.50
Sierra Madre	28-Jun-1991	5.80
Landers	28-Jun-1992	7.30
Northridge	17-Jan-1994	6.70
Ridgecrest	20-Sep-1995	5.80
Hector Mine	16-Oct-1999	7.10
Baja	22-Feb-2002	5.70
San Simeon	22-Dec-2003	6.50

Table 3.10. a and b values of California earthquake

Earthquake	b	a
Superstition Hill	1.05±0.02	5.40±0.05
Upland	0.92±0.03	4.39±0.09
Sierra Madre	0.53±0.01	2.61±0.03
Landers	0.88±0.01	5.71±0.03
Northridge	0.82±0.00	5.08±0.02
Ridgecrest	0.86±0.01	4.51±0.02
Hector Mine	0.94±0.01	5.55±0.03
Baja	1.11±0.03	4.88±0.08
San Simeon	1.03±0.02	5.34±0.07

Table 3.11. m_{ms}, Δm, m* and Δm* values of California earthquakes

Earthquake	m_{ms}	${m^{as}}_{max}$	Δm	m*	Δm*
Superstition Hill	6.60	4.70	1.90	5.12±0.09	1.48±0.09
Upland	5.50	4.70	0.80	4.80±0.17	0.70±0.17
Sierra Madre	5.80	4.30	1.50	4.87±0.11	0.93±0.11
Landers	7.30	6.30	1.00	6.46±0.05	0.84±0.05
Northridge	6.70	5.90	0.80	6.19±0.04	0.51±0.04
Ridgecrest	5.80	5.20	0.60	5.24±0.06	0.56±0.06
Hector Mine	7.10	5.80	1.30	5.90±0.06	1.20±0.06
Baja	5.70	4.10	1.60	4.39±0.13	1.31±0.13
San Simeon	6.50	4.70	1.80	5.16±0.12	1.34±0.12

The Northridge earthquake with mainshock magnitude $m_{ms} = 6.7$ had the largest detected aftershock of magnitude ${m_{as}}^{max}= 5.9$. From equation (2.11) the magnitude difference between the mainshock and the largest aftershock is $\Delta m = 0.8$. We found $b = 0.82 \pm 0.004$ and $a = 5.08 \pm 0.02$ from correlation of the aftershock frequency magnitude data given in Figure 3.43 with G-R scaling. From equation (2.12) the inferred magnitude of the largest aftershock is $m^* = 6.19 \pm 0.04$. From equation (2.13) the magnitude difference between the mainshock and the inferred largest aftershock is $\Delta m^* = 0.51 \pm 0.04$. The Northridge earthquake belongs to San Andreas Fault Zone.

3.3. Classification According to Fault Zones

The North Anatolian Fault Zone (NAFZ) is a major active right lateral strike-slip moving geologic fault in northern Anatolia which runs along the tectonic boundary between the Eurasian Plate and the Anatolian Plate. The fault extends westward from Karlıova, across northern Turkey and into the Mudurnu valley. The North Anatolian Fault is shown

Table 3.12. Comparison of our results with Shcherbakov and Turcotte's results for California earthquakes.

Earthquake	b	b(ST)	m^*	m^*(ST)	Δm^*	Δm^*(ST)
S. Hill	1.05±0.02	1.15±0.02	5.12±0.09	5.10±0.05	1.48±0.09	1.50±0.05
Upland	0.92±0.03	1.07±0.02	4.80±0.17	4.50±0.05	0.70±0.17	1.00±0.05
S. Madre	0.53±0.01	0.67±0.03	4.87±0.11	4.40±0.05	0.93±0.11	1.40±0.05
Landers	0.88±0.01	0.98±0.01	6.46±0.05	6.20±0.05	0.84±0.05	1.10±0.05
Northridge	0.82±0.00	0.95±0.02	6.19±0.04	6.10±0.05	0.51±0.04	0.60±0.05
Ridgecrest	0.86±0.01	1.00±0.01	5.24±0.06	5.05±0.05	0.56±0.06	0.75±0.05
Hector Mine	0.94±0.01	0.94±0.01	5.90±0.06	5.75±0.05	1.20±0.06	1.35±0.05
Baja	1.11±0.03	1.23±0.03	4.39±0.13	4.40±0.05	1.31±0.13	1.30±0.05
San Simeon	1.03±0.02	1.02±0.03	5.16±0.12	5.35±0.05	1.34±0.12	1.15±0.03

in Figure 3.44. The North Anatolian Fault is one of the most active and important faults in the world. Its length is approximately 1200 km and its width changes between 100 m and 10 km. Eight of our earthquakes take place on the North Anatolian Fault Zone. They are Mürefte-Şarköy, Yenice-Gönen, Bolu Abant, Adapazarı-Mudurnusuyu Valley, Kocaeli-Gölcük, Düzce, Karlıova-Bingöl1 and Karlıova-Bingöl2 earthquakes.

The East Anatolian Fault is a major geologic fault in eastern Turkey. It runs along the tectonic boundary between the Anatolian Plate and the northward-moving Arabian Plate. The difference in the relative motions of the two plates is manifest in the left lateral motion along the fault. The East Anatolian Fault runs in a northeasterly direction, starting from the Maraş Triple Junction at the northern end of the Dead Sea Transform, and ending at the Karlıova Triple Junction where it meets the North Anatolian Fault. The East Anatolian Fault is shown in Figure 3.44. Together with North Anatolian Fault Zone it undertakes westward escape of the Anatolian block. So, it has an important role

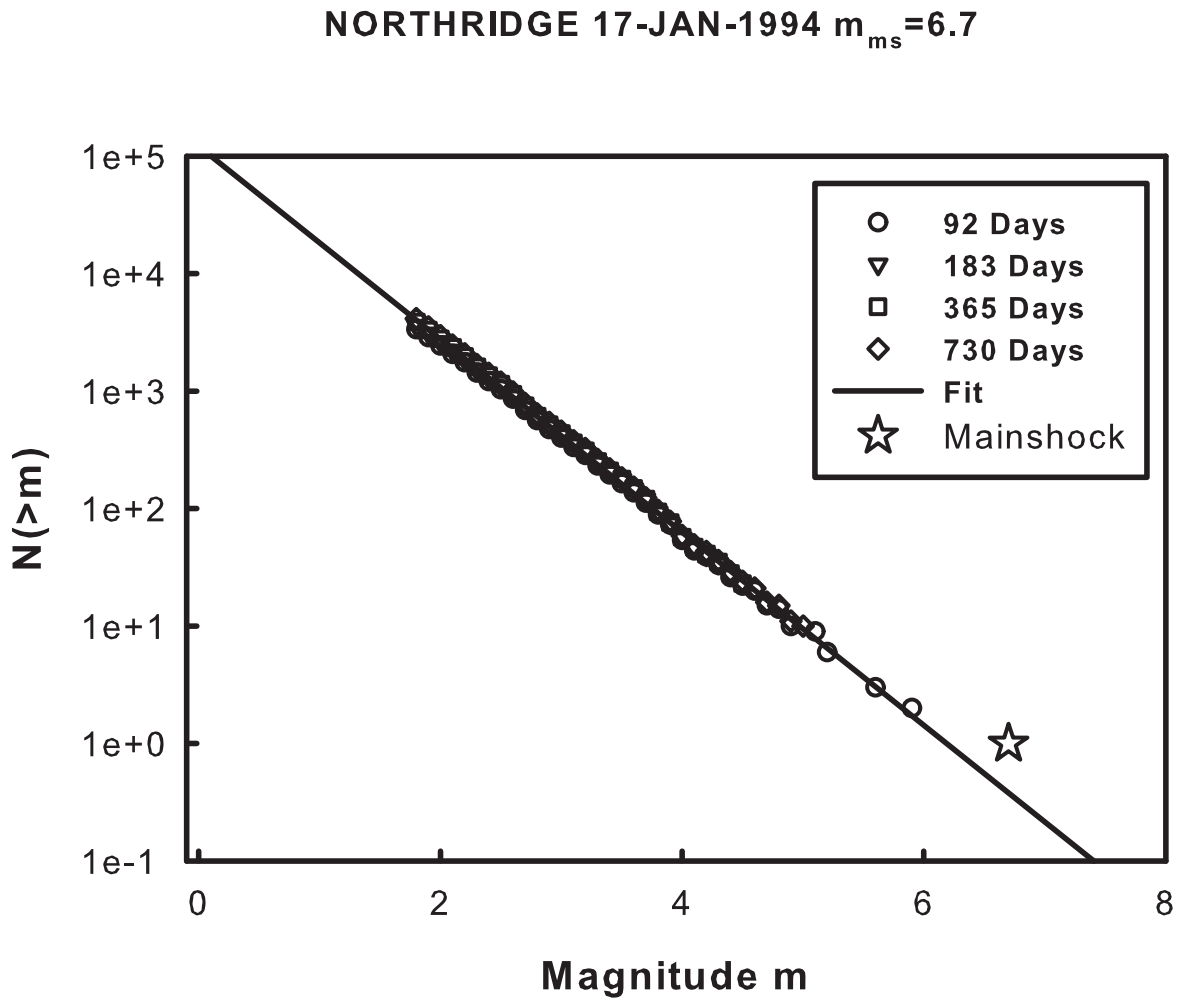

Figure 3.43. Frequency-magnitude distribution of Northridge earthquake

in the recent tectonics of the Eastern Mediterranean region. EAFZ is about 450 km-long in NE-SW trend. Three of our earthquakes take place on the East Anatolian Fault Zone. They are Turkey-Iran Border, Adana-Ceyhan and Pötürge-Malatya earthquakes. Narman-Erzurum earthquake takes place on the Erzurum Fault Zone which is left-lateral strike-slip fault zone. It shows the same characteristics with EAFZ, so we put Narman-Erzurum earthquake in the same category with the earthquakes that takes place on EAFZ.

Aegean Graben System consists of several grabens and horsts. From north to west,

Figure 3.44. Active fault map of Turkey [16].

these grabens are Edremit Bay, Bakırçay-Simav, Gediz-Küçük Menderes, Büyük Menderes, Gökova Bay. Aegean Graben system is exhibiting very complex tectonic structure in terms of plate tectonics. Aegean Graben System is shown in Figure 3.44. Fourteen of our earthquakes take place on Aegean Graben System. They are Burdur, Plovdiv, Gomati, Kütahya-Çavdarhisar, Thessaloniki, Karaburun-İzmir, Greece-Athens, Greece-Athens-2, Greece-Mount Athos, North Aegean Sea, Doğanbey-İzmir, Afyon-Dinar, Middle Aegean Sea and Sığacık-Seferihisar earthquakes. Bulgaria earthquake also took place on graben system in Bulgaria, so we put it in the same category with the earthquakes that take place on Aegean Graben System.

Cyprus arc extends from the Gulf of Antalya in the west, and the Gulf of İskenderun in the east, meets the Hellenic arc in the westernmost corner of Cyprus and joins the Eastern Anatolian Fault in the east. Cyprus arc zone is shown in Figure 3.44. There are many earthquakes that take place on the Hellenic arc in our analysis. We put these earthquakes in the same category with the earthquakes take place on the Cyprus Arc, because they

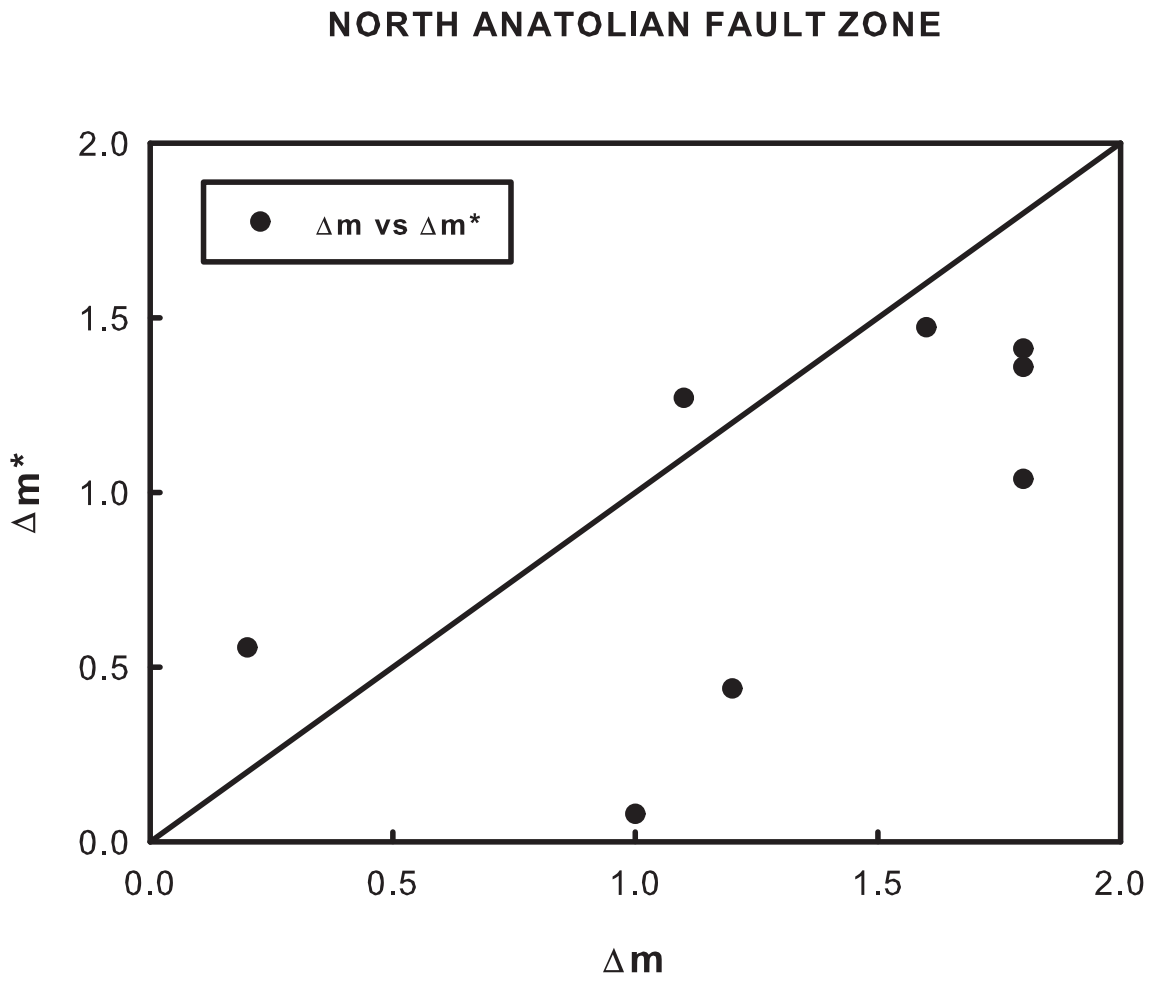

Figure 3.45. The Δm versus Δm^* graph of North Anatolian Fault Zone.

show same characteristics. Seven of them are in this category. They are Fethiye-Rodos, Kaş-Antalya, Aegean-12 Islands, Karpathos-12 Islands, Aegean Sea, Mediterrian Sea-Crete Island and Cyprus earthquakes.

South-East Anatolian Fault Zone extends from İskenderun bay to east part of Van. Hatay, Kahramanmaraş, Adıyaman, Malatya, Elazığ, Bitlis and Van are in this zone. South-East Anatolian Fault Zone meet the North Anatolian Fault Zone around the Bingöl-Karlıova. South-East Anatolian Fault is shown in Figure 3.44. Diyarbakır-Lice and Muş-Varto earthquakes took place on the South-East Anatolian Fault Zone. Armenia-Spitak

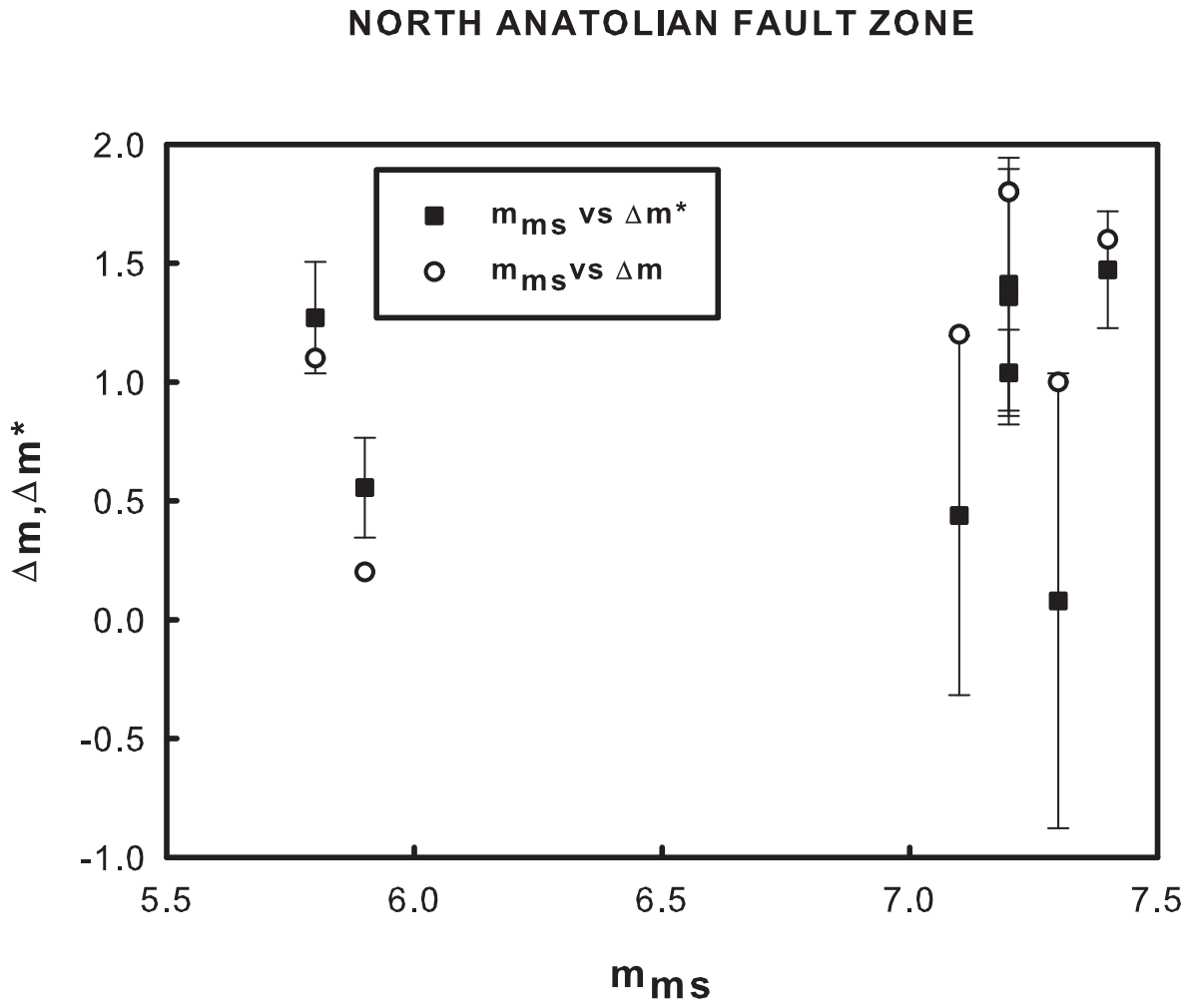

Figure 3.46. The Δm, Δm^* versus m_{ms} graph of North Anatolian Fault Zone.

and Racha earthquakes take place in Caucasians. We could not put them in any category. And Ukraine-Crimea earthquake could not be also put in any category because we do not have any information about the tectonic nature of the Ukraine.

The data of our classification are given in Table 3.13.

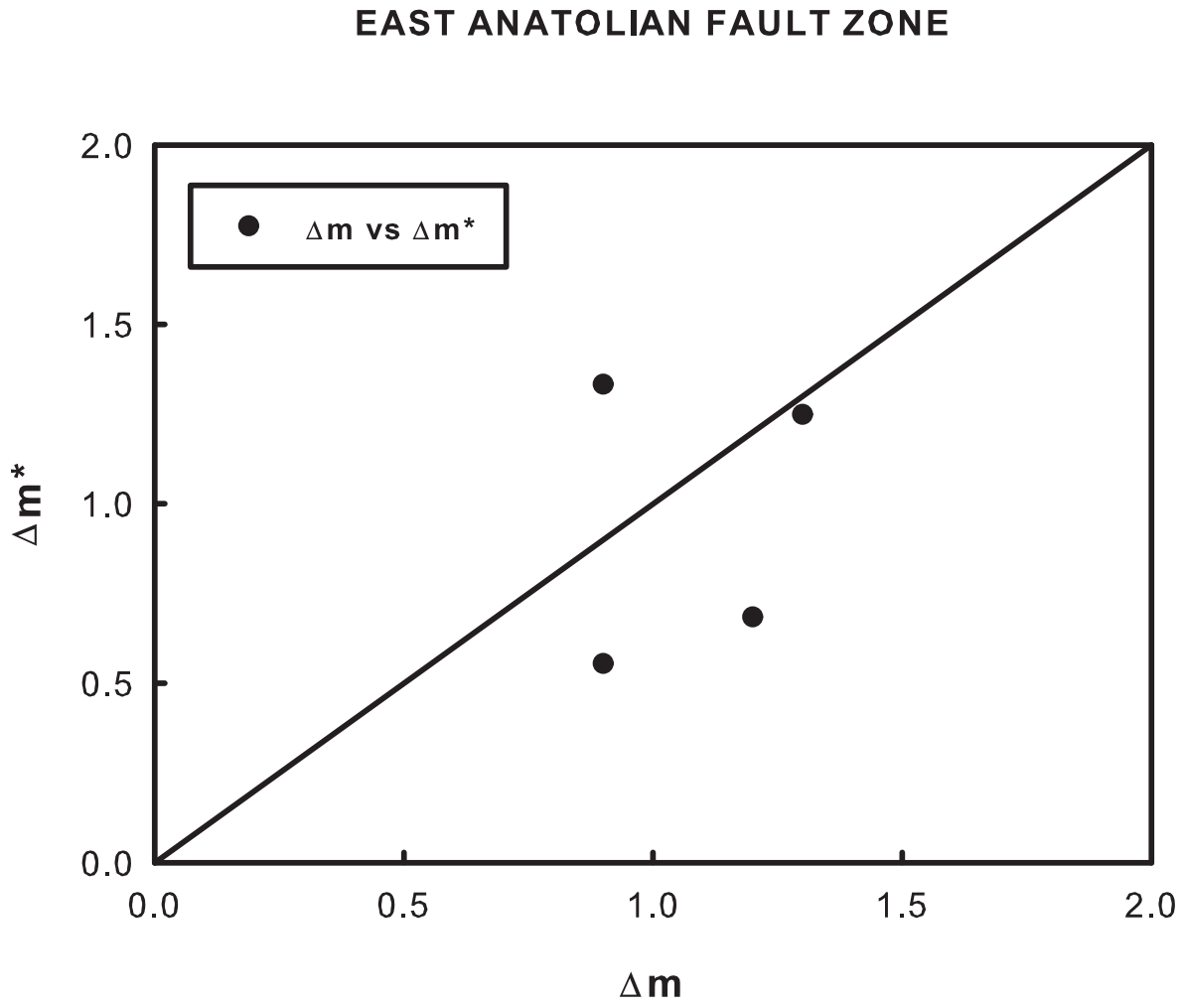

Figure 3.47. The Δm versus Δm^* graph of East Anatolian Fault Zone.

Table 3.13. Results of classifications

Parameters	NAFZ	EAFZ	Aegean Graben S.	Cyprus Arc Z.	SEAFZ
$\overline{\Delta m}$	1.31±0.52	1.08±0.18	1.23±0.44	1.14±0.40	2.10±0.5
$\overline{\Delta m^*}$	0.95±0.46	0.96±0.45	0.84±0.36	1.02±0.57	1.80±0.70
$\overline{b}$	0.72±0.04	0.75±0.05	0.90±0.05	0.81±0.06	1.04±0.10

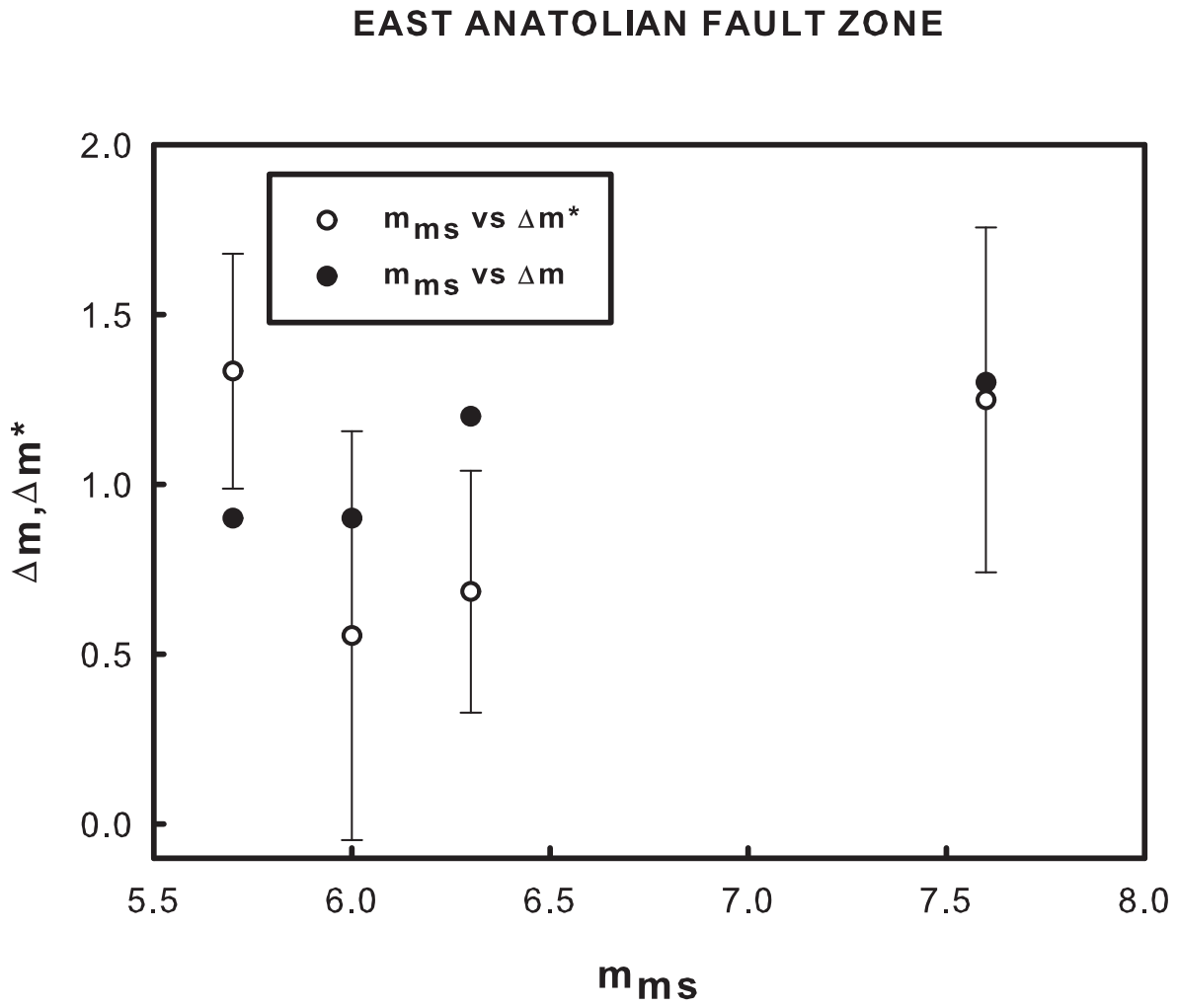

Figure 3.48. The Δm, Δm^* versus m_{ms} graph of East Anatolian Fault Zone.

3.4. GREECE CATALOG ANALYSIS

We analyzed 41 earthquakes that occurred in and near Turkey in this thesis. We wanted to check our data with other catalogs. Some earthquakes of our analysis occurred in Greece. Then we used catalog provided by Institute of Geodynamics National Observatory of Athens to make same analysis for Greece earthquakes [9]. Greece catalog provided data of earthquake that occurred between 1950 and 2008. There are 6 earthquakes that occurred in Greece in our analysis. They are Aegean Sea, Greece-Athens, Greece-Athens-2, Greece-

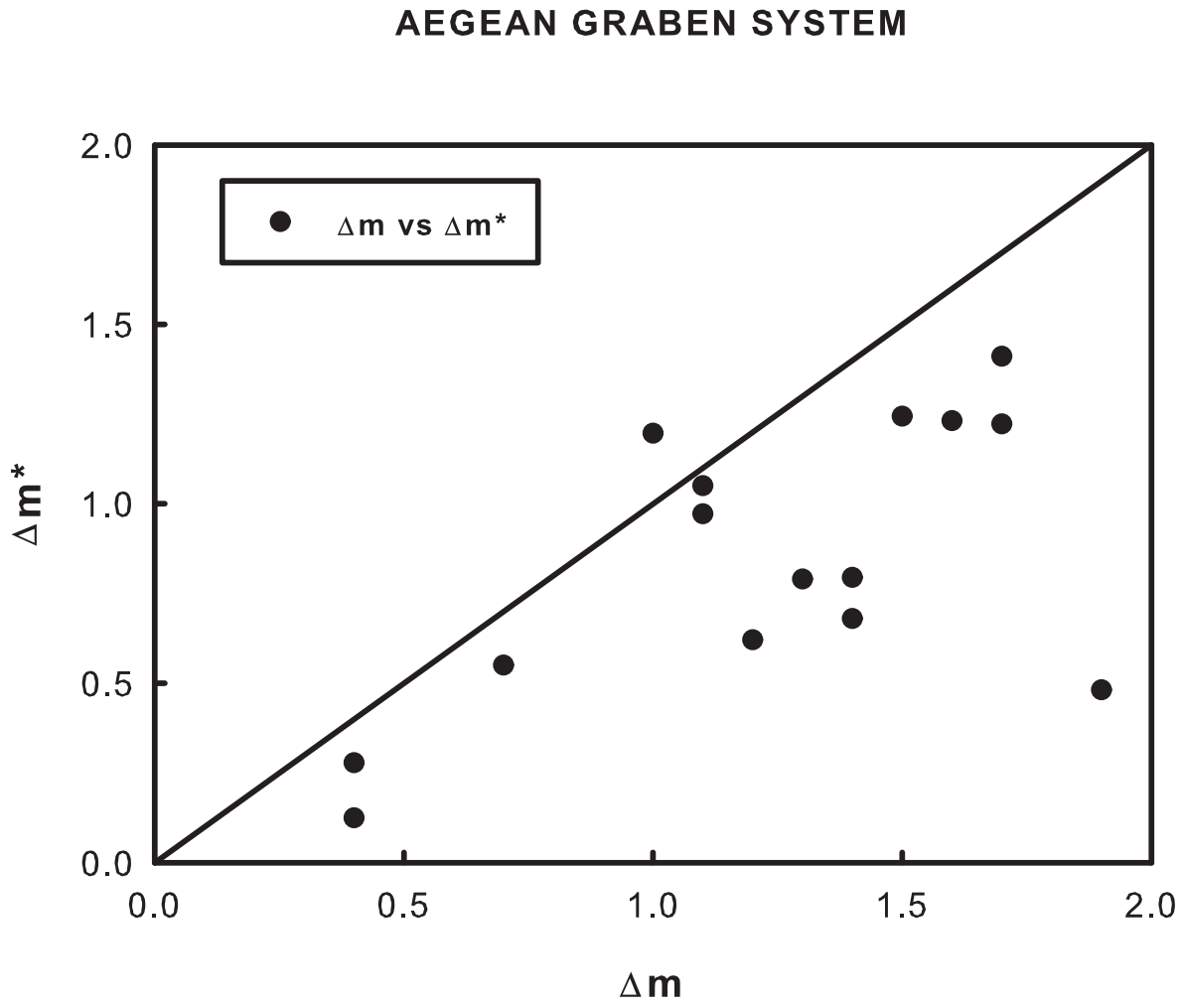

Figure 3.49. The Δm versus Δm^* graph of Aegean Graben System.

Mount Athos, North Aegean Sea, Middle Aegean Sea earthquakes. The graph of North Aegean Sea earthquake is given in Figure 3.55. The results of all earthquakes that were analysied by using Greece catalog are given in Table 3.14 and comparison of our catalog's results and Greece catalog's results is given in Table 3.15 and Table 3.16. Surface-wave magnitude m_s was given in years between 1950 and 1963 and Richter magnitude M_L was given in years between 1963 and 2000 in Greece catalog.

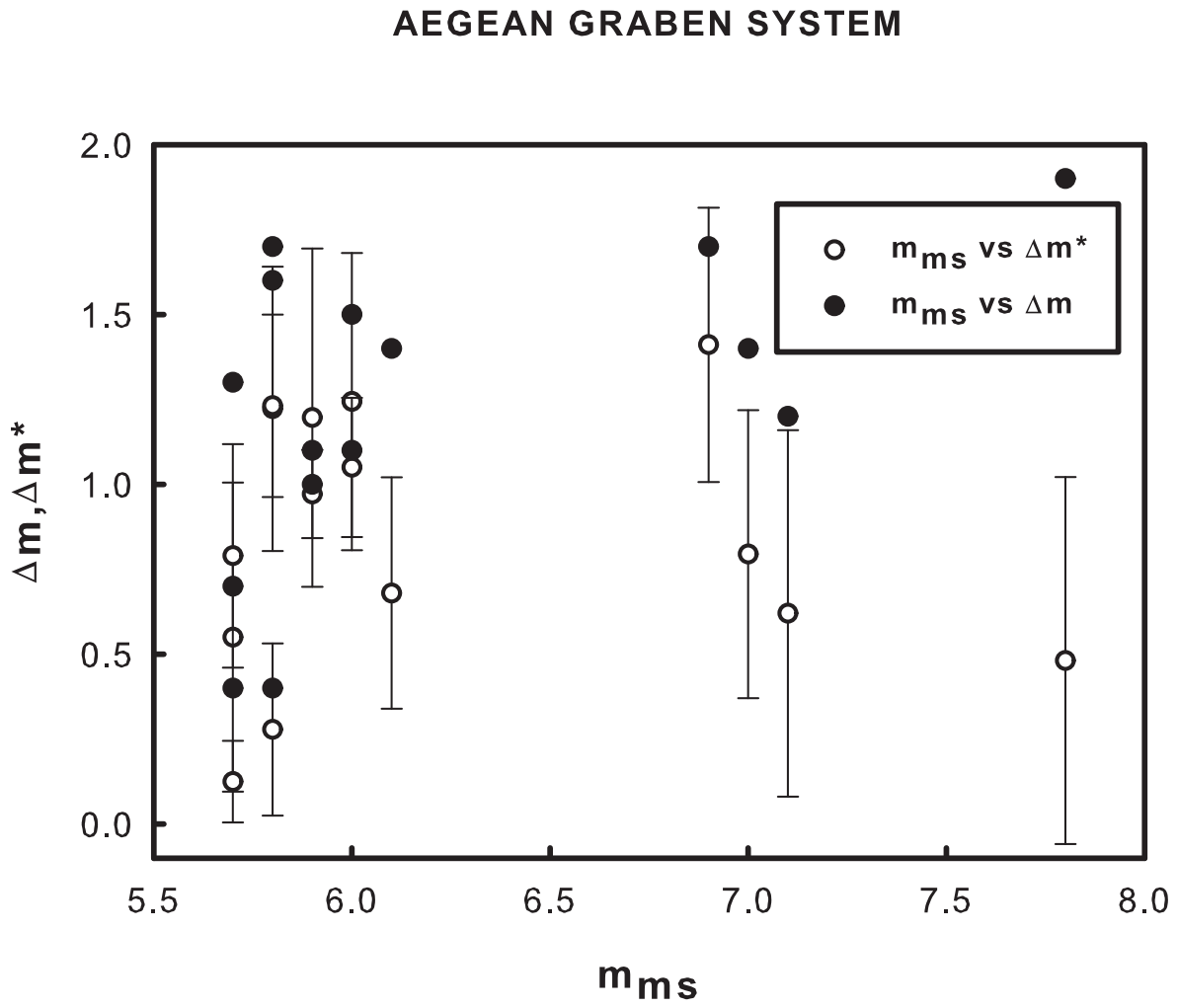

Figure 3.50. The Δm, Δm^* versus m_{ms} graph of Aegean Graben System.

3.5. U.S. CATALOG ANALYSIS

We used U.S. Geological Survey Earthquake Database to check our data with the other catalogs [8]. We did the same analysis for some earthquakes in Turkey by using U.S. catalog. They are Diyarbakır-Lice, Thessaloniki, Greece-Athens-2, Greece Mount Athos, North Aegean Sea, Doğanbey-İzmir, Afyon-Dinar, Cyprus, Middle Aegean Sea, Adana-Ceyhan, Düzce and Sığacık-Seferihisar earthquakes. The graph of Düzce earthquake is given in Figure 3.56. The results of all earthquakes that were analyzed by using U.S.

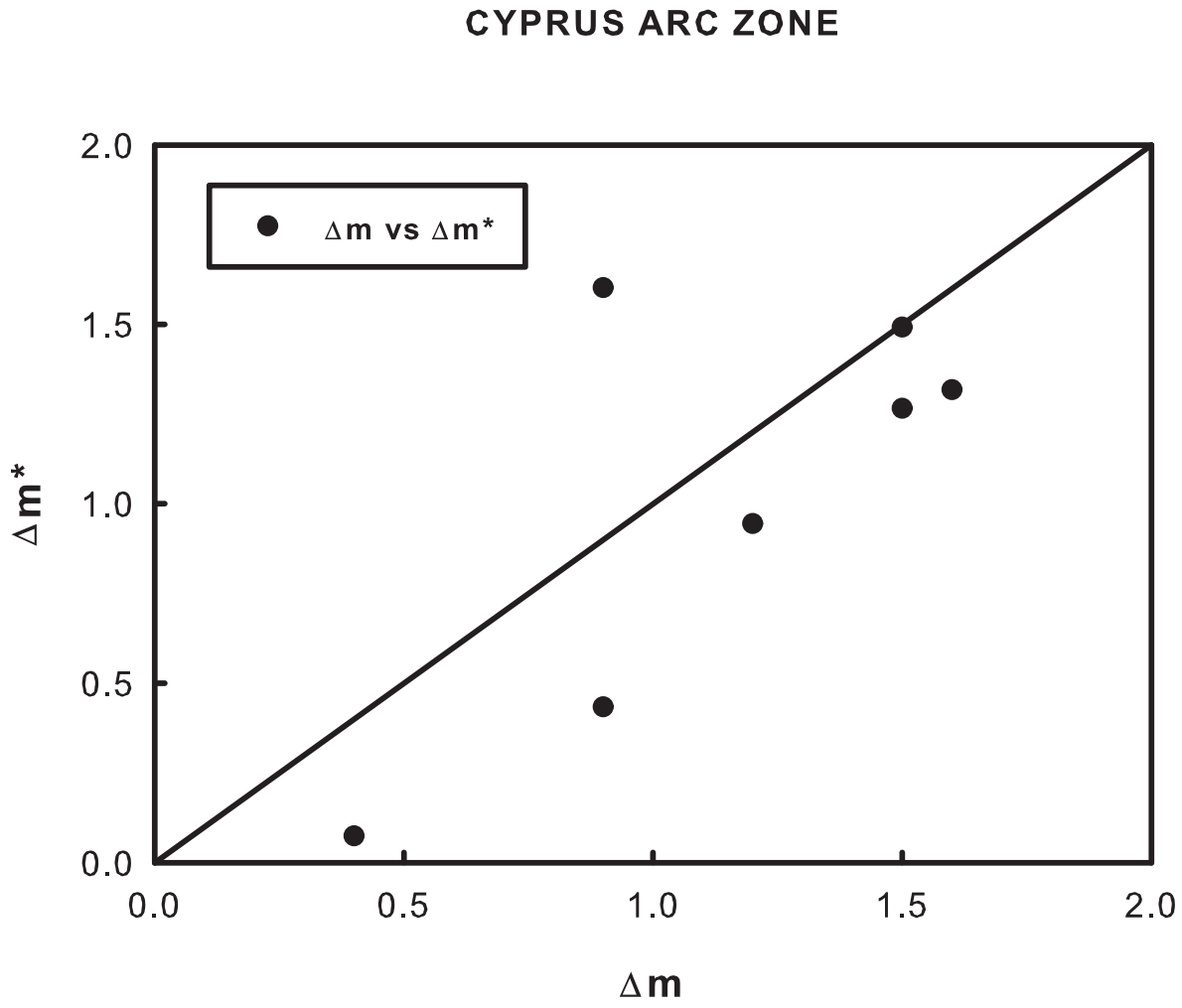

Figure 3.51. The Δm versus Δm^* graph of Cyprus Arc.

catalog are given in Table 3.17 and comparison of our catalog's results and U.S. catalog's results is given in Table 3.18 and Table 3.19. In U.S. catalog, the most of the magnitudes of earthquakes were taken from other stations, for example Kandilli, Athens, Pasadena, Thessaloniki etc. The surface-wave magnitude m_s was given from U.S. Geological Survey, because surface waves can propagate at long distances.

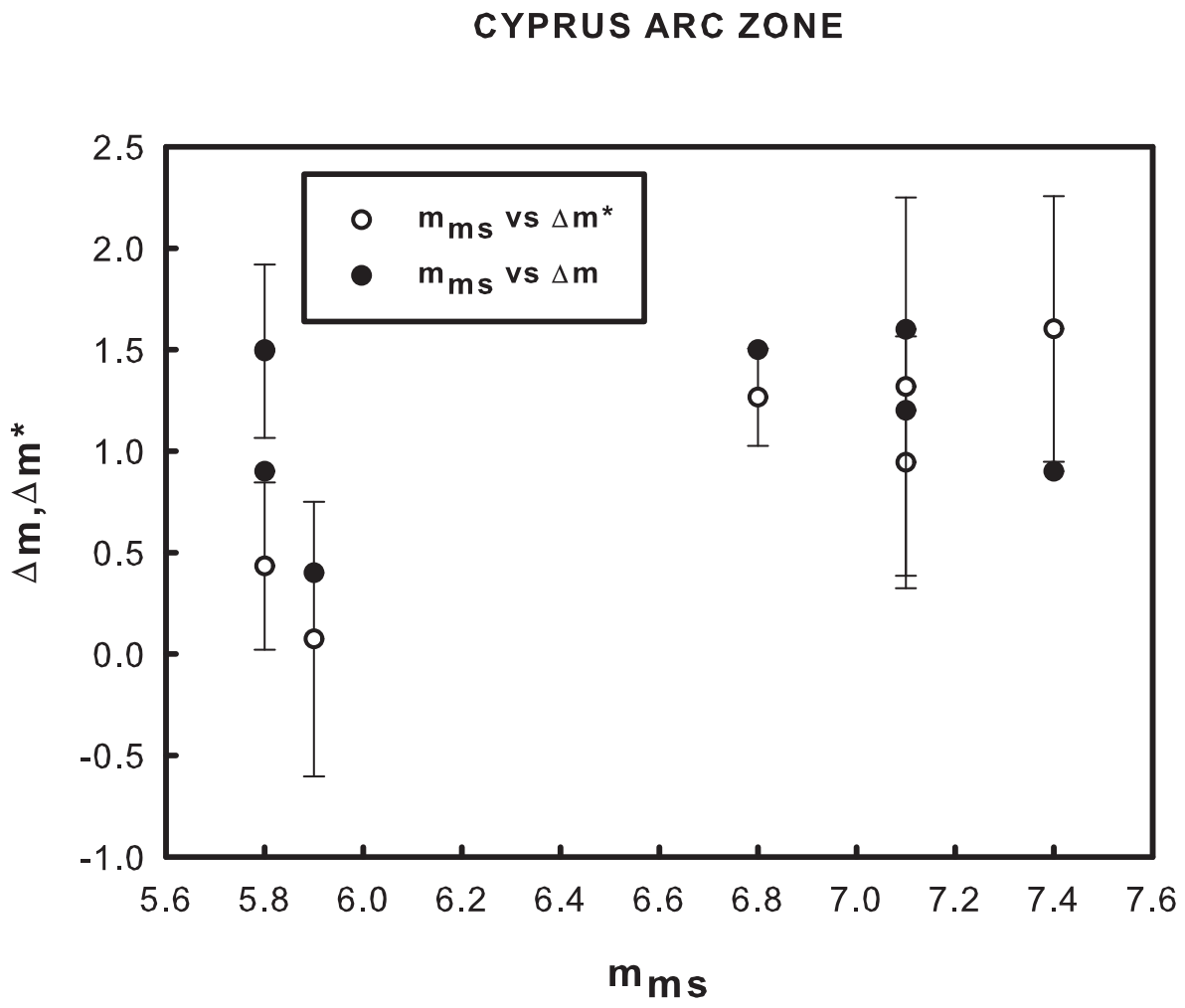

Figure 3.52. The Δm, Δm^* versus m_{ms} graph of Cyprus Arc.

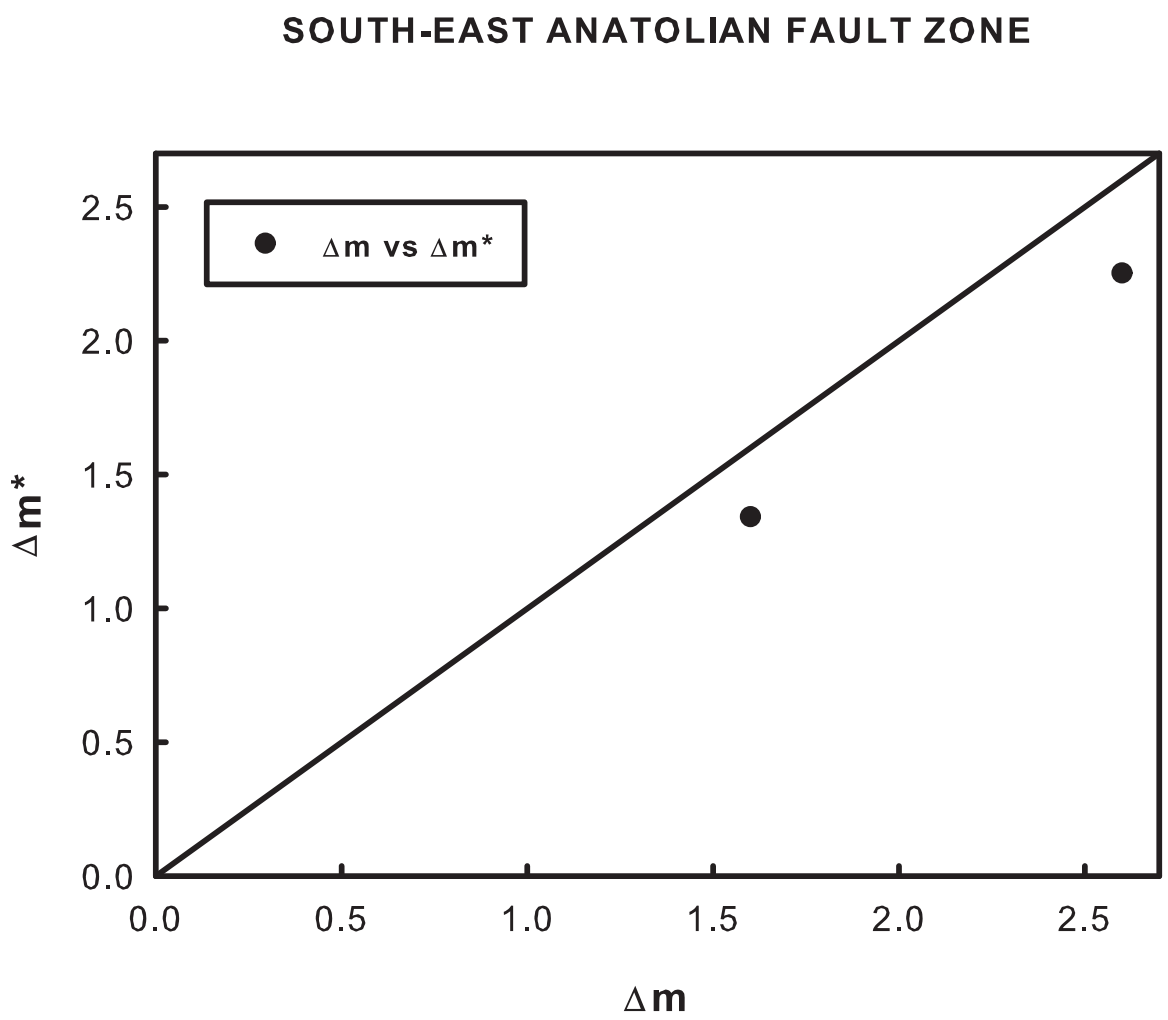

Figure 3.53. The Δm versus Δm^* graph of South-East Anatolian Fault Zone.

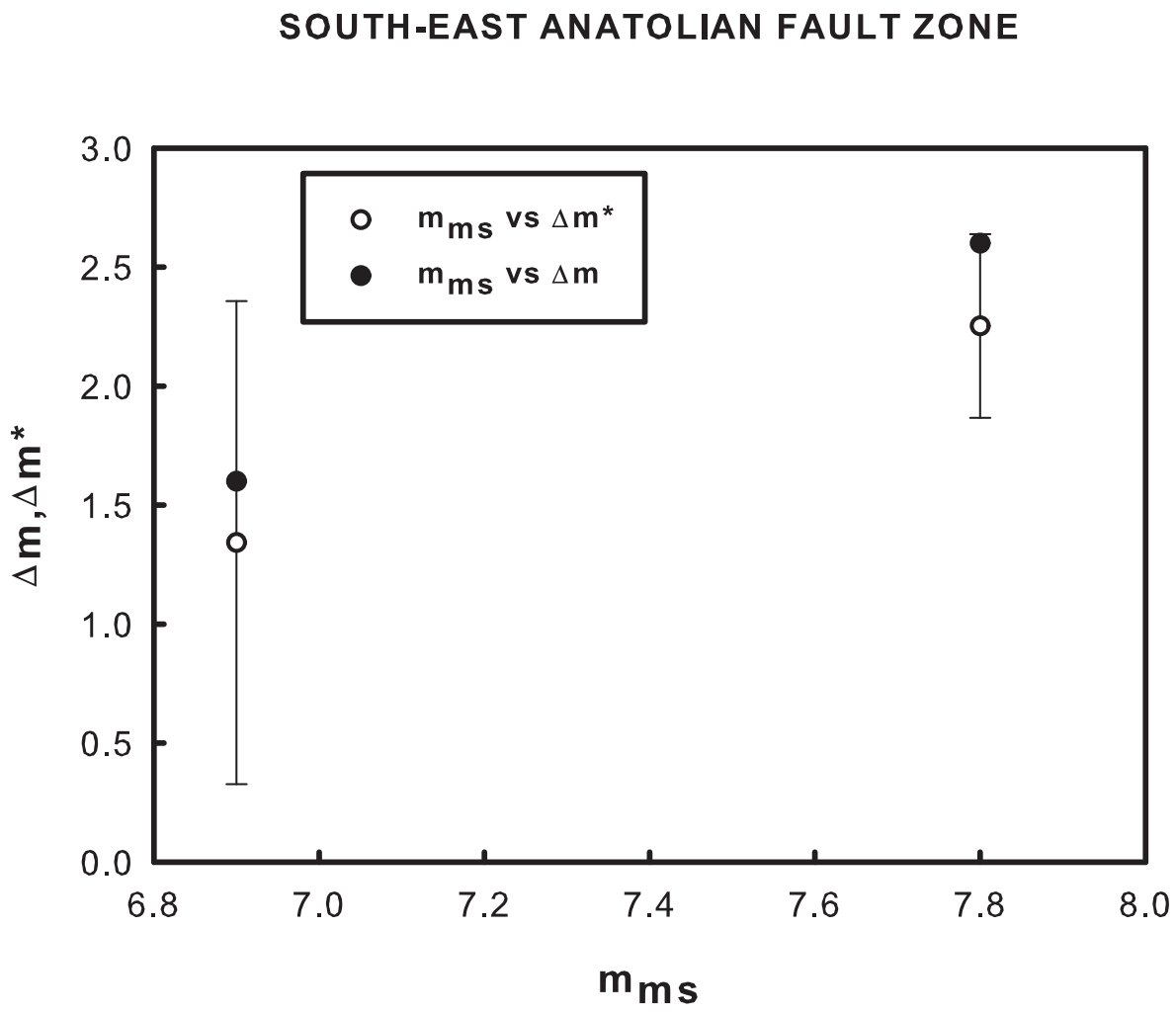

Figure 3.54. The Δm, Δm^* versus m_{ms} graph of South-East Anatolian Fault Zone.

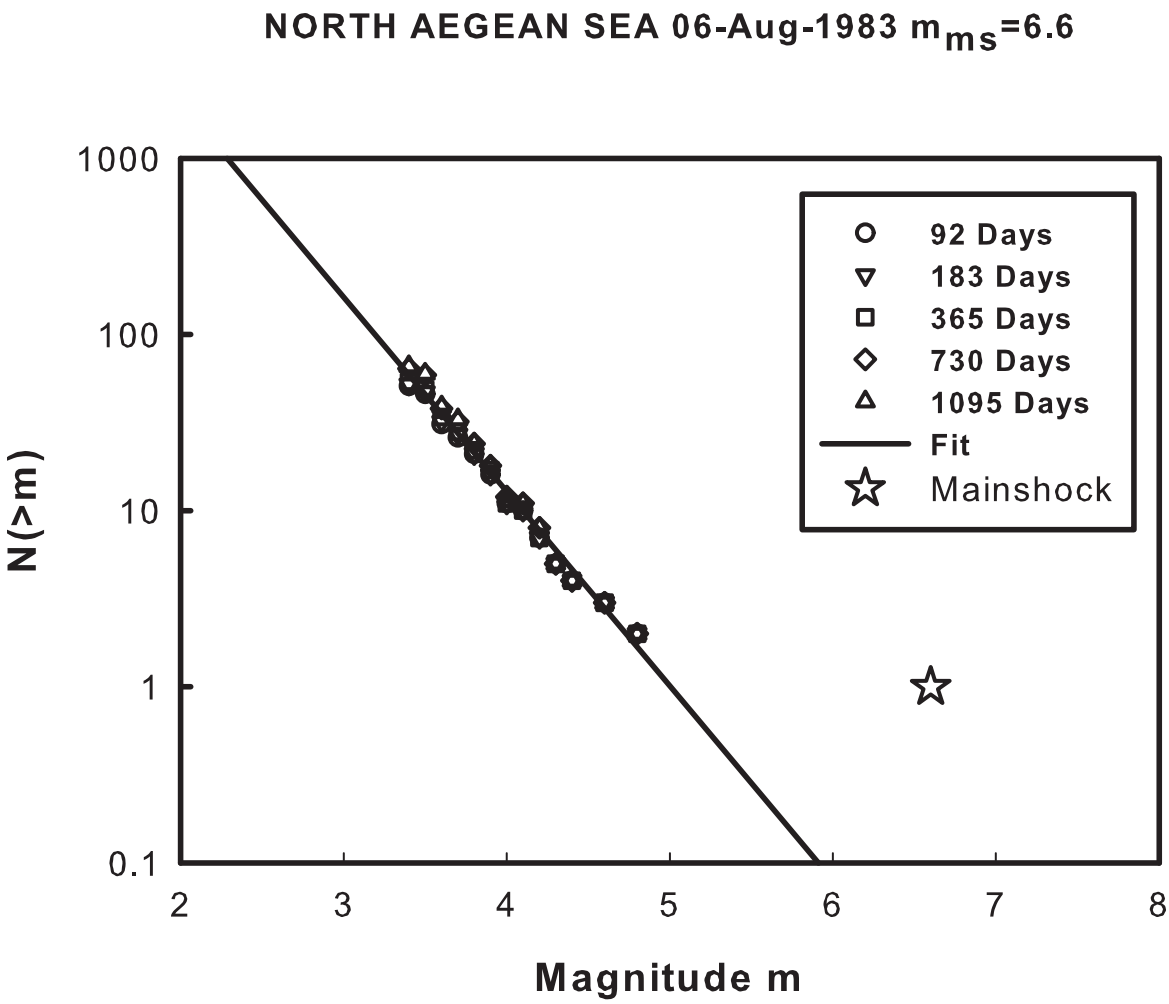

Figure 3.55. Frequency-magnitude distribution of North Aegean Sea earthquake with Greece Data

Table 3.14. Data of earthquakes that are analyzed by Greece data

Earthquake	a	b	m_{ms}	m^*	Δm	Δm^*
Aegean Sea	5.38±0.28	0.87±0.05	7.50	6.20±0.50	0.50	1.30±0.50
Greece-Athens	5.13±0.13	0.95±0.03	5.90	5.39±0.22	0.80	0.51±0.22
Greece-Athens-2	4.94±0.27	0.99±0.07	5.80	5.01±0.46	0.20	0.79±0.46
Greece-M. Athos	5.54±0.21	1.17±0.06	6.40	4.74±0.29	1.60	1.66±0.29
North Aegean Sea	5.52±0.13	1.10±0.03	6.60	5.00±0.19	1.80	1.60±0.19
Middle Aegean Sea	4.88±0.27	1.06±0.07	5.40	4.59±0.40	0.90	0.81±0.40

Table 3.15. Comparison of our catalog's results and Greece catalog's results.

Earthquake	b	b(G)	m_{ms}	m_{ms}(G)	m^*	m^*(G)
Aegean Sea	1.03±0.09	0.87±0.05	7.40	7.50	5.80±0.65	6.20±0.50
Greece-Athens	0.90±0.02	0.95±0.03	5.70	5.90	5.58±0.12	5.39±0.22
Greece-Athens-2	0.94±0.03	0.99±0.07	5.80	5.80	5.52±0.25	5.01±0.46
Greece-M. Athos	1.07±0.08	1.17±0.06	5.80	6.40	4.58±0.42	4.74±0.29
North Aegean Sea	1.41±0.10	1.10±0.03	6.00	6.60	4.76±0.44	5.00±0.19
Middle Aegean Sea	0.87±0.04	1.06±0.07	5.80	5.40	4.57±0.27	4.59±0.40

Table 3.16. Continuation of Table 3.15.

Earthquake	Δm	Δm (G)	Δm^*	Δm^*(G)
Aegean Sea	0.9	0.50	1.60±0.65	1.30±0.50
Greece-Athens	0.4	0.80	0.12±0.12	0.51±0.22
Greece-Athens-2	0.4	0.20	0.28±0.25	0.79±0.46
Greece-M. Athos	1.7	1.60	1.22±0.42	1.66±0.29
North Aegean Sea	1.5	1.80	1.24±0.44	1.60±0.19
Middle Aegean Sea	1.6	0.90	1.23±0.27	0.81±0.40

Table 3.17. Data of earthquakes that are analyzed by U.S. data

Earthquake	a	b	m_{ms}	m^*	Δm	Δm^*
Diyarbakır-Lice	5.08±0.27	0.90±0.06	6.70	5.64±0.47	1.50	1.06±0.47
Thessaloniki	5.72±0.33	1.12±0.08	6.60	5.09±0.47	1.50	1.51±0.47
Greece-Athens-2	5.57±0.26	0.99±0.06	6.60	5.62±0.44	0.90	0.98±0.44
Greece-M. Athos	4.38±0.09	0.76±0.02	7.00	5.74±0.20	1.50	1.26±0.20
North Aegean S.	5.49±0.16	1.03±0.04	7.30	5.31±0.26	2.20	1.99±0.26
Doğanbey-İzmir	3.40±0.15	0.64±0.04	6.10	5.30±0.41	1.70	0.80±0.41
Afyon-Dinar	3.59±0.13	0.63±0.03	6.40	5.70±0.36	1.10	0.70±0.36
Cyprus	5.05±0.08	0.80±0.02	6.90	6.30±0.17	1.00	0.60±0.17
Middle Aegean S.	4.42±0.30	0.93±0.08	6.10	4.75±0.51	1.80	1.35±0.51
Adana-Ceyhan	2.40±0.06	0.39±0.01	6.60	6.19±0.26	1.20	0.41±0.26
Düzce	4.51±0.15	0.73±0.04	7.50	6.15±0.37	1.70	1.35±0.37
Sığacık-Seferihisar	6.71±0.28	1.45±0.08	5.90	4.62±0.32	1.50	1.28±0.32

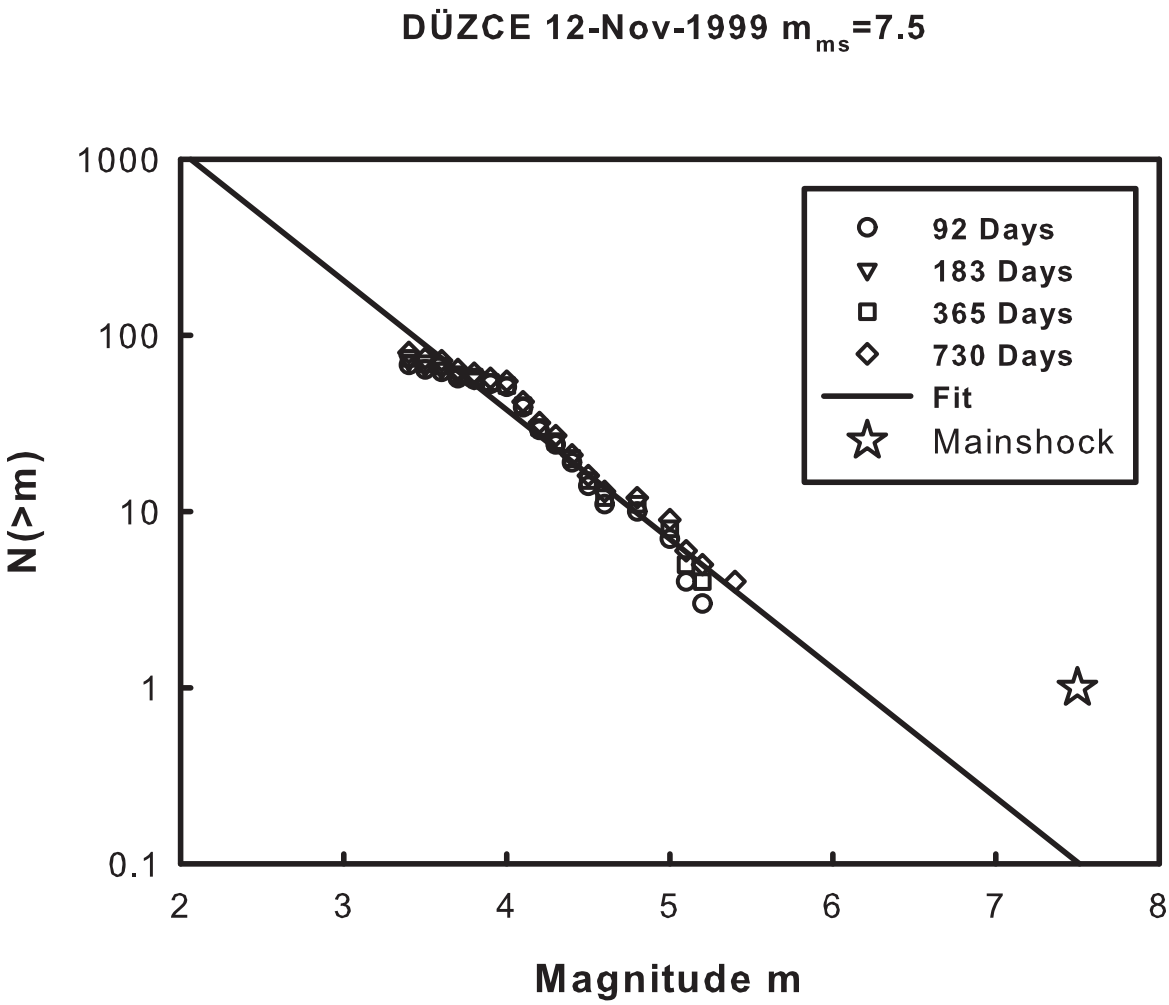

Figure 3.56. Frequency-magnitude distribution of Düzce earthquake with U.S. data

Table 3.18. Comparison of our catalog's results and U.S. catalog's results.

Earthquake	b	b(US)	m_{ms}	m_{ms}(US)	m^*	m^*(US)
Diyarbakır-Lice	1.08±0.06	0.90±0.06	7.8	6.70	5.55±0.39	5.64±0.47
Thessaloniki	0.77±0.04	1.12±0.08	6.1	6.60	5.42±0.34	5.09±0.47
Greece-Athens-2	0.94±0.03	0.99±0.06	5.8	6.60	5.52±0.25	5.62±0.44
Greece-M. Athos	1.07±0.08	0.76±0.02	5.8	7.00	4.58±0.42	5.74±0.20
North Aegean S.	1.41±0.10	1.03±0.04	6.0	7.30	4.76±0.44	5.31±0.26
Doğanbey-İzmir	0.65±0.04	0.64±0.04	5.7	6.10	4.91±0.33	5.30±0.41
Afyon-Dinar	1.20±0.04	0.63±0.03	6.0	6.40	4.95±0.20	5.70±0.36
Cyprus	0.99±0.03	0.80±0.02	6.8	6.90	5.53±0.24	6.30±0.17
Middle Aegean S.	0.87±0.04	0.93±0.08	5.8	6.10	4.57±0.27	4.75±0.51
Adana-Ceyhan	0.55±0.03	0.39±0.01	6.3	6.60	5.62±0.36	6.19±0.26
Düzce	0.78±0.02	0.73±0.04	7.2	7.50	6.16±0.18	6.15±0.37
Sığacık-Seferihisar	1.23±0.03	1.45±0.08	5.9	5.90	4.93±0.13	4.62±0.32

Table 3.19. Continuation of Table 3.18.

Earthquake	Δm	Δm(US)	Δm^*	Δm^*(US)
Diyarbakır-Lice	2.6	1.50	2.25±0.39	1.06±0.47
Thessaloniki	1.4	1.50	0.68±0.34	1.51±0.47
Greece-Athens-2	0.4	0.90	0.28±0.25	0.98±0.44
Greece-M. Athos	1.7	1.50	1.22±0.42	1.26±0.20
North Aegean S.	1.5	2.20	1.24±0.44	1.99±0.26
Doğanbey-İzmir	1.3	1.70	0.79±0.33	0.80±0.41
Afyon-Dinar	1.1	1.10	1.05±0.20	0.70±0.36
Cyprus	1.5	1.00	1.27±0.24	0.60±0.17
Middle Aegean S.	1.6	1.80	1.23±0.27	1.35±0.51
Adana-Ceyhan	1.2	1.20	0.68±0.36	0.41±0.26
Düzce	1.8	1.70	1.04±0.18	1.35±0.37
Sığacık-Seferihisar	1.1	1.50	0.97±0.13	1.28±0.32

4. CONCLUSION

Mainshocks are always followed by aftershocks which are caused by stress transfer during an earthquake. Several empirical scaling laws are valid for aftershocks. Aftershocks obey the Gutenberg-Richter frequency-magnitude scaling. Båth's law states that the difference between magnitude of mainshock and magnitude of the largest detected aftershock is a constant independent of mainshock magnitude. In 2004, Shcherbakov and Turcotte combined Båth's law and Gutenberg-Richter scaling to infer the largest aftershock by extrapolating G-R scaling for all observed aftershocks of a given mainshock.

Shcherbakov and Turcotte applied this modified form of Båth's law to San Andreas Fault Zone in California by considering 10 large earthquakes occurred between 1987 and 2003 with mainshock magnitudes equal to or greater than $m_{ms} \geq 5.5$.

We applied modified form of Båth's law to the fault zones in and near Turkey by considering 41 large earthquakes occurred between 1900 and 2005 with mainshock magnitudes equal to or greater than $m_{ms} \geq 5.7$. In Turkey, there are different fault zones that have different characteristics. They are the North Anatolian Fault Zone (NAFZ), the East Anatolian Fault Zone (EAFZ), Aegean Graben System and Cyprus Arc Zone. In Shcherbakov and Turcotte's application, there is one fault zone. So, we need to make a classification of these earthquakes. According to classification, the North Anatolian Fault Zone has eight earthquakes, the East Anatolian Fault Zone has four earthquakes, Aegean Graben System has fifteen earthquakes, Cyprus Arc Zone has seven earthquakes and Sout-East Anatolian Fault Zone has two earthquakes. The North Anatolian Fault Zone has the same characteristics with San Andreas Fault Zone, because they are both strike-slip faults. Earthquakes that occurred on San Andreas Fault Zone satisfy the modified form of Båth's law. Shcherbakov and Turcotte found same conclusion in their studies. We also found same conclusion with them. However, North Anatolian Fault Zone does not satisfy the modified

form of Båth's law, although it is a strike-slip fault zone as well. Only three eartquakes of NAFZ seem to satisfy the modified form of Båth's law. Aegean Graben System and Cyprus Arc Zone does not satisfy the modified form of Båth's law. The East Anatolian Fault Zone and The South-East Anatolian Fault Zone have four and two earthquakes respectively. So, they do not have enough earthquakes to show statistically important behavior.

We also checked our work with other catalogs that we found from Greece and U.S. Same analysis was made for twelve earthquakes by using U.S. earthquake catalog. The magnitudes were usually given as body-wave magnitude m_b for lower magnitude earthquakes and surface-wave magnitude m_s for higher magnitude earthquakes in their catalogs. However, in our catalog duration magnitude m_d was used in years between 1900 and 2001. The difference between our data and U.S. data is the result of the using different magnitude scales.

Same analysis was made for six earthquakes by using Greece earthquake catalog. Our data is more similar to Greece data than to U.S. data. They used surface-wave magnitude m_s in their catalogs in between 1950 and 1963. The Richter magnitude M_L was given in years between 1963 and 2000 in Greece catalog. There were not enough stations in these years in Greece. They were converting intensity to surface-wave magnitude by using empirical relations. However, duration magnitude m_d was given in years between 1900 and 2001 in our catalog. The difference between our data and Greece data is the result of the using different magnitude scales.

There were not enough stations in Turkey before 2000. Duration magnitudes were given by reading the duration of earthquakes from analog records until 2001. In our analysis, there were 34 earthquakes that occured before 2000. Most of the earthquakes that satisfy the modified form of Båth's law occured after 2000. The catalogs that we used may not be dense enough, especially for earlier earthquakes. Aftershocks of earlier earthquakes might not be recorded correctly. Therefore, the modified form of Båth's law

is not be applicable to the fault zones in Turkey.

APPENDIX-A CODES THAT WERE USED IN THE THESIS

Codes:

aftershock

```
function [N] = aftershock(D,first,quakename)
%[N] = quakegraph(D,first,quakename)
global main;
main=D(first,4);
L=0.01*10^(D(first,4)/2);
latlim=L/6378*180/pi;
lonlim=latlim/cos(D(first,2)*pi/180);
% 92 ——
last=D(first,1)+92;
[i, j]=find(D(:,1)>=last);
last=i(1);
[dt, quake]=cutoff(D(first:last,:),D(first,2)
,D(first,3),latlim,lonlim,0);
[n, x]=hist(quake(:,4),0:0.1:8);
N92=fliplr(cumsum(fliplr(n)));
% 183 ——
last=D(first,1)+183;
[i, j]=find(D(:,1)>=last); last=i(1);
[dt, quake]=cutoff(D(first:last,:),D(first,2)
,D(first,3),latlim,lonlim,0);
[n, x]=hist(quake(:,4),0:0.1:8);
N183=fliplr(cumsum(fliplr(n)));
```

```
% 365 ——— last=D(first,1)+365;
[i, j]=find(D(:,1)>=last); last=i(1);
[dt, quake]=cutoff(D(first:last,:),D(first,2)
,D(first,3),latlim,lonlim,0);
[n, x]=hist(quake(:,4),0:0.1:8);
N365=fliplr(cumsum(fliplr(n)));
% 730 ———
last=D(first,1)+730;
[i, j]=find(D(:,1)>=last); last=i(1);
[dt, quake]=cutoff(D(first:last,:),D(first,2)
,D(first,3),latlim,lonlim,0);
[n, x]=hist(quake(:,4),0:0.1:8);
N730=fliplr(cumsum(fliplr(n)));
% 1095 ———
last=D(first,1)+1095;
[i, j]=find(D(:,1)>=last); last=i(1);
[dt, quake]=cutoff(D(first:last,:),D(first,2)
,D(first,3),latlim,lonlim,0);
[n, x]=hist(quake(:,4),0:0.1:8);
N1095=fliplr(cumsum(fliplr(n)));
%———————
N=[N92; N183; N365; N730; N1095];
```

aftershockcal

```
function [N] = aftershockcal(D,first,quakename)
%[N] = quakegraphcal(D,first,quakename)
global main;
main=D(first,4);
```

```
L=0.01*10^(D(first,4)/2);
latlim=L/6378*180/pi;
lonlim=latlim/cos(D(first,2)*pi/180);
% 92 ———
last=D(first,1)+92;
[i, j]=find(D(:,1)>=last);
last=i(1);
[dt, quake]=cutoff(D(first:last,:),D(first,2)
,D(first,3),latlim,lonlim,0);
[n, x]=hist(quake(:,4),0:0.1:8);
N92=fliplr(cumsum(fliplr(n)));
% 183 ———
last=D(first,1)+183;
[i, j]=find(D(:,1)>=last); last=i(1);
[dt, quake]=cutoff(D(first:last,:),D(first,2)
,D(first,3),latlim,lonlim,0);
[n, x]=hist(quake(:,4),0:0.1:8);
N183=fliplr(cumsum(fliplr(n)));
% 365 ———
last=D(first,1)+365;
[i, j]=find(D(:,1)>=last); last=i(1);
[dt, quake]=cutoff(D(first:last,:),D(first,2)
,D(first,3),latlim,lonlim,0);
[n, x]=hist(quake(:,4),0:0.1:8);
N365=fliplr(cumsum(fliplr(n)));
% 730 ———
last=D(first,1)+730;
[i, j]=find(D(:,1)>=last); last=i(1);
[dt, quake]=cutoff(D(first:last,:),D(first,2)
```

,D(first,3),latlim,lonlim,0);

$[n, x]$=hist(quake(:,4),0:0.1:8);

N730=fliplr(cumsum(fliplr(n)));

% 1095 ———

N=[$N92$; $N183$; $N365$; $N730$];

cutoff

function $[dt, Bnew]$ = cutoff(B,lat,lon,latlim,lonlim,cut);

%$[dt, Bnew]$ = cutoff(B,lat,lon,latlim,lonlim,cut);

s=size(B); dt=[0];

Bnew=zeros(1,s(2)); for i=1:s(1);

if (B(i,2)>=lat-latlim) & (B(i,2)<=lat+latlim)

& (B(i,3)>=lon-lonlim) & (B(i,3)<=lon+lonlim)

& (B(i,4)>=cut)

dt(end+1)=B(i,1)*24*3600;

Bnew(end+1,:)=B(i,:);

end;

end; dt=dt(2:end); dt=diff(dt);

Bnew=Bnew(2:end,:);

REFERENCES

1. Gutenberg, B. and Richter, C. F., *Seismicity of the Earth and Associated Phenomena* (Princeton Univ. Press, Princeton, New Jersey, 1954).

2. Helmstetter, A. and Sornette, D., Diffusion of epicenters of earthquake aftershocks, Omoris law, and generalized continuous-time random walk models *Physical Review* **E 66**, 061104 (2002).

3. Båth, M., Lateral inhomogeneities in the upper mantle, *Tectonophysics*. **2**, 483–514 (1965).

4. Shcherbakov, R. and Turcotte, D. L., A Modified Form of Båth's Law, *Bulletin of the Seismological Society of America*. **94**, 1968–1975 (2004).

5. Boğaziçi University Kandilli Observatory and Earthquake Research Institute, www.koeri.boun.edu.tr, 2007.

6. Southern California Earthquake Center, Southern California Seismic Network catalog, www.data.scec.org, 2008.

7. Northern California Earthquake Data Center, Northern California Seismic Network catalog, http://quake.geo.berkeley.edu/ncedc/, 2008.

8. U. S. Geological Survey Earthquake Database, http://neic.usgs.gov/neis/epic/, 2008.

9. Institute of Geodynamics National Observatory of Athens, http://www.gein.noa.gr/services/cat.html, 2008.

10. Gülen L., Surface Fault Breaks, Aftershock Distribution, and Rupture Process of the

17 August 1999 İzmit, Turkey, Earthquake, *Bulletin of the Seismological Society of America*. **92**, 230–244 (2002).

11. Kanamori, H. and Brodsky, E. E., The Physics of Earthquakes, *Reports on Progress in Physics*. **67**, 1429–1496 (2004).

12. Vere-Jones D., A note on the statistical interpretation of Båth's law, *Bulletin of the Seismological Society of America*. **59**, 1535–1541 (1969).

13. Helmstetter, A. and Sornette, D., Båth's law derived from the Gutenberg-Richter law and from aftershock properties, *Geophysical Research Letters*. **30**, 2069 (2003).

14. Shcherbakov, R., Turcotte, D. L. and Rundle, J. B., Aftershock Statistics, *Pure and Applied Geophysics*. **162**, 1051–1076 (2005).

15. Kagan, Y. Y., Aftershock Zone Scaling, *Bulletin of Seismological Society of America*. **92**, 641–655 (2002).

16. General Directorate of Mineral Research and Exploration, http://www.mta.gov.tr, 2008.